UC Berkeley
UC Berkeley Electronic Theses and Dissertations

Title

Cation Exchange Reactions for Improved Quality and Diversity of Semiconductor Nanocrystals

Permalink

https://escholarship.org/uc/item/4gx4f76d

Author

Beberwyck, Brandon James

Publication Date

2014

Peer reviewed|Thesis/dissertation

Cation Exchange Reactions for Improved Quality and Diversity of Semiconductor Nanocrystals

By

Brandon James Beberwyck

A dissertation submitted in partial satisfaction of the

requirements for the degree of

Doctor of Philosophy

in

Engineering- Materials Science and Engineering

in the

Graduate Division

Of the

University of California, Berkeley

Committee in charge:

Professor A. Paul Alivisatos, Chair
Professor Peidong Yang
Professor Jeffrey R. Long

Fall 2014

Cation Exchange Reactions for Improved Quality and Diversity of Semiconductor Nanocrystals

Copyright 2014

By

Brandon James Beberwyck

Abstract

Cation Exchange Reactions for Improved Quality and Diversity of Semiconductor Nanocrystals

By

Brandon James Beberwyck

Doctor of Philosophy in Materials Science and Engineering

University of California, Berkeley

Professor A. Paul Alivisatos, Chair

Observing the size and shape dependent physical properties of semiconductor nanocrystals requires synthetic methods capable of not only composition and crystalline phase control but also molecular scale uniformity for a particle consisting of tens to hundreds of thousands of atoms. The desire for synthetic methods that produce uniform nanocrystals of complex morphologies continues to increase as nanocrystals find roles in commercial applications, such as biolabeling and display technologies, that are simultaneously restricting material compositions. With these constraints, new synthetic strategies that decouple the nanocrystal's chemical composition from its morphology are necessary.

This dissertation explores the cation exchange reaction of colloidal semiconductor nanocrystals, a template-based chemical transformation that enables the interconversion of nanocrystals between a variety of compositions while maintaining their size dispersity and morphology. Chapter 1 provides an introduction to the versatility of this replacement reaction as a synthetic method for semiconductor nanocrystals. An overview of the fundamentals of the cation exchange reaction and the diversity of products that are achievable is presented. Chapter 2 examines the optical properties of nanocrystal heterostructures produced through cation exchange reactions. The deleterious impact of exchange on the photoluminescence is correlated to residual impurities and a simple annealing protocol is demonstrated to achieve photoluminescence yields comparable to samples produced by conventional methods. Chapter 3 investigates the extension of the cation exchange reaction beyond ionic nanocrystals. Covalent III-V nanocrystal of high crystallinity and low size dispersity are synthesized by the cation exchange of cadmium pnictide nanocrystals with group 13 ions. Lastly, Chapter 4 highlights future studies to probe cation exchange reactions in colloidal semiconductor nanocrystals and progress that needs to be made for its adoption as a routine synthetic approach.

For family and friends.
You know who you are.

Table of Contents

List of Figures

List of Tables

Chapter 1.

Cation Exchange as a Versatile Tool for Nanomaterials Synthesis

The development of nanomaterials for next generation photonic, optoelectronic, and catalytic applications requires a robust synthetic toolkit for systematically tuning composition, phase, and morphology at nanometer length scales. While de novo synthetic methods for preparing nanomaterials from molecular precursors have advanced considerably in recent years, post-synthetic modifications of these pre-formed nanostructures have enabled the step-wise construction of complex nanomaterials. Among these post-synthetic transformations, cation exchange reactions, in which the cations ligated within a nanocrystal host lattice are substituted with those in solution, have emerged as particularly powerful tools for fine-grained control over nanocrystal composition and phase. In this feature article, we review the fundamental thermodynamic and kinetic basis for cation exchange reactions in colloidal semiconductor nanocrystals and highlight its synthetic versatility for accessing nanomaterials intractable by direct synthetic methods from molecular precursors. Unlike analogous ion substitution reactions in extended solids, cation exchange reactions at the nanoscale benefit from rapid reaction rates and facile modulation of reaction thermodynamics via selective ion coordination in solution. The preservation of the morphology of the initial nanocrystal template upon exchange, coupled with stoichiometric control over the extent of reaction, enables the formation of nanocrystals with compositions, morphologies, and crystal phases that are not readily accessible by conventional synthetic methods.

1.1 Chemical Transformations as a Synthetic Method

The physical and chemical properties of periodic extended solids change drastically as the crystallite size is reduced to nanometer dimensions.[1] A quantitative understanding of these fundamental scaling laws has emerged as a direct result of synthetic advances that permit the preparation of monodisperse crystallites of diverse nanoscale size and shape. The direct synthesis of nanocrystal colloids is most practically achieved using a hot-injection protocol, in which molecular precursors are rapidly decomposed at elevated temperatures to produce a burst of nanocrystal nucleation followed by uniform steady-state growth.[2,3] Hot-injection synthetic methods have proven particularly powerful for accessing monodisperse II-VI and IV-VI compound semiconductor nanocrystals. Indeed, a wide array of morphological diversity can be achieved among the II-VI class of

nanocrystals and has enabled their widespread utilization in optoelectronic,[4] photocatalytic,[5] and bioimaging applications.[6]

Direct nanocrystal synthesis methods require a careful tuning of nucleation, growth, and surface ligation kinetics at temperatures sufficient to crystallize phase-pure extended solids.[2,3] All of these kinetic processes remain poorly understood and, as a consequence, there remain no *general* design principles for the *de novo* synthesis of a nanocrystal of arbitrary composition, phase, morphology, or surface structure. However, synthetic protocols have been extensively refined for several classes of compound semiconductor nanocrystals which may serve as general anion host lattices for the preparation of compositionally diverse, morphologically well-defined nanomaterials provided that post synthetic methods for cation substitution can be broadly applied. Recent developments suggest that a post-synthetic cation exchange strategy might prove particularly versatile for the synthesis of large classes of binary nanocrystalline phases that would otherwise be inaccessible by application of direct hot-injection synthetic methods.[7] In this article, we highlight the thermodynamic and mechanistic basis for cation exchange reactions at the nanoscale and use this as a backdrop to illustrate selected applications of cation exchange for the preparation of nanocrystals that are challenging to access by direct synthesis from molecular precursors. For a broader view of cation exchange in nanostructures including applications beyond synthesis, we direct the readers to a recent tutorial review.[8]

1.2 Fundamentals of Cation Exchange at the Nanoscale

Ion exchange, the substitution of ions in an extended solid with those in solution, is an age-old strategy for modifying the composition and properties of crystalline materials. Ion substitution reactions are responsible for various re-equilibration processes in rocks,[9] displacement reactions in metal oxides,[10] and of more technological relevance, serve as a simple processing technique for thin film semiconductors.[11] In particular, cation exchange of thin film semiconductors has been utilized to form a broad range of structures including optical waveguides, heterojunctions for optoelectronic devices, and alloys for infrared photodetectors.[11]

In recent years, cation exchange reactions have been increasingly applied as a synthetic tool for accessing novel nanomaterials. For both nanocrystalline colloids and bulk extended solids, a typical cation exchange procedure is extremely simple. For example, exposing nanocrystal colloids of CdSe to a methanolic solution of Ag^+ ions leads to rapid formation of Ag_2Se colloids with liberation of Cd^{2+} from the reactant host lattice (Figure 1.1).[7] Microscopically, each individual cation substitution reaction can be viewed as the extended solid analog of transmetallation reactions commonly observed for molecular coordination compounds.[12] In addition to their simplicity, nanoscale cation exchange reactions typically exhibit excellent morphology retention, rapid reaction rates, and tunable thermodynamics making them a particularly attractive synthetic tool. While complimentary anion exchange reactions have also been demonstrated,[13,14,15] the larger

size and lower diffusivity of lattice anions leads to sluggish reaction kinetics and poor morphology retention, often giving rise to hollow nanostructures.[16]
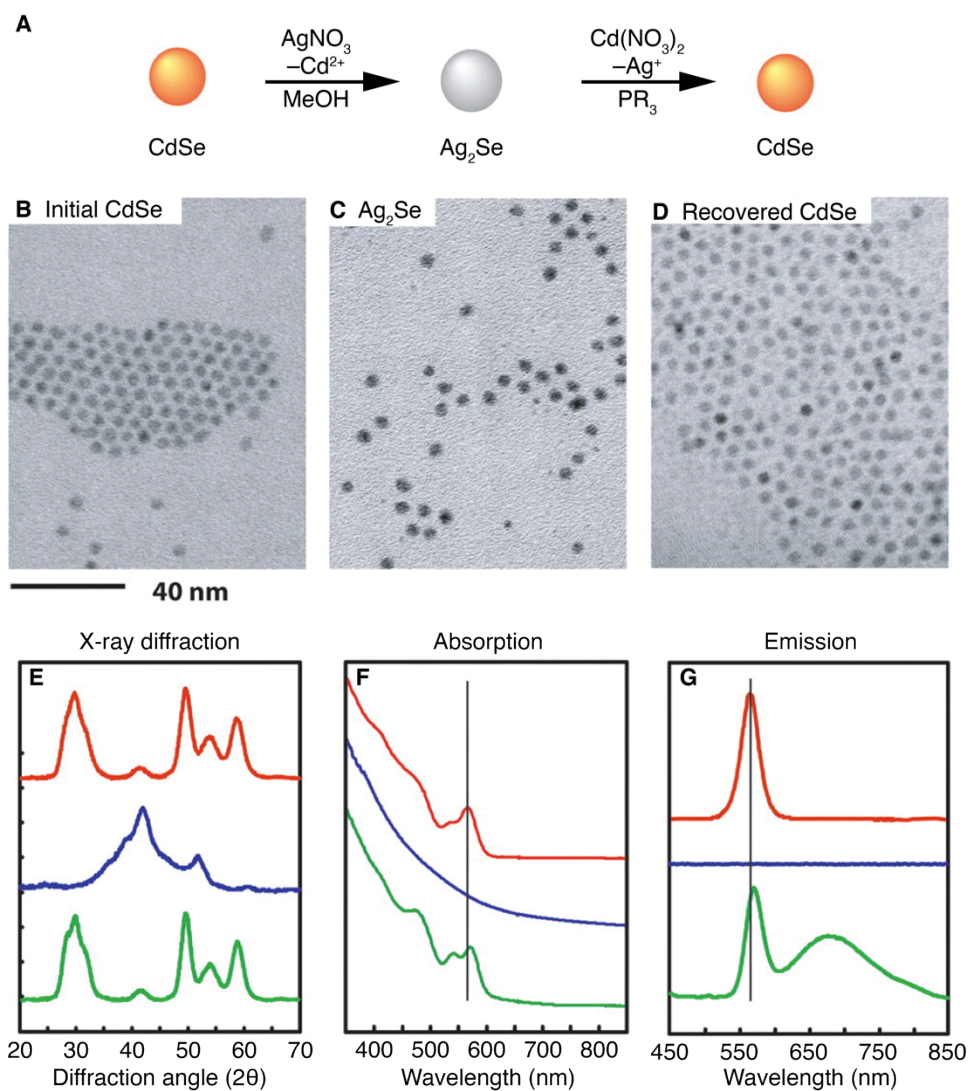
Figure 1.1. Cation exchange reaction of nanocrystalline colloids. (A) Reaction scheme for the conversion of CdSe to Ag_2Se and Ag_2Se to CdSe. Exposure of CdSe to a methanolic solution of Ag^+ leads to the rapid formation of Ag_2Se. Ag_2Se is exchanged back to CdSe by exposure of the Ag_2Se nanocrystals to excess Cd^{2+} in the presence of a tri-alkyl phosphine. TEM images of (B) as synthesized CdSe nanocrystals, (C) Ag_2Se nanocrystals synthesized via cation exchange, and (D) CdSe nanocrystals recovered from the reverse cation exchange reaction. XRD patterns (E), absorption spectra (F), and emission spectra (G) of initial CdSe (red), Ag_2Se (blue), and recovered CdSe (green) nanocrystals, respectively. Adapted with permission from ref. 7, copyright 2005 AAAS.

While a cation exchange reaction is remarkably simple to execute, the outcome of the reaction and the structure of the product obtained are dictated by subtle thermodynamic and kinetic factors. First among these are the relative thermodynamic stabilities of the reactant and product phases. Second are the relative thermodynamics of cation solvation and/or specific ligation in the liquid phase. While these two parameters, cation solvation and phase stability, can predict, to a first approximation, the thermodynamic feasibility of an overall ion exchange reaction, they provide little insight into the reaction pathway or the structure of the product. Since ion exchange reactions must proceed through partially substituted alloy intermediates, the thermodynamics of the *interphase* between reactant and product phases, referred to as the exchange reaction zone, dictates the structure and morphology of the product crystallite. While these principles apply to solid-state ion exchange reactions broadly, regardless of crystallite size, we will use contemporary examples of ion exchange reactions at the nanoscale to illustrate the importance of bulk, solution, and interfacial thermodynamics in dictating the reaction outcome.

Kinetic factors are also key in determining the feasibility of an ion exchange reaction. In this respect, the kinetics of ion exchange at the nanoscale differ substantially from those observed for bulk extended solids because limits on long-range solid-state ion diffusion are significantly relaxed by the large surface-to-volume ratios of nanoscale crystallites. Indeed, solid-state diffusion limitations in bulk crystallites often necessitate the application of high temperatures and pressures to achieve rapid product formation.[11] As an example, Ag^+, which possesses a relatively high ion diffusivity,[17] sluggishly converts a thin film (500 nm) of CdSe to Ag_2Se, requiring several hours at 80 °C,[18] whereas the similar reaction in CdSe nanocrystals (see above) proceeds to completion in $\ll 1$ s at room temperature.[7] In the subsequent section, we will highlight recent mechanistic studies of ion exchange kinetics at the nanoscale to illustrate the mechanistic consequences of relaxing limitations on solid-state ion diffusion.

1.3 Thermodynamics of Cation Exchange

The synthetic feasibility of a cation exchange reaction is determined by its net thermodynamic driving force and intervening activation barriers.[19] For cation exchange to become a general synthetic tool, a quantitative understanding of the thermodynamics of the exchange process is desired to permit the rational design of future exchange reactions. Consider, for example, an arbitrary ion exchange reaction between two metal sulfides,

$$AS + B^{2+} \leftrightarrows BS + A^{2+} \qquad \text{(eq. 1)}$$
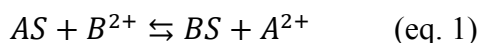
where A and B represent divalent metal ions. This overall exchange reaction can be divided into two hypothetical electrochemical half reactions,

$$AS \leftrightarrows A^{2+} + 2e^- + S^0 \qquad \text{(eq. 2)}$$

$$B^{2+} + 2e^- + S^0 \leftrightarrows BS \qquad \text{(eq. 3)}$$
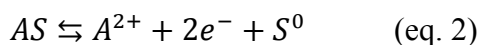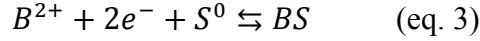
Each of which may be further decomposed into the corresponding standard free energy of formation (ΔG_f^0) of each phase and the standard reduction potential (E^0) of the metal ion in question,

$$AS \rightleftarrows A^0 + S^0 \qquad -\left(\Delta G_f^0\right)_{AS} \qquad \text{(eq. 4)}$$

$$A \rightleftarrows A^{2+} + 2e^- \qquad -(E^0)_{A^{2+}} \qquad \text{(eq. 5)}$$

$$B^0 + S^0 \rightleftarrows BS \qquad \left(\Delta G_f^0\right)_{BS} \qquad \text{(eq. 6)}$$

$$B^{2+} + 2e^- \rightleftarrows B \qquad (E^0)_{B^{2+}} \qquad \text{(eq. 7)}$$
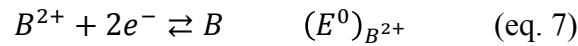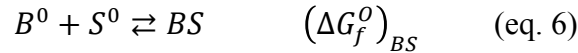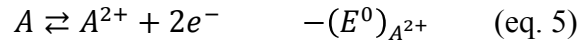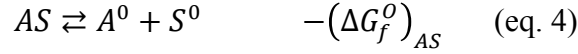
Thus, for this example, the overall aqueous driving force for ion exchange (eq. 1) is given by,

$$\Delta G_{reaction} = \left(\Delta G_f^0\right)_{BS} - \left(\Delta G_f^0\right)_{AS} - 2F[(E^0)_{B^{2+}} - (E^0)_{A^{2+}}] \qquad \text{(eq. 8)}$$

where F is Faraday's constant. Since tabulated formation energies[20] are available for a number of binary chalcogenides, oxides, and pnictides and aqueous redox potentials[21] are known for virtually every metal ion in the periodic table, the aqueous thermodynamics of any given ion exchange reaction can be readily calculated.[22] We wish to stress that this strategy provides a convenient method for calculating ion exchange thermodynamics but does not imply anything about the mechanistic pathway by which ion exchange proceeds. Using this simple methodology, aqueous driving forces are presented in Table 1.1 for a select number of metal sulfide phases.

The foregoing discussion highlights the two key determinants of ion exchange thermodynamics: the difference in formation energies of the reactant and product phases and the difference in redox potentials of the exchanging ions. For simplicity, the above calculation and the values in Table 1.1 take into account only the bulk lattice formation energies for each phase and aqueous redox potentials for the attendant metal ions. In practice, the thermodynamic driving force for an ion exchange may significantly differ from these estimates for the following two principle reasons.

First, nanostructuring is expected to significantly depress the formation energies of each phase. Formation energies for the product and reactant colloid may be highly dependent on crystallite size and shape, and significant thermodynamic contributions to phase stability may arise from ligands bound to the surface of the nanocrystal. If these energy contributions scale unevenly between the reactant and product phase, the actual thermodynamics of an exchange reaction may deviate significantly for the values calculated in Table 1.1. These effects are expected to be particularly pronounced for very small crystallites (< 2 nm), in which a majority of the metal ions reside on the surface.

Table 1.1. Calculated aqueous reaction free energies per sulfur equivalent, $\Delta G^{0}_{reaction}$ (kJ mol^{-1}), for the cation exchange of reactant (abscissa) to product (ordinate) metal sulfides.

Reactant

PdS	HgS	Ag$_2$S	Cu$_2$S	SnS	PbS	CdS	ZnS	CoS	NiS	Product
0.0	-33.8	-55.5	-63.5	-169.0	-176.8	-182.1	-198.7	-207.5	-214.60	PdS
	0.0	-21.7	-29.7	-135.2	-143.0	-148.3	-165.0	-173.7	-180.8	HgS
		0.0	-8.0	-113.5	-121.3	-126.6	-143.2	-152.0	-159.1	Ag$_2$S
			0.0	-105.5	-113.3	-118.6	-135.2	-144.0	-151.1	Cu$_2$S
				0.0	-7.8	-13.1	-29.8	-38.5	-45.6	SnS
					0.0	-5.3	-21.9	-30.7	-37.8	PbS
						0.0	-16.6	-25.4	-32.5	CdS
							0.0	-8.8	-15.9	ZnS
								0.0	-7.1	CoS
									0.0	NiS

Second, the ligating environment in solution is expected to significantly alter the reduction potential of each metal ion.[23] While readily accessible aqueous redox potentials provide a starting point for estimating ion exchange free energies, these potentials are known to vary significantly, depending on the solvating/ligating environment of the solution in which the exchange occurs. As a consequence, the thermodynamic preference for a given ion exchange can be easily reversed (Figure 1.1) if the ions discharged from the reactant lattice can be *preferentially* ligated in solution. A ligand's propensity for selective ion binding can be qualitatively understood in the context of Pearson's hard soft acid base (HSAB) theory, which classifies Lewis acids and bases by varying degrees of hardness, η, based on their polarizability.[24] Hardness serves as a qualitative predictor of selective ion binding because like interactions, hard-hard and soft-soft, are favored relative to opposing, soft-hard, interactions. This principle has been exploited to drive the replacement of soft Ag^+ (η = 6.96 eV) and Cu^+ (η = 6.28 eV) ions in chalcogenide host lattices with harder metal ions including Cd^{2+} (η = 10.29 eV),[7] Zn^{2+} (η = 10.88 eV),[25,26] and Pb^{2+} (η = 8.46 eV)[27] via preferential ligation to soft tertiary phosphines ($\eta \sim$ 6 eV). This strategy has, thereby, enabled both reversible and sequential exchanges.

While a quantitative assessment of nanostructuring and specific ligation effects awaits detailed thermochemical studies of nanoscale cation exchange reactions, the above crude calculations can provide a starting point for designing ion exchange synthetic protocols that take advantage of intrinsic thermodynamics or preferential ion ligation.

1.4 Mechanistic Insights into Nanoscale Cation Exchange

While thermodynamic considerations can serve to guide the development of new cation exchange syntheses, many of these reactions proceed under non-equilibrium conditions, necessitating a careful consideration of the mechanistic pathways by which they proceed. While a detailed microkinetic description of solid-state cation exchange remains elusive, qualitative mechanistic pathways have been proposed for these reactions in minerals[9] and thin film semiconductors.[11] For ion exchanges in semiconductor thin films, which are most analogous to the corresponding reactions in colloidal nanocrystals, appreciable rates of heterogeneous ion substitution at crystallite surfaces and rapid solid-state diffusion of the exchanging cation are required. Experimental results indicate that the rate of diffusion within each crystallite is typically much slower that the rate of substitution at the crystallite surface. Thus, the composition at the surface of the substrate remains in quasi-equilibrium and is dictated by the solution composition and temperature, independent of the time duration of the reaction. The disparity between the surface and bulk composition during a cation exchange establishes a chemical potential gradient within the film, providing a driving force for directional diffusion of the replacing ion in the parent lattice. Reaction progress is then kinetically limited by the rate of solid-state diffusion. Indeed, the compositional profile of a thin film undergoing a cation exchange can be used to measure the self-diffusion coefficients of the constituent ions, finding good agreement with values determined by established radiotracer techniques.[11]

In both mineral replacement reactions and semiconductor thin film ion exchange, the transport of ions to the boundary between reactant and product phases is believed to be the rate-limiting step.[9,11] The ion exchange reaction can then be viewed as the propagation of this phase boundary across the crystallite. In this fashion, ion exchange reactions can be described by analogy to the solid-state heterophase concept of a reaction zone.[28] The reaction zone, typically a several atomic layer thick region between two materials, represents a local variation in the chemical composition and charge distribution relative to either bulk phase.

The stability and propagation of the reaction zone has direct consequences for particle size-dependent morphology retention during a nanocrystal cation exchange.[7] For example, nanorod morphology retention is strongly dependent on the rod diameter for CdSe to Ag_2Se ion exchange reactions (Figure 1.2). Small diameter (~3.5 nm) CdSe nanorods transformed into spherical Ag_2Se nanocrystals upon Ag^+ exchange (Figure 1.2A) whereas larger diameter (~5 nm) CdSe nanorods maintained their morphology upon conversion to Ag_2Se (Figure 1.2B). These results can be rationalized if we invoke a reaction zone on the order of 3 nm in diameter. For thin nanorods, wherein the reaction zone dimensions are comparable to the particle diameter, the entire structure will reside in a non-equilibrium state during the exchange such that both cations and anions can rearrange to generate the thermodynamically preferred, spherical morphology (Figure 1.2C). However, if the size of the nanocrystal is significantly larger than the reaction zone, only a portion of the crystallite experiences significant structural distortions during the exchange while the remainder of the lattice remains intact, templating retention of the nanorod morphology (Figure 1.2C). In this fashion, the anion sublattice is subject to minimal net reorganization over the course of the exchange if the crystal size is much larger than the dimensions of the reaction zone.

When nanoscale crystallites are large enough to preserve anionic framework stability, the crystal structure and nanoscale morphology remain robust, as demonstrated by performing forward and reverse exchanges between CdSe→Ag_2Se→CdSe.[7] As a result of quantum confinement, CdSe nanocrystals exhibit a characteristic excitonic absorption and narrow emission band that is highly sensitive to the size of the particle. Through sequential forward and reverse exchanges that serve to regenerate the starting phase, the absorption and emission maxima remain largely unchanged, indicating that the crystallite size and anion stoichiometry remain largely invariant during the cation exchange process (Figure 1.1E, F). The same phenomenon has been observed for exchanges conducted on nanoheterostructures, consisting of a CdSe sphere embedded in a CdS rod.[29] Ion substitution with Cu^+ was followed by reintroduction of Cd^{2+} to regenerate the initial CdSe/CdS core-shell heterostructure. Through this series of ion exchange reactions, negligible shifts in the photoluminescence peak maxima were observed indicating preservation of the Se core sublattice within the S anion shell sublattice. Additionally, minimal structural and compositional changes were observed by scanning transmission electron microscopy high angle annular dark field (STEM-HAADF) imaging. These results establish that for sufficiently large crystallites, cation exchange reactions can effectively preserve the size, position, and interfacial structure of one or more anion sublattices.
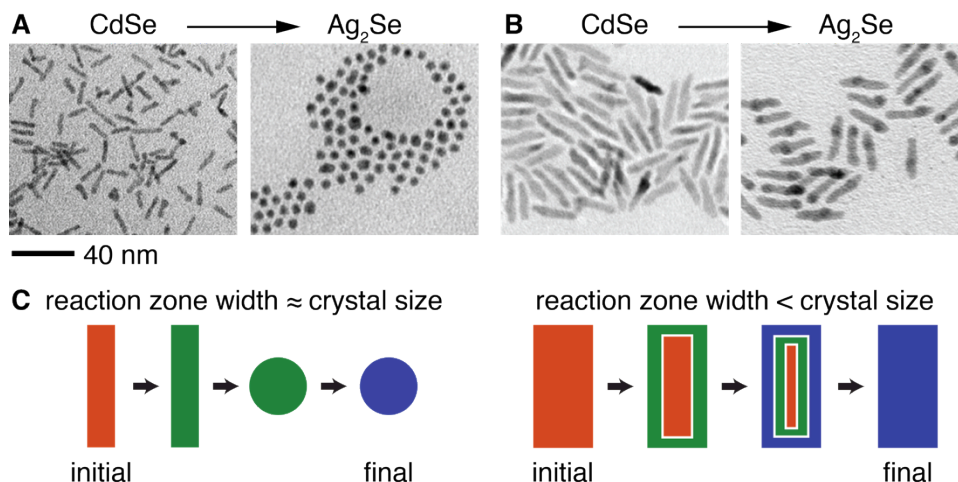
Figure 1.2. Effect of reaction zone size on morphology retention. TEM images of CdSe nanorods and the product Ag_2Se nanocrystals for (A) small diameter nanorods in which the reaction zone is comparable to the crystallite dimensions and (B) large diameter nanorods in which the reaction zone is significantly smaller than the crystallite dimensions. (C) Schematic of size dependent morphology changes during the CdSe to Ag_2Se exchange reaction. Orange and blue colors indicate the regions of initial reactant and final product phase, respectively. The green region indicates the reaction zone. Adapted with permission from ref. 7, copyright 2005 AAAS.

While cation exchanges can be executed for material systems with very high volume changes, in the extreme limit, crystallite size is a key determinant of morphology retention. This was directly investigated in the case of ion exchange from cadmium to platinum and palladium chalcogenides, $CdE \rightarrow Pt_xE_y$, P_xdE_y, (E = S, Se, Te).[19] For each chalcogenide, this exchange reaction is accompanied by a substantial contraction of the unit cell volume ($\Delta V/V \sim -30\%$). By comparison, the canonical $CdSe \rightarrow Ag_2Se$ exchange results in a <1% change in the unit cell volume ($\Delta V/V$ <1%). The ability of the host lattice to accommodate large volume changes is highly dependent on crystallite size. Small spherical nanocrystals conserved their original morphology and transformed into a kinetically frozen metastable state until thermally annealed. However, the additional stress accumulated in larger spherical particles and anisotropic rod structures reached a critical point such that void formation or fragmentation occurred during the exchange to relieve stress due to the extreme lattice mismatch.

The above examples showcase the endpoint structures that result from cation exchange. On the pathways towards these products, the interfacial thermodynamics of the reaction front define the structures of alloy intermediates. By directly probing the alloy structures that result from partial ion substitution in a nanocrystal host, mechanistic insights into the site selectivity of initiation and propagation of the reaction front have been revealed.

Cation exchanges of CdS nanorods with fast diffusing monovalent ions (Cu^+, Ag^+) provide a clear example of the unique nature of the initiation and propagation of cation

exchange reactions amongst nanocrystals.[30,31,32] As these reactions are highly exergonic at room temperature and exhibit facile kinetics,[33] the extent of reaction can be easily controlled by introducing sub-stoichiometric amounts of the substituting ion. Since CdS is largely immiscible with Ag_2S and Cu_2S,[34,35] incomplete exchange of CdS with Cu^+ or Ag^+ will lead to phase segregated CdS-Cu_2S and CdS-Ag_2S alloy structures. However, the heterostructures produced during incomplete exchange are remarkably different for copper vs. silver (Figure 1.3 A-D), highlighting the disparate interfacial formation energetics of the two systems. These differential energetics include contributions from the chemical formation energies at each heterophase junction and lattice strain contributions arising from epitaxial mismatch.

The chemical formation energy, reflecting the strength of the Cd-S-Ag bond, is negative for the Ag_2S-CdS interfaces.[31] Thus, for Ag^+ exchange of CdS nanorods, low Ag^+ concentration leads to the nonselective nucleation of Ag_2S islands embedded along the periphery of the CdS nanorod, showing no preference for nucleation at specific facets (Figure 1.3A). However, epitaxy of the orthorhombic Ag_2S and wurtzite CdS phases requires a 4% expansion of the Ag_2S lattice along the plane of the interface and a 15% contraction perpendicular to it, adding an elastic strain energy contribution to the formation energy.[30,32] As the Ag^+ exchange progresses, these Ag_2S islands begin to grow, increasing the elastic strain in the Ag_2S segments. Eventually, the elastic strain results in a positive total interfacial formation energy of the Ag_2S-CdS segments, causing the larger Ag_2S islands to absorb the smaller ones by Ostwald ripening, facilitated by the high diffusivity of the Ag^+. Once the Ag_2S segments have spanned the diameter of the CdS rod, the Ag_2S-CdS regions spontaneously self order due to the elastic repulsion between neighboring segments of Ag_2S arising from the lattice-mismatch-induced strain field (Figure 1.3B).[30,31,32] Upon addition of more Ag^+, the Ag_2S segments become larger until the entire CdS structure has been transformed into Ag_2S.

In contrast, positive chemical interface formation energies of Cu_2S-CdS and small elastic contributions from nearly identical sulfur sublattices, leads to a strongly facet dependent exchange of CdS nanorods with Cu^+ (Figure 1.3C, D).[31] Epitaxial chemical formation energy calculations show that Cu_2S attachment to the $(000\bar{1})$ facet of CdS, parallel to the rod cross-section, leads to the lowest energy interface, whereas attachment to the opposing (0001) facet entails a 2.5 times larger energy penalty. These unfavorable interface energies dictate that interfacial surface area is minimized and aligned perpendicular to the long axis of the CdS rod. In agreement, at low Cu^+ concentration, nucleation of Cu_2S appears at the $(000\bar{1})$ end facet of the CdS rod, forming a Cu_2S-CdS interface parallel to the rod cross-section. As the Cu^+ exchange progresses with the addition of Cu^+, this interface continues to propagate along the length of the rod while maintaining its orientation. At even higher Cu^+ concentration, the nucleation of Cu_2S on the opposite end of the rod ((0001) CdS) begins and progresses, though these two Cu_2S region maintain high asymmetry, consistent with the difference in formation energies of these two interfaces (Figure 1.3D). These Cu_2S regions continue to propagate until they meet and the entire rod has been exchanged.
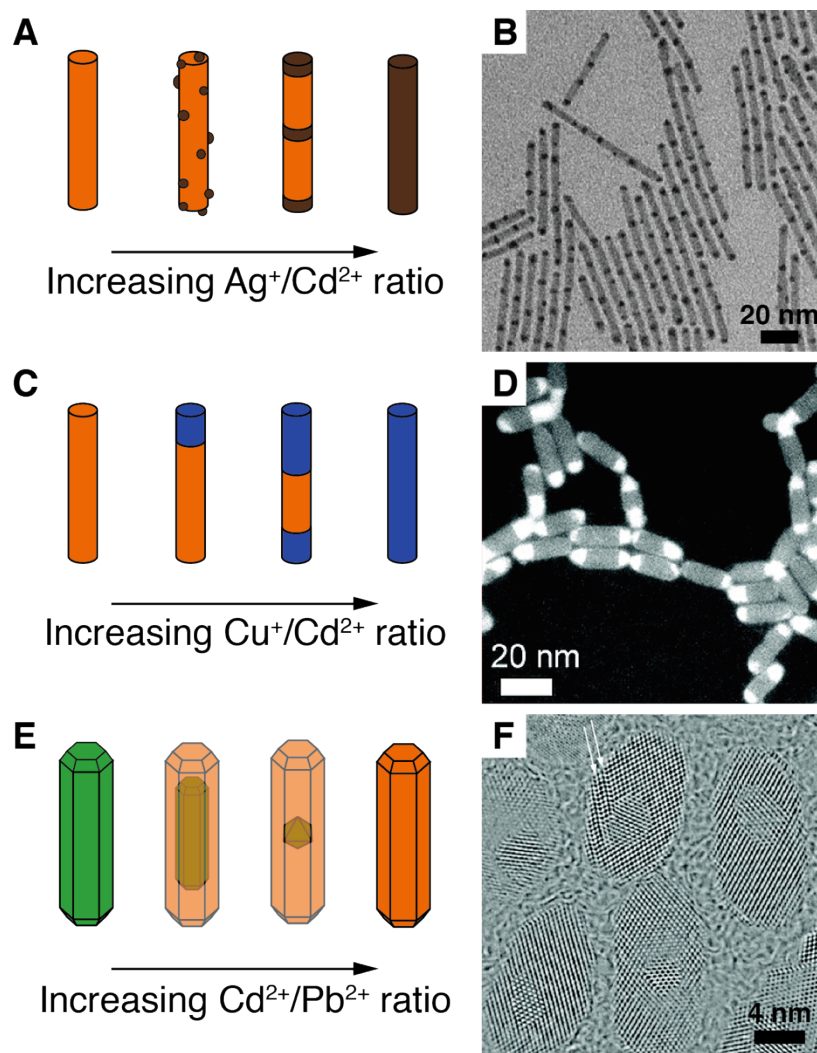
Figure 1.3. Progression of cation exchange reaction for various materials. (A) Schematic of the progressive exchange of CdS nanorods with Ag^+. (B) TEM image of CdS-Ag_2S nanorods formed from partial Ag^+ exchange displaying superlattices. Adapted with permission from ref. 30, copyright 2007 AAAS. (C) Schematic of the progressive exchange of CdS nanorods with increasing Cu^+ concentration. (D) Cu energy filtered TEM image of CdS-Cu_2S binary nanorods. The bright regions in the images correspond to Cu_2S and the gray regions correspond to the CdS portions of the nanorods. Adapted with permission from ref. 31, copyright 2009 American Chemical Society. (E) Schematic of the progressive exchange of PbSe nanorods with increasing Cd^{2+} concentration. (F) High resolution TEM images of PbSe nanorods at intermediate stage of Cd^{2+} exchange, displaying rock salt PbSe dots embedded in a zinc blende CdSe rod. Adapted with permission from ref. 37, copyright 2012 American Chemical Society.

The propagation of the reaction front can also be observed in the isovalent exchange of PbE→CdE (E = S, Se, Te).[36] In contrast to Ag^+ and Cu^+ exchange reactions of CdE, this reaction exhibits a larger activation barrier, permitting facile control over reaction

progress by incrementally adjusting the reaction temperature. The partial conversion of PbSe→CdSe on faceted PbSe nanocrystals including cubes, stars, and rods displayed similar progression of exchange, implying that this conversion is not preferentially nucleated by selective adsorption of the Cd at specific facets.[37] However, similar to the Cu^+ exchange, the propagation of the Cd^{2+} exchange appears to be strongly facet dependent, proceeding in a strongly anisotropic <111> direction, leading to the formation of primarily {111} interfaces between the zinc blende CdSe and rock salt PbSe (Figure 1.3E, F).[37,38,39] As each {111} layer consists of only Cd, Pb, or Se, a sharp interface boundary between these immiscible phases may be achieved by propagation along the <111> direction. The highly anisotropic nature of this reaction leads to the formation of octahedral cores of PbSe within a CdSe rod when subject to partial ion exchange.

Relative to their bulk crystalline analogues, the reduced volume of nanoscale materials significantly relaxes the kinetic demands of solid-state diffusion. For example, using bulk diffusion coefficients,[17] Ag^+, Cu^+, and Au^+ ions can diffuse the entire length of a 5 nm diameter InAs crystal in less than a second at ambient temperature.[40,41] Thus, the diffusion mediated propagation of the reaction zone may no longer be rate limiting for many nanoscale cation exchange reactions.[7] Indeed, time-resolved micro-X-ray absorption spectroscopy (XAS) and stopped flow absorption measurements of the topotaxial Ag^+ exchange of 3.5 nm CdSe nanocrystals indicates rapid conversion ($t_{1/2}$ < 100 ms), a strong dependence on the concentration of the coordinating ligand, and second order kinetics consistent with a rate-limiting surface reaction step.[33] The short time scale and low activation energy (estimated to be 5 kcal mol^{-1}) emphasize the dramatically accelerated kinetics on the nanoscale. While a detailed mechanistic understanding of nanoscale cation exchange reactions awaits further study, the evidence accumulated thus far suggests that the reactions bear more kinetic resemblance to transmetallation reactions of molecular coordination complexes than bulk solid-state transformations. As anticipated, the kinetics of ion exchange transition from molecular-like to bulk-like behavior as the crystallite size increases. This transition has been observed for 30 nm diameter CdSe nanowires that exhibit solid-state diffusion limited kinetics for Ag^+ substitution.[42]

The isovalent exchange of PbE→CdE (E = S, Se, Te)[36] appears to exhibit a significantly larger activation energy than the Ag^+ exchange. The reaction is self-limiting, forming a shell of the exchanged material, which serves to impede further ion substitution. The reaction rate appears to follow typical Arrhenius behavior for a temperature dependent activation process. These strongly temperature dependent kinetics, as well as the layer-by-layer nature of the exchange (see above) imply a vacancy assisted diffusion mechanism.[37,38]

1.5 Synthetic Versatility of Cation Exchange

Recent advances in colloidal nanoparticle synthesis have provided access to a vast library of high quality monodisperse semiconductor, metal, and metal oxide nanocrystals, with

exquisite control of size and morphology.[3,43,44] By in large, these nanocrystals have been prepared by a hot-injection synthesis from molecular precursors, wherein delicate control over precursor decomposition kinetics, nanocrystal nucleation and growth rates, and surfactant binding energies are required to achieve size and shape control.[2,3] This is especially true for the synthesis of morphologically anisotropic nanoparticles which rely heavily on facet-selective surfactant binding[43,45] and precise control over crystallographic polymorphism.[44] No general rules exist for achieving this across broad classes of materials. Thus, despite the exquisite size and shape control accessible for certain materials systems via hot-injection methods, such as II-VI semiconductors, there remain large classes of nanomaterials for which morphology-controlled syntheses remain elusive.

Cation exchange is a powerful tool for circumventing many of these challenges because morphological well-defined nanocrystals, prepared by traditional hot-injection methods, can be used as anion templates for the preparation of compositionally diverse pure and alloy phases that would be inaccessible by direct methods. In this section, we review recent applications of cation exchange to synthesize covalent phases, meta-stable nanostructures, multi-component alloys, and doped nanocrystals that are all inaccessible by direct synthetic methods. We conclude with examples in which cation exchange is combined in-situ with hot-injection strategies to generate complex nanomaterials in a simple, one-pot procedure.

1.5.1 Synthesis of Covalent Nanocrystal Phases

Whereas numerous direct synthetic methods exist for accessing monodisperse II-VI semiconductor nanocrystals, hot-injection syntheses of III-V nanocrystals fail to generate nanoparticles with narrow size dispersity and high crystallinity. Unlike their II-VI analogs, III-V semiconductors exhibit highly covalent lattices, requiring relatively high temperatures to access crystalline materials. However, the molecular precursors available for the direct synthesis of III-V nanocrystals decompose rapidly at low temperature. Thus, it has proven difficult to balance high precursor reactivity with high crystallization temperatures to achieve sufficient temporal separation of nucleation and growth, a key requirement for the synthesis of monodisperse nanoparticles.[46] Indeed, mechanistic studies indicate rapid depletion of molecular precursors during III-V syntheses mandating that growth occurs via Ostwald ripening and gives rise to broad size distributions.[47]

Cation exchange methods have proven invaluable for overcoming this obstacle and have enabled the synthesis of monodisperse III-V nanocrystals including GaP and GaAs.[48] Utilizing monodisperse Cd_3As_2 and Cd_3P_2 nanocrystals as host anion lattices, III-V nanocrystals can be obtained by treatment with group 13 ions (In^{3+} or Ga^{3+}) at elevated temperature. The difference in lattice energy provides sufficient driving force for the conversion of $Cd_3E_2 \rightarrow GaE$, InE (E = P, As) while maintaining a narrow size distribution. This example illustrates the versatility of cation exchange for accessing monodisperse nanomaterials recalcitrant to traditional hot-injection methods.

1.5.2 Synthesis of Meta-Stable Nanocrystals

The mild reaction conditions attendant to most cation exchange reactions enables the synthesis of non-equilibrium crystal morphologies inaccessible by direct hot-injection methods. As highlighted above, kinetically controlled morphologies including rods and tetrapods can be readily prepared among the cadmium chalcogenides and post-synthetically converted into silver or copper chalcogenides with excellent morphology retention by exposure to Ag^+ or Cu^+-containing solutions at room temperature.[7,31] Through preferential ligation of tri-alkyl phosphines to soft Ag^+ and Cu^+ ion, subsequent exchanges with Pb^{2+} or Zn^{2+} can be used to further extend these complex morphologies to the lead and zinc chalcogenides (Figure 1.4).[26,27] This cation exchange strategy, therefore comprises a simple three-step synthetic route to anisotropic nanorod morphologies of isotropic crystal phases, such as rock salt PbS.[27]

Since cation exchange is a low-temperature, template-based synthetic method, it is well suited to the preparation of kinetically trapped, meta-stable crystal phases. The sequential exchange of CdSe→Cu_2Se→ZnSe nanocrystals transferred not only the size and shape of the parent nanocrystal but the crystal structure as well (Figure 1.4).[26] Wurtzite CdSe was transformed to a metastable hexagonal close packed (HCP) phase of Cu_2Se by Cu^+ exchange and subsequent exchange with Zn^{2+} yielded nanocrystals of ZnSe in the pure HCP phase. These examples illustrate that, in certain cases, the anion host lattice remains sufficiently rigid to template meta-stable product nanostructures with excellent crystallographic and morphological fidelity, independent of cation composition.

1.5.3 Synthesis of Alloy Nanocrystals

Exchange reactions in which only a fraction of the cations in the host lattice are replaced permit incremental compositional control and convenient access to both solid solutions and phase segregated alloy nanocrystals. As II-VI compounds are known to form solid solutions with other group 12 ions,[11] partial exchange of II-VI nanocrystals with Cd^{2+}, Zn^{2+}, or Hg^{2+} can be used to form homogenously alloyed nanocrystals of constant morphology. This has enabled the investigation of the electronic structure of the nanocrystal as a function of composition at constant size. For instance, Hg^{2+} exchange of CdTe nanocrystals produces $Hg_xCd_{1-x}Te$ nanocrystals with incrementally tunable Hg content from 0-60% (x=0-0.6).[49] The similar lattice parameters but distinct band gaps of CdTe and HgTe allow the absorption and fluorescence of the nanocrystals to be smoothly varied from the visible to near infrared (NIR) by increasing the extent of Hg^{2+} substitution. Similarly, cation exchange induced alloying has been used to form ternary, $Cd_xZn_{1-x}Se$,[50] and quaternary, Cu-In-Zn-S,[51] chalcogenide nanocrystals.
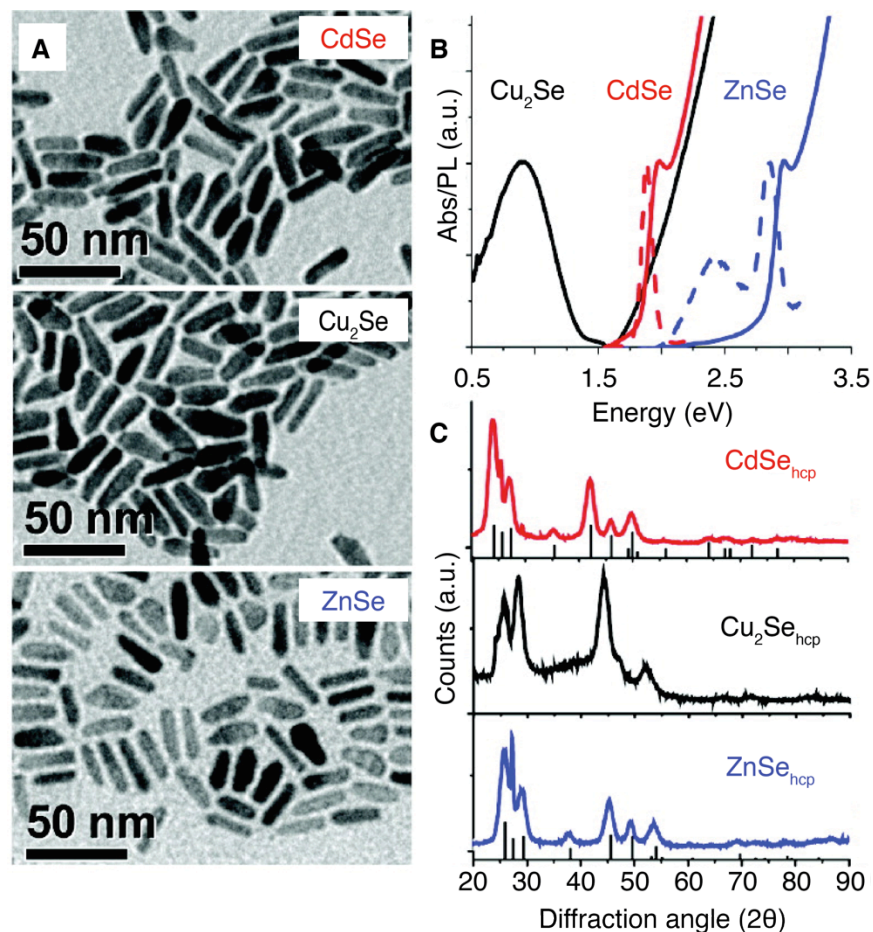
Figure 1.4. Meta-stable structures produced by cation exchange. (A) TEM images of CdSe, Cu$_2$Se, and ZnSe nanorods and their corresponding (B) optical absorption/emission spectra and (C) XRD patterns. The morphology and crystal structure of the initial CdSe template is transferred to the Cu$_2$Se and ZnSe product nanocrystals. Adapted with permission from ref. 26, copyright 2011 American Chemical Society.

Cation exchange methods are also well suited to the synthesis of phase-segregated alloy nanostructures, also known as nanoheterostructures.[52] A wide array of nanoheterostructures[53-57] have been synthesized by hot-injection methods and these syntheses principally rely on seeded growth, in which a nanoparticle serves to induce the heterogeneous nucleation of the product phase, giving rise to a multi-component product containing two or more phases in direct contact with each other.[52] Seeded growth protocols require exceptionally well-tuned precursor decomposition and growth kinetics to prevent parasitic homogeneous nucleation of the second phase and Ostwald ripening of the seed particles during the reaction.[36,52] Additionally, seeded growth protocol often require registry between the lattices of the two materials to encourage efficient heterogeneous nucleation.[52]

Cation exchange provides an alternative approach for the formation of nanoheterostructures. At the most elementary level, complete cation exchange of a nanoparticle containing two anion sublattices can yield novel heterostructures difficult to access by direct synthetic methods. This has been demonstrated in the case of CdSe/CdS seeded rods, a unique class of heterostructures, in which the band alignment of the selenide and sulfide phases and the wavelength of emission can be tuned simply by changing the size of the CdSe seed.[56,57] Remarkably, treatment of CdSe/CdS heterostructures with Cu^+ generates Cu_2Se/Cu_2S heterostructures in which the anion sublattice has been largely undisturbed.[29,58] Subsequent treatment with Pb^{2+} or Zn^{2+} generates PbSe/PbS[29] and ZnSe/ZnS[58] seeded rods, respectively, providing opportunities for band engineering in the NIR and UV-blue region. Despite the low temperatures of these exchange reactions, the product nanoheterostructures are of high optical quality.[59]

Nanocrystals possessing a single anion host lattice can also serve as synthons for the preparation of nanoheterostructures via cation exchange. Provided that reactant and product phases are immiscible, partial cation exchange of a single-phase nanocrystal can generate a heterostructured product. This strategy affords significant advantages relative to traditional seeded growth methods because it obviates any complications that may arise from homogeneous nucleation of the product phase. As discussed above, the interfacial energetics of the two co-existing phases dictate the propagation of the reaction zone, leading to various structural intermediates over the course of a cation exchange reaction. By choosing a starting nanocrystal of appropriate composition, morphology, and crystal structure, various novel heterostructures can be readily synthesized via incomplete cation exchange.

For example, partial Cd^{2+} exchange of spherical PbE (E = S, Se, Te) forms PbE/CdE core-shell nanocrystals displaying a type-I structure, improving their optoelectronic performance and environmental stability.[36] The mild conditions required for this surface cation exchange reaction enables the formation of PbE/CdE core/shell nanocrystals with negligible ripening of the seed particle, a common complication associated with traditional overcoating procedures of PbE. As the substitution of Pb^{2+} with Cd^{2+} is thermally activated, the thickness of the CdE shell can be controlled by varying the reaction temperature. The cubic phase of the parent PbE is bestowed upon the CdE shell with high fidelity during the exchange, resulting in a core-shell structure with a small lattice mismatch.

The anisotropic nature (see above) of many cation exchange reactions can be utilized to generate diverse nanoheterostructures when partial exchanges are applied to anisotropic nanoparticles. As described above, the partial Cu^+ exchange of CdS nanorods leads to highly asymmetric binary Cu_2S-CdS heterostructures.[31] Performing the Cu^+ exchange on self assembled, aligned CdS nanorods can be used to further increase the asymmetry of this exchange, forming nanorods with a single interface Cu_2S-CdS primed for directional charge separation and extraction.[60] Likewise, binary nanorod superlattices can be formed by partial Ag^+ exchange of CdS nanorods[30] and these complex heterostructure morphologies can be further elaborated to generate divalent metal chalcogenide superlattices via two sequential ion substitutions.[27] Heterostructures analogous to seeded

rods but composed of two different cations within a common anion sublattice can also be synthesized via partial exchange. Due to the preference of the Cd^{2+} exchange of lead chalcogenides to progress along the <111> direction, partial Cd^{2+} exchange of anisotropic PbS or PbSe rods form PbE-CdE (E = S, Se) single and multiple dot-in-rod heterostructures,[37,61] which are practically impossible to access by conventional hot-injection synthesis methods.

The common requirement for hetero-epitaxy during traditional seeded growth is relaxed considerably for cation exchange reactions. Indeed, single crystalline semiconductor shells can be formed around metal cores through nonepitaxial growth.[62] For example, the large lattice mismatch between CdS and Au (43%) would preclude the formation of conformal Au/CdS core/shell structures by traditional methods. However, the Cd^{2+}, Pb^{2+}, or Zn^{2+} cation exchange of amorphous, conformal Ag_2S shells surrounding Au cores generates the desired Au/CdS, Au/PbS, and Au/ZnS heterostructures, respectively, despite the fact that the metal chalcogenide shells are not in lattice registry with the gold core.

1.5.4 Synthesis of Doped Nanomaterials

The above examples illustrate the utility of quantitative and sub-stoichiometric cation exchange. At severe sub-stoichiometry, cation exchange can be used to incorporate low concentrations of defects or dopants into an otherwise pure nanocrystal host. The ability to controllably dope semiconductors with impurities allows the modulation of electronic,[63,64] optical,[65,66] and magnetic properties[67] of nanocrystals. However, development of hot-injection syntheses for the formation of impurity-doped nanocrystals has been challenging.[68] Kinetic competition between dopant inclusion and further overgrowth of the host material typically leads to much lower concentrations of dopants in the particle than in solution. Furthermore, the addition of dopants during the synthesis alters nucleation and growth kinetics, greatly complicating nanocrystal syntheses.[69,70] Post-synthetic control of doping via cation exchange is, therefore, highly desirable. As the size, shape, and quality of the nanocrystal host are retained during the exchange reaction, the influence of the impurity and its concentration on the nanocrystal's properties can be investigated in a controlled fashion. Fine-grained control over the number of impurities introduced by cation exchange can either be achieved by regulating the stoichiometry or kinetics of the ion substitution reaction.

Metal impurity doping of InAs nanocrystals was achieved by exposing InAs nanocrystals to dilute solutions of dissolved Ag, Cu, and Au salts.[41] The post-synthetic incorporation of these ions into the InAs host lattice likely occurs by substitution of In^{3+} with Au^{3+} or Ag^+ or the formation of interstitial Cu^+ ions. Using scanning tunneling spectroscopy (STS), the effects of the impurities on the electronic properties and Fermi level of the InAs nanocrystals were systematically probed (Figure 1.5). STS spectra reveal that the Fermi level and band structure remain largely unchanged upon isovalent Au^{3+} substitution. However, incorporation of interstitial Cu^+ and substitutional Ag^+ led to large

changes in the Fermi energy and the formation of mid-gap states. The creation of these mid-gap states and the associated shift in the Fermi energy suggests that ion exchange may be a promising strategy for the controlled doping of nanocrystals.
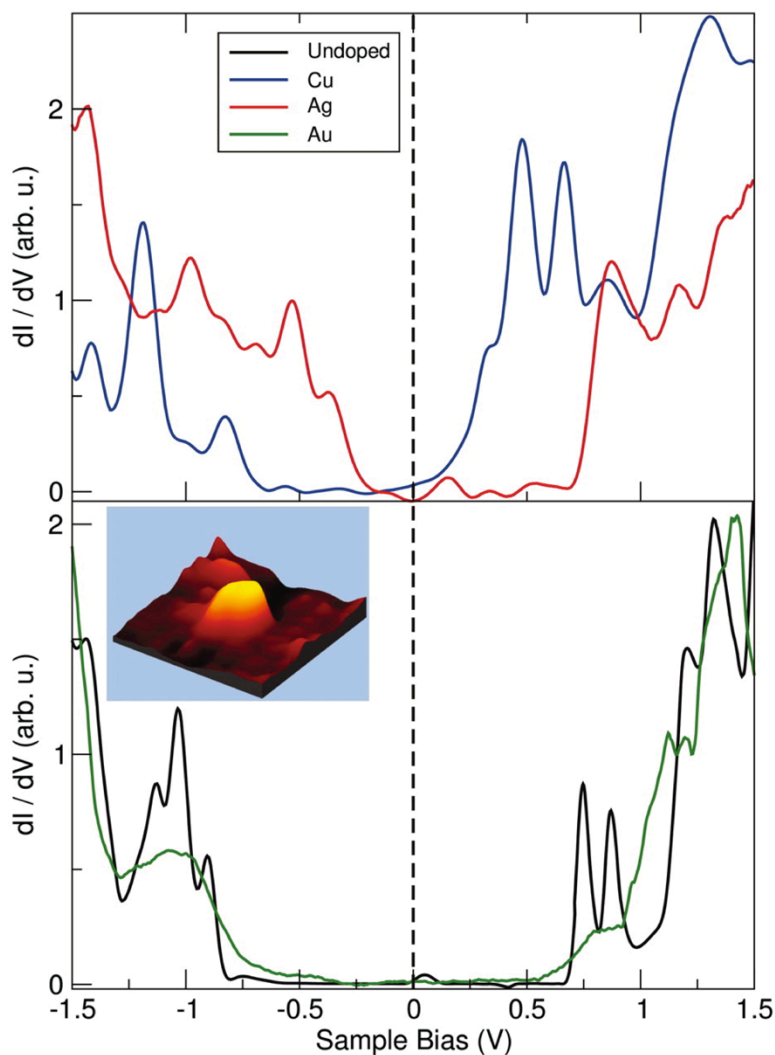
Figure 1.5. Scanning tunneling microscopy (STM) tunneling spectra of undoped (black trace), Au-doped (green trace), Cu-doped (blue trace), and Ag-doped (red trace) InAs nanocrystals, highlighting the relative shifts of the band edges in the doped samples. The inset shows an STM image of a single nanocrystal. Reproduced with permission from ref. 41, copyright 2011 AAAS.

Cation exchange has also been utilized to dope CdSe with Ag^+.[71] Utilizing conditions similar to the reverse exchange reaction from $Ag_2Se \rightarrow CdSe$, CdSe nanocrystals were exposed to Ag^+ in the presence of a large excess of a tri-alkyl phosphine. Preferential phosphine ligation to Ag^+ reduced the driving force for ion substitution, permitting the

controlled incorporation of Ag^+ impurities at concentrations as low as ~1 Ag^+ per nanocrystal. This methodology has been extended to Ag^+ doping of PbSe films, demonstrating its broad applicability to synthesizing electronically active materials.[72]

Cation exchange has also been employed to incorporate magnetically active dopants, such as Co^{2+} and Mn^{2+}. Co^{2+} doping in iron oxide nanocrystals is achieved by selective substitution of Fe^{2+} by Co^{2+}, permitting the modulation of the magnetic properties of the hematite host due to the stronger spin-orbit coupling of Co^{2+} sites.[73] The valence selectivity of this exchange reaction has been utilized to selectively dope the core of core/shell $FeO/CoFe_2O_4$ nanoparticles with Co^{2+} without modifying the Fe^{3+} containing shell. Analogously, the commonly employed magnetically active dopant, Mn^{2+}, can also be incorporated by cation exchange.[74] ZnTe magic size nanocrystals exposed to a Mn(II) precursor at elevated temperature display characteristic emission of a Mn^{2+} dopant level in a ZnTe matrix, indicating successful ion substitution.

1.5.5 In-situ Cation Exchange Syntheses

While we have, thus far, drawn stark distinctions between conventional hot-injection synthesis and cation exchange, it is important to highlight the overlap between these two methods. Clearly, the template nature of cation exchange requires robust methods, such as hot-injection synthesis, for accessing high quality nanocrystal scaffolds. However, in-situ cation exchange, in which cation exchange reactions are combined in a one-pot fashion with conventional synthetic methods, may provide better synthetic control and enable the development of novel nanocrystals. One such strategy involves applying cation exchange to generate the desired seed particles in-situ for immediate use in a subsequent growth step. In this approach, nucleation and growth can be temporally separated to achieve highly monodisperse nanocrystals. For example, a highly reactive precursor of one metal cation can efficiently nucleate nanocrystals of a different metal cation, provided rapid exchange occurs, as successfully demonstrated for the formation of monodisperse PbSe nanocrystals using the Sn(II) precursor, $Sn[N(SiMe_3)_2]$.[75] Additionally, multi-component heterostructures can be synthesized by in-situ cation exchange followed by seeded growth. The hot-injection of large cubic phase $Cu_{2-x}Se$ nanocrystals into a reaction mixture optimized for CdS growth leads to the rapid exchange of $Cu_{2-x}Se \rightarrow CdSe$ with the growth of CdS shells nucleated by the newly-formed CdSe seed particles.[76] The particular habit of the $Cu_{2-x}Se$ seed is transferred to the CdSe seed upon exchange, leading to the nucleation of octagonally symmetric CdS arms, resulting in unique CdSe/CdS octapods.

In-situ cation exchange can further be utilized at intermediate stages of nanocrystal growth. The combination of conventional growth and conformal surface exchange can provide a method for radial engineering of nanocrystal composition using a simple one-pot method. For example, applying the surface-selective Hg^{2+} exchange of growing CdS nanocrystals leads to the formation of CdS/HgS/CdS quantum dots, colloidal nanocrystal analogs to thin film quantum well structures.[77] These surface exchanges also provide a

simple route for the creation of buffer layers to minimize lattice mismatch during overcoating procedures, preventing the formation of misfit dislocations that lead to deleterious effects on optical quality.[78] The in-situ Ga^{3+} surface exchange on InP nanocrystals alters the lattice parameter sufficiently to permit epitaxial growth of ZnS shells, yielding highly luminescent nanocrystals.[79]

1.6 Outlook

In summary, cation exchange reactions have proven to be an invaluable synthetic tool for accessing colloidal semiconductor nanocrystals of diverse composition, phase, and morphology. The ability to easily tune reaction thermodynamics via preferential ion ligation in solution has enabled nanocrystal cation exchange reactions with a great diversity of metal ions, including Ag^+,[7] Au^{3+},[41] Bi^{3+},[14] Cd^{2+},[7] Co^{2+},[73] Cu^+,[31] Cu^{2+},[7] Eu^{3+},[80] Ga^{3+},[48,79] Gd^{3+},[80] Hg^{2+},[49,77] In^{3+},[48] La^{3+},[80] Mn^{2+},[74] Pb^{2+},[25,27] Pt^{2+},[19] Pd^{2+},[19] Sb^{3+},[14] and Zn^{2+}.[25,26] Furthermore, the mild reaction conditions attendant to most exchanges makes it a particularly powerful strategy for accessing many non-equilibrium morphologies, crystal phases, and materials that are difficult to prepare by direct hot-injection methods. Control over the extent of the exchange reaction further extends the utility of cation exchange for accessing a wide variety of heterostructures and doped nanocrystals.

The continued development of cation exchange as a synthetic tool would benefit from additional studies of the fundamentals of the exchange reaction. Accurate quantification of overall reaction thermodynamics and ligand binding energies is needed to enable the rational design of nanocrystal ion exchanges spanning the periodic table. In-situ observation of reaction intermediates in nanocrystal ion exchanges would serve to clarify lingering mechanistic questions. These studies may benefit from recent advances in in-situ TEM observation in the liquid phase.[81,82] Additional studies of nanocrystal ion exchange kinetics are essential to establish a unifying mechanistic picture across a broad range of anion host lattices, exchanging ions, and ligating environments. In this regard, the influence of surface ligation and its role in inhibiting or catalyzing ion exchange reactions remains under-investigated. While cation exchange reactions have, thus far, largely focused on ionic metal chalcogenide phases, future work should expand the focus towards a broader class of nanomaterials inaccessible by direct synthetic methods.

1.7. Chapter 1 References

1.   Alivisatos, A. P. Perspectives on the Physical Chemistry of Semiconductor Nanocrystals. *J. Phys. Chem.* **1996**, *100*, 13226–13239.
2.   Yin, Y.; Alivisatos, A. P. Colloidal Nanocrystal Synthesis and the Organic–Inorganic Interface. *Nature* **2005**, *437*, 664–670.

3. Park, J.; Joo, J.; Kwon, S. G.; Jang, Y.; Hyeon, T. Synthesis of Monodisperse Spherical Nanocrystals. *Angew. Chem. Int. Ed.* **2007**, *46*, 4630–4660.

4. Talapin, D. V.; Lee, J.-S.; Kovalenko, M. V.; Shevchenko, E. V. Prospects of Colloidal Nanocrystals for Electronic and Optoelectronic Applications. *Chem. Rev.* **2010**, *110*, 389–458.

5. Han, Z.; Qiu, F.; Eisenberg, R.; Holland, P. L.; Krauss, T. D. Robust Photogeneration of H_2 in Water Using Semiconductor Nanocrystals and a Nickel Catalyst. *Science* **2012**, *338*, 1321–1324.

6. Michalet, X.; Pinaud, F. F.; Bentolila, L. A.; Tsay, J. M.; Doose, S.; Li, J. J.; Sundaresan, G.; Wu, A. M.; Gambhir, S. S.; Weiss, S. Quantum Dots for Live Cells, in Vivo Imaging, and Diagnostics. *Science* **2005**, *307*, 538–544.

7. Son, D. H.; Hughes, S. M.; Yin, Y.; Alivisatos, A. P. Cation Exchange Reactions in Ionic Nanocrystals. *Science* **2004**, *306*, 1009-1012.

8. Rivest, J. B.; Jain, P. K. Cation Exchange on the Nanoscale: An Emerging Technique for New Material Synthesis, Device Fabrication, and Chemical Sensing. *Chem. Soc. Rev.* **2013**, *42*, 89-96.

9. Putnis, A. Mineral Replacement Reactions: From Macroscopic Observations to Microscopic Mechanisms. *Mineral. Mag.* **2002**, *66*, 689–708.

10. Schmalzried, H. *Solid State Reactions*; Verlag Chemie: Weinheim, Germany, 1981.

11. Fedorov, V. A.; Ganshin, V. A.; Korkishko, Y. N. Ion Exchange in II-VI Crystals: Thermodynamics, Kinetics, and Technology. *Phys. Status Solidi A* **1993**, *139*, 9–65.

12. Osakada, K.; Yamamoto, T. Transmetallation of Alkynyl and Aryl Complexes of Group 10 Transition Metals. *Coord. Chem. Rev.* **2000**, *198*, 379–399.

13. Dloczik, L.; Engelhardt, R.; Ernst, K.; Fiechter, S.; Sieber, I.; Könenkamp, R. Hexagonal Nanotubes of ZnS by Chemical Conversion of Monocrystalline ZnO Columns. *Appl. Phys. Lett.* **2001**, *78*, 3687-3689.

14. Dloczik, L.; Könenkamp, R. Nanostructure Transfer in Semiconductors by Ion Exchange. *Nano Lett.* **2003**, *3*, 651–653.

15. Park, J.; Zheng, H.; Jun, Y.-W.; Alivisatos, A. P. Hetero-Epitaxial Anion Exchange Yields Single-Crystalline Hollow Nanoparticles. *J. Am. Chem. Soc.* **2009**, *131*, 13943–13945.

16. Yin, Y.; Rioux, R. M.; Erdonmez, C. K.; Hughes, S. M.; Somorjai, G. A.; Alivisatos, A. P. Formation of Hollow Nanocrystals Through the Nanoscale Kirkendall Effect. *Science* **2004**, *304*, 711-714.

17. Dutt, M. B.; Sharma, B. L. *3 Diffusion in Compound Semiconductors*; Beke, D. L., Ed.;SpringerMaterials—The Landolt-Börnstein Database (http://www.springermaterials.com). DOI: 10.1007/10426818_10.

18. Lokhande, C. D.; Gadave, K. M. A Simple Chemical Method for Conversion of CdS into Ag_2S and CdSe into Ag_2Se. *Mater. Chem. Phys.* **1993**, *36*, 119–123.

19. Wark, S.; Hsia, C.-H.; Son, D. H. Effects of Ion Solvation and Volume Change of the Reaction on the Equilibrium and Morphology in Cation-Exchange Reaction of Nanocrystals. *J. Am. Chem. Soc.* **2008**, *130*, 9550–9555.

20. Collaboration: Scientific Group Thermodata Europe (SGTE). *Thermodynamic Properties of Compounds*; SpringerMaterials - The Landolt-Börnstein Database http://www.springermaterials.com).

21. Vanysek, P. Electrochemical Series. In *CRC Handbook of Chemistry and Physics*, 87th ed.; Lide, D. R., Ed.; CRC Press: Boca Raton, FL, 2006; pp 8/20− 8/29.

22. Engelken, R. D.; Ali, S.; Chang, L. N.; Brinkley, C.; Turner, K.; Hester, C. Study and Development of a Generic Electrochemical Ion-Exchange Process to Form M_xS Optoelectronic Materials from ZnS Precursor Films Formed by Chemical-Precipitation Solution Deposition. *Mater. Lett.* **1990**, *10*, 264–274.

23. Chaudhry, M.; Persson, I. Transfer Thermodynamic Study on the Copper(II) Ion from Water to Methanol, Acetonitrile, Dimethyl Sulfoxide and Pyridine. *J. Chem. Soc. Faraday Trans.* **1994**, *90*, 2243-2248.

24. Pearson, R. G. Absolute Electronegativity and Hardness: Application to Inorganic Chemistry. *Inorg. Chem.* **1988**, *27*, 734–740.

25. Camargo, P. H. C.; Lee, Y. H.; Jeong, U.; Zou, Z.; Xia, Y. Cation Exchange: A Simple and Versatile Route to Inorganic Colloidal Spheres with the Same Size but Different Compositions and Properties. *Langmuir* **2007**, *23*, 2985–2992.

26. Li, H.; Zanella, M.; Genovese, A.; Povia, M.; Falqui, A.; Giannini, C.; Manna, L. Sequential Cation Exchange in Nanocrystals: Preservation of Crystal Phase and Formation of Metastable Phases. *Nano Lett.* **2011**, *11*, 4964-4970.

27. Luther, J. M.; Zheng, H.; Sadtler, B.; Alivisatos, A. P. Synthesis of PbS Nanorods and Other Ionic Nanocrystals of Complex Morphology by Sequential Cation Exchange Reactions. *J. Am. Chem. Soc.* **2009**, *131*, 16851–16857.

28. Backhaus-Ricoult, M. Solid-State Reactivity at Heterophase Interfaces. *Annu. Rev. Mater. Res.* **2003**, *33*, 55–90.

29. Jain, P. K.; Amirav, L.; Aloni, S.; Alivisatos, A. P. Nanoheterostructure Cation Exchange: Anionic Framework Conservation. *J. Am. Chem. Soc.* **2010**, *132*, 9997-9999.

30. Robinson, R. D.; Sadtler, B.; Demchenko, D. O.; Erdonmez, C. K.; Wang, L.-W.; Alivisatos, A. P. Spontaneous Superlattice Formation in Nanorods Through Partial Caiton Exchange. *Science* **2007**, *317*, 355–358.

31. Sadtler, B.; Demchenko, D. O.; Zheng, H.; Hughes, S. M.; Merkle, M. G.; Dahmen, U.; Wang, L.-W.; Alivisatos, A. P. Selective Facet Reactivity During Cation Exchange in Cadmium Sulfide Nanorods. *J. Am. Chem. Soc.* **2009**, *131*, 5285–5293.

32. Demchenko, D. O.; Robinson, R. D.; Sadtler, B.; Erdonmez, C. K.; Alivisatos, A. P.; Wang, L.-W. Formation Mechanism and Properties of CdS-Ag_2S Nanorod Superlattices. *ACS Nano* **2008**, *2*, 627–636.

33. Chan, E. M.; Marcus, M. A.; Fakra, S.; ElNaggar, M.; Mathies, R. A.; Alivisatos, A. P. Millisecond Kinetics of Nanocrystal Cation Exchange Using Microfluidic X-ray Absorption Spectroscopy. *J. Phys. Chem. A* **2007**, *111*, 12210–12215.

34. Kubaschewski O. Silver-Cadmium-Sulfur. In *Ternary Alloys: a Comprehensive Compendium of Evaluated Constitutional Data and Phase Diagrams*, Vol. 1, Petzow, G.; Effenberg, G., Eds.; VCH: Weinheim, 1988; pp 419-428.

35. Mizetskaya, I.B.; Oleinik, G.S.; Trishchuk, L.I. Phase Diagram of the Cu_2S-CdS System. *Inorg. Mater.* **1982**, *18*, 581–582.

36. Pietryga, J. M.; Werder, D. J.; Williams, D. J.; Casson, J. L.; Schaller, R. D.; Klimov, V. I.; Hollingsworth, J. A. Utilizing the Lability of Lead Selenide to Produce Heterostructured Nanocrystals with Bright, Stable Infrared Emission. *J. Am. Chem. Soc.* **2008**, *130*, 4879–4885.

37. Casavola, M.; van Huis, M. A.; Bals, S.; Lambert, K.; Hens, Z.; Vanmaekelbergh, D. Anisotropic Cation Exchange in PbSe/CdSe Core/Shell Nanocrystals of Different Geometry. *Chem. Mater.* **2012**, *24*, 294–302.

38. Bals, S.; Casavola, M.; van Huis, M. A.; Van Aert, S.; Batenburg, K. J.; Van Tendeloo, G.; Vanmaekelbergh, D. Three-Dimensional Atomic Imaging of Colloidal Core-Shell Nanocrystals. *Nano Lett.* **2011**, *11*, 3420-3424.

39. Lambert, K.; De Geyter, B.; Moreels, I.; Hens, Z. PbTe|CdTe Core|Shell by Cation Exchange, a HR-TEM Study. *Chem. Mater.* **2009**, *21*, 778–780.

40. Mokari, T.; Aharoni, A.; Popov, I.; Banin, U. Diffusion of Gold into InAs Nanocrystals. *Angew. Chem. Int. Ed.* **2006**, *45*, 8001–8005.

41. Mocatta, D.; Cohen, G.; Schattner, J.; Millo, O.; Rabani, E.; Banin, U. Heavily Doped Semiconductor Nanocrystal Quantum Dots. *Science* **2011**, *332*, 77–81.

42. Dorn, A.; Allen, P. M.; Harris, D. K.; Bawendi, M. G. In Situ Electrical Monitoring of Cation Exchange in Nanowires. *Nano Lett.* **2010**, *10*, 3948–3951.

43. Peng, X.; Manna, L.; Yang, W.; Wickham, J.; Scher, E.; Kadavanich, A.; Alivisatos, A. P. Shape Control of CdSe Nanocrystals. *Nature* **2000**, *404*, 59–61.

44. Manna, L.; Milliron, D. J.; Meisel, A.; Scher, E. C.; Alivisatos, A. P. Controlled Growth of Tetrapod-Branched Inorganic Nanocrystals. *Nat. Mater.* **2003**, *2*, 382–385.

45. Puzder, A.; Williamson, A. J.; Zaitseva, N.; Galli, G.; Manna, L.; Alivisatos, A. P. The Effect of Organic Ligand Binding on the Growth of CdSe Nanoparticles Probed by Ab Initio Calculations. *Nano Lett.* **2004**, *4*, 2361–2365.

46. Heath, J. R.; Shiang, J. J. Covalency in Semiconductor Quantum Dots. *Chem. Soc. Rev.* **1998**, *27*, 65-71.

47. Allen, P. M.; Walker, B. J.; Bawendi, M. G. Mechanistic Insights into the Formation of InP Quantum Dots. *Angew. Chem. Int. Ed.* **2009**, *49*, 760–762.

48. Beberwyck, B. J.; Alivisatos, A. P. Ion Exchange Synthesis of III-V Nanocrystals. *J. Am. Chem. Soc.* **2012**, *134*, 19977-19980.

49. Smith, A. M.; Nie, S. Bright and Compact Alloyed Quantum Dots with Broadly Tunable Near-Infrared Absorption and Fluorescence Spectra Through Mercury Cation Exchange. *J. Am. Chem. Soc.* **2011**, *133*, 24-26.

50. Zhong, X.; Feng, Y.; Zhang, Y.; Gu, Z.; Zou, L. A Facile Route to Violet- to Orange-Emitting $Cd_xZn_{1-x}Se$ Alloy Nanocrystals via Cation Exchange Reaction. *Nanotechnology* **2007**, *18*, 385606.

51. De Trizio, L.; Prato, M.; Genovese, A.; Casu, A.; Povia, M.; Simonutti, R.; Alcocer, M. J. P.; D'Andrea, C.; Tassone, F.; Manna, L. Strongly Fluorescent Quaternary Cu–In–Zn–S Nanocrystals Prepared from $Cu_{1-x}InS_2$ Nanocrystals by Partial Cation Exchange *Chem. Mater.* **2012**, *24*, 2400–2406.

52. Carbone, L.; Cozzoli, P. D. Colloidal Heterostructured Nanocrystals: Synthesis and Growth Mechanisms. *Nano Today* **2010**, *5*, 449-493.

53. Hines, M. A.; Guyot-Sionnest, P. Synthesis and Characterization of Strongly Luminescing ZnS-Capped CdSe Nanocrystals *J. Phys. Chem.* **1996**, *100*, 468–471.

54. Peng, X.; Schlamp, M. C.; Kadavanich, A. V.; Alivisatos, A. P. Epitaxial Growth of Highly Luminescent CdSe/CdS Core/Shell Nanocrystals with Photostability and Electronic Accessibility. *J. Am. Chem. Soc.* **1997**, *119*, 7019–7029.

55. Kim, S.; Fisher, B.; Eisler, H.-J.; Bawendi, M. Type-II Quantum Dots: CdTe/CdSe(Core/Shell) and CdSe/ZnTe(Core/Shell) Heterostructures. *J. Am. Chem. Soc.* **2003**, *125*, 11466–11467.

56. Talapin, D. V.; Nelson, J. H.; Shevchenko, E. V.; Aloni, S.; Sadtler, B.; Alivisatos, A. P. Seeded Growth of Highly Luminescent CdSe/CdS Nanoheterostructures with Rod and Tetrapod Morphologies. *Nano Lett.* **2007**, *7*, 2951–2959.

57. Carbone, L.; Nobile, C.; De Giorgi, M.; Sala, F. D.; Morello, G.; Pompa, P.; Hytch, M.; Snoeck, E.; Fiore, A.; Franchini, I. R.; Nadasan, M.; Silvestre, A. F.; Chiodo, L.; Kudera, S.; Cingolani, R.; Krahne, R.; Manna, L. Synthesis and Micrometer-Scale Assembly of Colloidal CdSe/CdS Nanorods Prepared by a Seeded Growth Approach. *Nano Lett.* **2007**, *7*, 2942–2950.

58. Li, H.; Brescia, R.; Krahne, R.; Bertoni, G.; Alcocer, M. J. P.; D'Andrea, C.; Scotognella, F.; Tassone, F.; Zanella, M.; De Giorgi, M.; Manna, L. Blue-UV-Emitting ZnSe(Dot)/ZnS(Rod) Core/Shell Nanocrystals Prepared from CdSe/CdS Nanocrystals by Sequential Cation Exchange. *ACS Nano* **2012**, *6*, 1637-1647.

59. Jain, P. K.; Beberwyck, B. J.; Fong, L.-K.; Polking, M. J.; Alivisatos, A. P. Highly Luminescent Nanocrystals From Removal of Impurity Atoms Residual From Ion-Exchange Synthesis. *Angew. Chem. Int. Ed.* **2012**, *51*, 2387–2390.

60. Rivest, J. B.; Swisher, S. L.; Fong, L.-K.; Zheng, H.; Alivisatos, A. P. Assembled Monolayer Nanorod Heterojunctions. *ACS Nano* **2011**, *5*, 3811-3816.

61. Justo, Y.; Goris, B.; Kamal, J. S.; Geiregat, P.; Bals, S.; Hens, Z. Multiple Dot-in-Rod PbS/CdS Heterostructures with High Photoluminescence Quantum Yield in the Near-Infrared. *J. Am. Chem. Soc.* **2012**, *134*, 5484–5487.

62. Zhang, J.; Tang, Y.; Lee, K.; Ouyang, M. Nonepitaxial Growth of Hybrid Core-Shell Nanostructures with Large Lattice Mismatches. *Science* **2010**, *327*, 1634–1638.

63. Orlinskii, S.; Schmidt, J.; Baranov, P.; Hofmann, D.; de Mello Donegá, C.; Meijerink, A. Probing the Wave Function of Shallow Li and Na Donors in ZnO Nanoparticles. *Phys. Rev. Lett.* **2004**, *92*, 047603.

64. Roy, S.; Tuinenga, C.; Fungura, F.; Dagtepe, P.; Chikan, V.; Jasinski, J. Progress Toward Producing n-Type CdSe Quantum Dots: Tin and Indium Doped CdSe Quantum Dots. *J. Phys. Chem. C* **2009**, *113*, 13008–13015.

65. Bhargava, R. N.; Gallagher, D.; Hong, X.; Nurmikko, A. Optical Properties of Manganese-Doped Nanocrystals of ZnS. *Phys. Rev. Lett.* **1994**, *72*, 416–419.

66. Pradhan, N.; Goorskey, D.; Thessing, J.; Peng, X. An Alternative of CdSe Nanocrystal Emitters: Pure and Tunable Impurity Emissions in ZnSe Nanocrystals. *J. Am. Chem. Soc.* **2005**, *127*, 17586–17587.

67. Bryan, J. D.; Gamelin, D. R. Doped Semiconductor Nanocrystals: Synthesis, Characterization, Physical Properties, and Applications. *Prog. Inorg. Chem.* **2005**, *54*, 47–126.

68. Norris, D. J.; Efros, A. L.; Erwin, S. C. Doped Nanocrystals. *Science* **2008**, *319*, 1776-1779.

69. Tuinenga, C.; Jasinski, J.; Iwamoto, T.; Chikan, V. In Situ Observation of Heterogeneous Growth of CdSe Quantum Dots: Effect of Indium Doping on the Growth Kinetics. *ACS Nano* **2008**, *2*, 1411–1421.

70. Beulac, R.; Ochsenbein, S. T.; Gamelin, D. R. Colloidal Transition-Metal-Doped Quantum Dots. In *Nanocrystal Quantum Dots*; Klimov, V. I., Ed.; CRC Press: Boca Raton, FL, 2010; p397-453.

71. Sahu, A.; Kang, M. S.; Kompch, A.; Notthoff, C.; Wills, A. W.; Deng, D.; Winterer, M.; Frisbie, C. D.; Norris, D. J. Electronic Impurity Doping in CdSe Nanocrystals. *Nano Lett.* **2012**, *12*, 2587–2594.

72. Kang, M. S.; Sahu, A.; Frisbie, C. D.; Norris, D. J. Influence of Silver Doping on Electron Transport in Thin Films of PbSe Nanocrystals. *Adv. Mater.* **2012**, *25*, 725–731.

73. Sytnyk, M.; Kirchschlager, R.; Bodnarchuk, M. I.; Primetzhofer, D.; Kriegner, D.; Enser, H.; Stangl, J.; Bauer, P.; Voith, M.; Hassel, A. W.; Krumeich, F.; Ludwig, F.; Meingast, A.; Kothleitner, G.; Kovalenko, M. V.; Heiss, W. Tuning the Magnetic Properties of Metal Oxide Nanocrystal Heterostructures by Cation Exchange. *Nano Lett.* **2013**, *13*, 586–593.

74. Eilers, J.; Groeneveld, E.; de Mello Donegá, C.; Meijerink, A. Optical Properties of Mn-Doped ZnTe Magic Size Nanocrystals. *J. Phys. Chem. Lett.* **2012**, *3*, 1663–1667.

75. Kovalenko, M. V.; Talapin, D. V.; Loi, M. A.; Cordella, F.; Hesser, G.; Bodnarchuk, M. I.; Heiss, W. Quasi-Seeded Growth of Ligand-Tailored PbSe Nanocrystals Through Cation-Exchange-Mediated Nucleation. *Angew. Chem. Int. Ed.* **2008**, *47*, 3029–3033.

76. Deka, S.; Miszta, K.; Dorfs, D.; Genovese, A.; Bertoni, G.; Manna, L. Octapod-Shaped Colloidal Nanocrystals of Cadmium Chalcogenides via "One-Pot" Cation Exchange and Seeded Growth. *Nano Lett.* **2010**, *10*, 3770–3776.

77. Mews, A.; Eychmüller, A.; Giersig, M.; Schooss, D.; Weller, H. Preparation, Characterization, and Photophysics of the Quantum Dot Quantum Well System CdS/HgS/CdS. *J. Phys. Chem.* **1994**, *98*, 934–941.

78. Dabbousi, B. O.; Rodriguez-Viejo, J.; Mikulec, F. V.; Heine, J. R.; Mattoussi, H.; Ober, R.; Jensen K. F.; Bawendi, M. G. (CdSe)ZnS Core−Shell Quantum Dots: Synthesis and Characterization of a Size Series of Highly Luminescent Nanocrystallites. *J. Phys. Chem. B* **1997**, *101*, 9463–9475.

79. Kim, S.; Kim, T.; Kang, M.; Kwak, S. K.; Yoo, T. W.; Park, L. S.; Yang, I.; Hwang, S.; Lee, J. E.; Kim, S. K.; Kim, S.-W. Highly Luminescent InP/GaP/ZnS

Nanocrystals and Their Application to White Light-Emitting Diodes. *J. Am. Chem. Soc.* **2012**, *134*, 3804-3809.

80. Dong, C.; van Veggel, F. C. J. M. Cation Exchange in Lanthanide Fluoride Nanoparticles. *ACS Nano* **2008**, *3*, 123–130.

81. Zheng, H.; Smith, R. K.; Jun, Y.-W.; Kisielowski, C.; Dahmen, U.; Alivisatos, A. P. Observation of Single Colloidal Platinum Nanocrystal Growth Trajectories. *Science* **2009**, *324*, 1309–1312.

82. Yuk, J. M.; Park, J.; Ercius, P.; Kim, K.; Hellebusch, D. J.; Crommie, M. F.; Lee, J. Y.; Zettl, A.; Alivisatos, A. P. High-Resolution EM of Colloidal Nanocrystal Growth Using Graphene Liquid Cells. *Science* **2012**, *336*, 61–64.

Chapter 2.

Highly Luminescent Nanocrystals from Removal of Impurity Atoms Residual from Ion Exchange Synthesis

Ion exchange of semiconductor nanocrystals, while promising for synthesizing otherwise inaccessible quantum heterostructures, yields materials with poor optoelectronic properties, most manifestly their photoluminescence quantum yields. We trace the cause of the low quantum yield of ion-exchange-obtained nanocrystals to impurities at the level of few atoms per nanocrystal. Cation-exchanged nanostructures, however, can be purified of such detrimental impurities post exchange, resulting in materials with quantum yields up to 400-fold enhanced and approaching the superior quality of nanocrystals made from hot injection. Impurity purification enables practical utilization of ion exchange for developing functional quantum heterostructures and may be generalizable to other nanostructure fabrication methods that yield impure samples.

2.1 Optical Quality of Nanocrystal Heterostructures Produced by Ion Exchange

Ion exchange of nanocrystals has the potential to emerge as an alternative to conventional routes for synthesis of ionic nanocrystals.[1-9] The facile ability to replace all cations of a nanocrystal with another cation, while preserving size and shape, allows one to employ nanocrystals as templates for the fabrication of other nanocrystals of interest.[6] Such a templated synthesis strategy is especially useful where the chemistry or crystallographic phase of the target nanocrystals is difficult to access via hot-injection methods. For instance, we recently showed[10] that Cu(I) sulfide quantum dots prepared via hot-injection mostly result in the highly Cu-deficient djurleite phase.[11,12] The stoichiometric chalcocite phase is achievable, however, via room-temperature cation exchange of template CdS quantum dots with Cu^+.

Cation exchange holds particular promise for the fabrication of multicomponent heterostructured nanocrystals,[6,9] which allow independent tunability of electron and hole wavefunctions, but present potential synthetic challenges due to their greater structural complexity. Here, it is advantageous that the anionic framework of the heterostructure is maintained during cation exchange, allowing structural preservation of interfaces and junctions that define the electronic band alignment within the heterostructure. This has

made possible the design and templated fabrication of novel semiconductor heterostructures that can range[13,14] from type-I, with high quantum yield emission useful for imaging and light-emitting diodes,[15,16] to type-II, which allow charge separation for photovoltaic and photocatalytic applications.[9,17]

However, the ion exchange technique has been found to present a severe drawback: it results in nanocrystals with poor optoelectronic properties.[1] This is clear from a quantitative comparison of the optical properties of nanocrystals obtained from cation exchange with those prepared via standard hot-injection for the model CdSe/CdS dot/rod heterostructure.[13-141516] In this work, we trace the cause of the poor optical properties of cation-exchange-obtained nanocrystals to chemical impurities on the few atom per nanocrystal level. We have also found a method to purify the nanocrystals of these detrimental impurities post exchange and achieve optical properties comparable to those of hot-injection synthesized nanocrystals.

2.2 Characterization of Cation Exchanged Products

Hot-injection synthesis of CdSe/CdS dot/rods with a 3.9-nm dot yields highly photoluminescent (PL) nanorods with a quantum yield (QY) of over 55%, enabled by the type-I band-alignment. On the other hand, CdSe/CdS dot/rods obtained from the room-temperature exchange of Cu_2Se/Cu_2S dot/rods with Cd^{2+} (see Appendix for methods) exhibit relatively negligible emission, i.e., QY of 0.07%, almost 3 orders of magnitude smaller. This is despite the fact that the nanorods prepared by the two methods possess similar heterostructure morphologies, especially seed sizes, and consequently identical excitonic structures, as evidenced by the similarity of their absorption and PL spectra (Figure 2.1). The QY of emission is a useful optical probe of sample quality.[18] The insubstantial PL yield of the cation-exchanged samples is likely due to their poor crystallographic quality: cation exchange yields nanocrystals with a relatively high density of defect sites for non-radiative carrier recombination.

Optical and structural characterization of the cation-exchanged nanocrystals elucidated the presence of a variety of crystallographic defects, some or all of which may be responsible for the high rate of non-radiative carrier recombination. High-resolution transmission electron microscopy (HRTEM) of the cation-exchanged rods shows the presence of zinc blende regions and associated stacking faults, as well as grain boundaries, absent in the hot-injection-synthesized nanorods, further supported by X-ray diffraction (XRD) (Figure 2.2) and previous evidence from Son et al.[1] It has also been suggested that cation exchange results in poorly passivated nanocrystal surfaces, which may enhance the surface trapping of carriers.[1] However, for our model type-I heterojunction system, the detrimental effect of a poorly passivated surface on the PL is expected to be much smaller than that observed here due to the excitonic confinement within the CdSe dot. This implies that the surface is an unlikely contributor to the PL deterioration. However, the interface between the dot and rod may itself have a defective
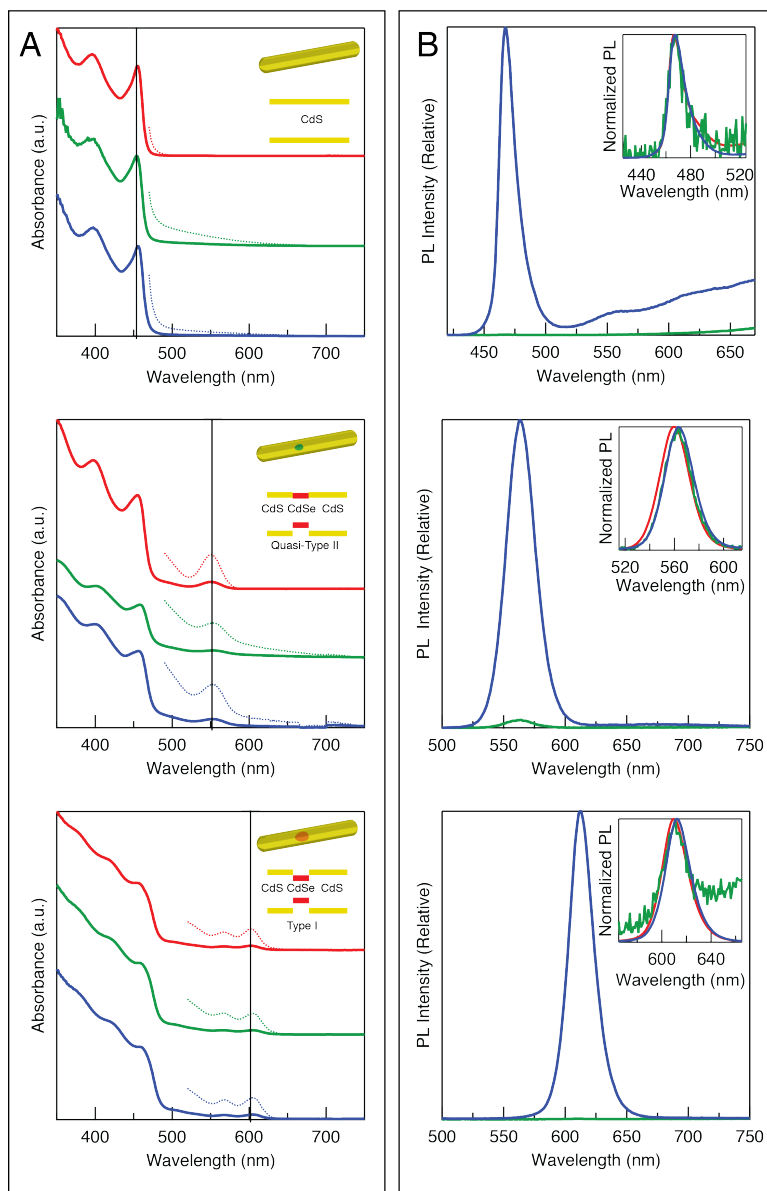
Figure 2.1. Impact of ion exchange on the optical properties of nanoheterostructures. (A) Absorbance and (B) photoluminescence (PL) spectra of CdS nanorods (top), CdSe/CdS dot/rods with a 2.5-nm dot (middle), and CdSe/CdS dot/rods with a 3.9-nm dot (bottom) obtained from hot-injection (red), cation exchange (green), and post-exchange purification (blue). Dotted line shows the magnified (x5) absorption spectrum highlighting the absorption of the dot. Vertical black line in the left panel graphs indicates the peak position of the lowest exciton showing the similarity in excitonic structure for nanorod samples obtained from the three methods. (Inset of A) Model of nanorod heterostructure and its band alignment. (Inset of B) Normalized PL showing similarity in PL peak positions between samples obtained from the three different methods. All PL spectra were corrected for absorbed intensity at the excitation wavelength and for self-absorption at the emission wavelength. Corrected PL spectra following integration show that the PL yield was enhanced 363-fold (top), 35-fold (middle), and 413-fold (bottom) respectively upon defect purification.

or strained epitaxy, serving as a strong channel for carrier dissipation. Yet another possibility is the presence of Cu impurities remnant from the cation exchange process, the likelihood of which is supported by the common occurrence of Cu doping in CdS and CdSe materials.[19-22]
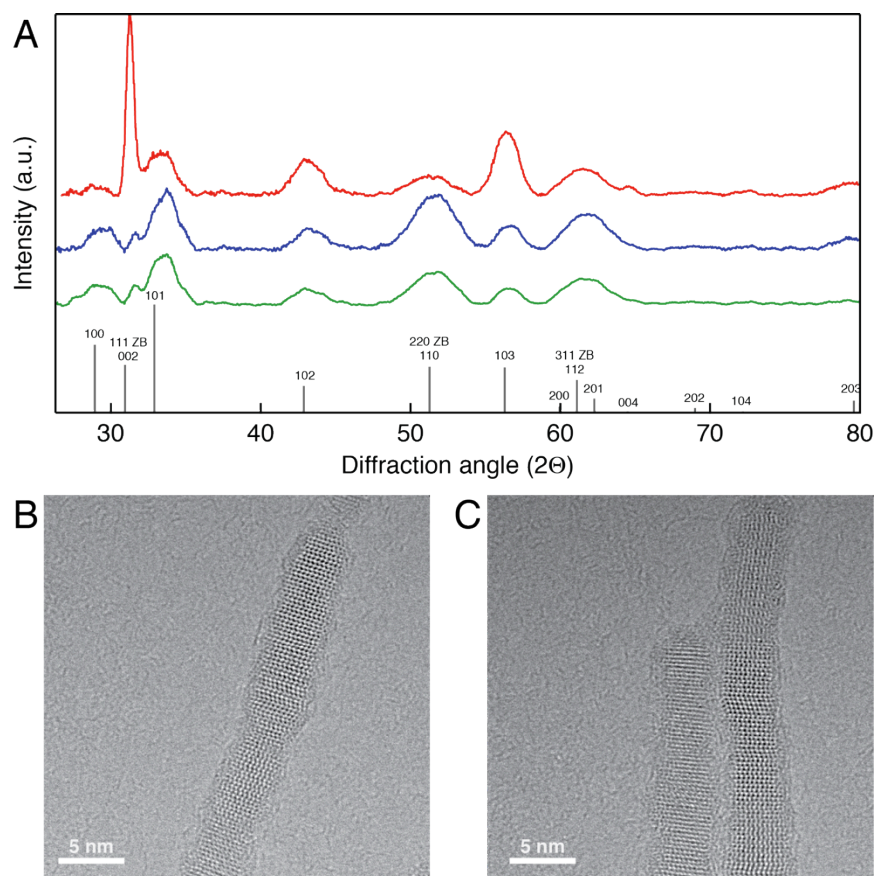
Figure 2.2. Structural impact of ion exchange on nanoheterostructures. (A) X-ray diffraction pattern of CdSe/CdS dot/rods with 2.5-nm dot obtained from hot-injection (red), cation exchange (blue), and post-exchange purification (green). A slight increase in peaks associated with zinc blende structure is seen following cation exchange but negligible difference is found following post-exchange purification. HRTEM images of CdSe/CdS dot/rods with 3.9-nm dot (B) from cation exchange and (C) from post-exchange purification. Both samples show grain boundaries and stacking faults.

2.3   Photoluminescence   Recovery   of   Cation   Exchanged Nanoheterostructures

Semiconductor nanocrystals synthesized by careful hot-injection can be made in such a way as to have negligible number of defects (structural or chemical impurities).[23,24] It has been suggested, although without conclusive experimental verification, that defects, if

any, are "self-purified" during the nanocrystal growth process or even post synthesis (typically on the time-scale of minutes to hours), possibly due to the ease with which defects can migrate to the surface of the nanocrystal.[23-2425] The anomalously high density of defects resulting from cation exchange may be a result of the fast kinetics (millisecond timescale[26]) of the process relative to thermal energy at room temperature, resulting in the defects being kinetically frozen.[27] One may therefore extrapolate that the defective nanocrystals made via exchange can undergo self-purification over time.

Indeed, CdSe/CdS dot/rods obtained from cation exchange recovered their QY up to several-fold over a period of few months at room temperature, likely due to slow purification of defects post exchange. Such purification or expulsion of defects is expected to be thermally activated. Consistently, by heating of colloidal solutions of the dot/rods (with a 3.9-nm dot) at 100°C, we obtained a 400-fold enhancement in their PL yield within 30 hours (Figure 2.1B bottom). No significant change in the excitonic spectra or PL peak position was observed during the purification process, implying that no significant compositional or morphological changes accompanied the process. Control experiments with dot/rods made via hot-injection showed no increase or rather a small decrease (possibly due to ligand loss) in QY under identical heating conditions.

2.4 Physical Manifestation of Photoluminescence Recovery

2.4.1 Role of Structural Defects on PL Recovery

HRTEM images of the purified nanorods show no appreciable difference in the density of grain boundaries, zinc-blende regions, or stacking faults compared to nanorods immediately following exchange (Figure 2.2B, C). Thus, the PL recovery is not due to the annealing of these structural defects. Likewise, the XRD pattern stays relatively unchanged through the purification process (Figure 2.2A). Thus, the above-mentioned structural defects are not the primary cause of the poor QY and inferior optoelectronic properties of exchanged nanorods.

Attempts to passivate the surface of exchanged dot/rods by excess addition of ligands such as oleic acid did not provide any significant QY enhancement (Table A.1.1), proving that loss of ligands is not a major cause of poor QY. The poor QY cannot be attributed to a defective CdSe/CdS interface either: CdS nanorods without a CdSe dot show a similar purification effect. The QY of CdS nanorods obtained from exchange is enhanced 360-fold within 61 hours upon heating at 65°C (Figure 2.1B top).

2.4.2 Role of Residual Impurities on PL Recovery

While structural defects appear to be relatively benign, Cu impurities remnant from cation exchange can serve as non-radiative electron deep traps or recombination centers.[28]

We tested this possibility by intentionally doping CdSe/CdS dot/rods (with a 3.9-nm dot) made via hot-injection with a small percentage of Cu impurities. Cu^+ impurities, being highly diffusive in a CdS lattice,[29,30] can be easily incorporated into the nanorod. There is an appreciable reduction in the PL yield even at the lowest doping of 0.02% or 4×10^{18} cm^{-3}. The latter amounts to two impurities per nanorod on average, implying that the PL and possibly other optoelectronic properties of a nanocrystal could be sensitive to the presence of single impurity atoms. Doping with 0.4% Cu is found to result in a 100-fold reduction in the PL QY (Figure 2.3A), clearly showing the detrimental effect of Cu impurities. At such a low doping percentage, no change in excitonic absorption of the rods is observed (Figure 2.3A inset), eliminating any morphological or compositional changes, especially the formation of Cu_2S domains.
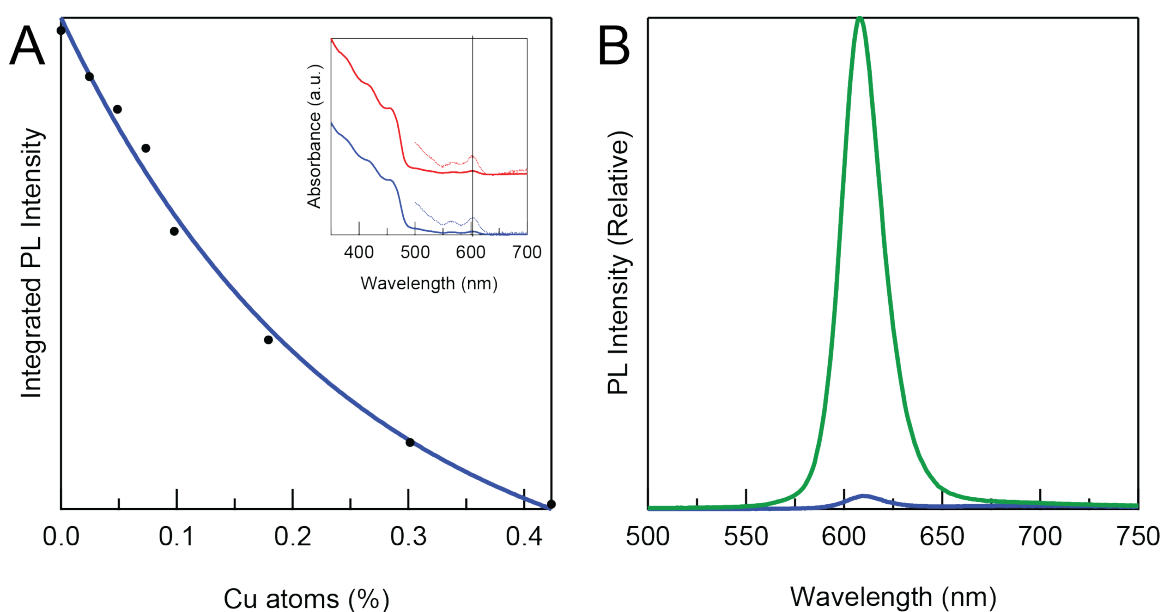
Figure 2.3. Role of Cu impurities on photoluminescence quenching. (A) Integrated photoluminescence of hot-injection-synthesized CdSe/CdS dot/rods with a 3.9-nm dot with various percentages of Cu doping. The Cu doping percentage is an upper limit arrived at by assuming that the intentional doping method has a 100% yield. The inset shows the absorbance spectra of the dot/rods showing that the excitonic spectra are identical for as-synthesized rods (red) and those following 0.4% Cu doping, indicating that no compositional or morphological changes accompany the intentional doping at such a low doping percentage. (B) Photoluminescence spectrum of CdSe/CdS dot/rods with a 3.9-nm dot from hot-injection with 0.4% Cu doping (blue) and defect-purified (green) by standing in solution in the presence of tri-butyl phosphine at room-temperature for 24 hours. The PL spectra were corrected as described in Figure 2.1 captions. Corrected PL spectra following integration show that the PL yield was enhanced 38-fold upon impurity purification.

Thus, Cu impurities, even on the level of few atoms per nanocrystal, are enough to result in suppressed emission in the dot/rods made by cation exchange. Note that at such low

impurity concentrations, analysis of Cu impurity levels by inductively coupled plasma mass spectroscopy is bound to be unreliable due a much higher background of Cu^+ ions in solution, remnant from the cation exchange step. The amount of Cu is too low to be even detected in elemental analyses of the nanorods via energy dispersive x-ray spectroscopy.[6]

The intentionally doped dot/rods, when allowed to stand in solution in the presence of tri-butyl phosphine (TBP), conditions similar to nanorod samples obtained from cation exchange, show an enhancement in QY nearly 40–fold over 24 hours at room temperature (Figure 2.2, right). No significant change in excitonic absorption was seen. Phosphines, being soft bases, are common binding ligands for Cu^+, a soft acid,[31-34] providing an additional driving force for the expulsion of Cu impurities. Control experiments with undoped dot/rods from hot-injection allowed to stand in the presence of TBP did not show any QY enhancement, rather a slight decrease by 13%.

Purification of Cu impurities from cation-exchanged nanorods is thus aided by the driving force provided by selective binding of Cu^+ by the phosphine and thermal activation of impurity diffusion via heating. It is possible that there is an equilibrium between Cu^+ impurities within the lattice and those bound to phosphine. Addition of excess TBP during cation exchange would favor Cu^+ expulsion, however, severe ligand exchange and nanorod etching limit high TBP concentrations.

2.5 High Optical Quality Nanoheterostructures by Cation Exchange Reactions

Cation-exchanged nanorods following purification compare well with those made via conventional synthesis, in terms of their QY (Table A.1.1-A.1.3). For instance, exchanged dot/rods (with a 3.9-nm dot) following purification exhibit a QY of 30% approaching the 55% QY of dot/rods obtained from hot-injection synthesis. When the marginal reduction in PL due to heating-induced ligand loss is accounted for by a heating control, we found that the QYs of these dot/rods are similar for exchanged and hot-injection synthesized samples. Similarly, exchange-obtained CdS nanorods (without a dot) following purification achieve a QY that is three-fifths that of nanorods obtained from hot-injection, even without accounting for ligand loss. Impurity purification thus allows exchanged nanocrystals to achieve a QY approaching the inherent value in the absence of detrimental impurities.

Dot/rods with a smaller 2.5-nm dot (quasi type-II alignment[13]) show order-of-magnitude QY recovery, but lower compared to the above two cases: following purification we obtain a QY that is one quarter the QY of dot/rods from hot-injection. It is likely, due to entropic reasons that, even following purification, a small number of impurities remain behind, distributed over the ensemble of nanocrystals. Since the quasi type-II dot/rod is a charge-separated system with a more delocalized electronic wavefunction,[13,14,17] the efficiency of radiative e-h recombination would be more sensitive to these remnant

impurities. On the other hand, in the type-I dot/rods and the CdS rods, where the e-h pair is relatively bound,[35,36] the effect of remnant impurities on radiative recombination would be lower. For CdS nanorods (Fig 2.1B top), in addition to excitonic emission, surface trap emission (at $\lambda > 600$ nm) is also enhanced upon purification, corroborating the role of Cu impurities as non-radiative traps or recombination centers. While it is difficult to ascertain the location of the Cu impurities, if the impurities were localized chiefly to the surface of the nanorod, the emission of the type-I dot-rods (where the exciton is shielded from the surface) would not be affected as drastically.

In summary, we have found that by providing appropriate thermal activation and driving force, nanocrystals obtained from ion exchange can be purified of residual impurities, resulting in high optoelectronic grade materials. It is possible that the relative ease and speed of the purification process is unique to nanosized crystals, which has implications for models of doping and self-purification on the nanoscale.[18] The activated dopant purification method demonstrated here may extend to other nanostructure fabrication methods that result in inherently impure samples.

2.6 Chapter 2 References

1.   Son, D. H.; Hughes, S. M.; Yin, Y.; Alivisatos, A. P. Cation Exchange Reactions in Ionic Nanocrystals. *Science* **2004**, *306*, 1009-1012.

2.   Robinson, R. D.; Sadtler, B.; Demchenko, D. O.; Erdonmez, C. K.; Wang, L.-W.; Alivisatos, A. P. Spontaneous Superlattice Formation in Nanorods Through Partial Caiton Exchange. *Science* **2007**, *317*, 355–358.

3.   Luther, J. M.; Zheng, H.; Sadtler, B.; Alivisatos, A. P. Synthesis of PbS Nanorods and Other Ionic Nanocrystals of Complex Morphology by Sequential Cation Exchange Reactions. *J. Am. Chem. Soc.* **2009**, *131*, 16851–16857.

4.   Pietryga, J. M.; Werder, D. J.; Williams, D. J.; Casson, J. L.; Schaller, R. D.; Klimov, V. I.; Hollingsworth, J. A. Utilizing the Lability of Lead Selenide to Produce Heterostructured Nanocrystals with Bright, Stable Infrared Emission. *J. Am. Chem. Soc.* **2008**, *130*, 4879–4885.

5.   Sadtler, B.; Demchenko, D. O.; Zheng, H.; Hughes, S. M.; Merkle, M. G.; Dahmen, U.; Wang, L.-W.; Alivisatos, A. P. Selective Facet Reactivity During Cation Exchange in Cadmium Sulfide Nanorods. *J. Am. Chem. Soc.* **2009**, *131*, 5285–5293.

6.   Jain, P. K.; Amirav, L.; Aloni, S.; Alivisatos, A. P. Nanoheterostructure Cation Exchange: Anionic Framework Conservation. *J. Am. Chem. Soc.* **2010**, *132*, 9997-9999.

7.   Smith, A. M.; Nie, S. Bright and Compact Alloyed Quantum Dots with Broadly Tunable Near-Infrared Absorption and Fluorescence Spectra Through Mercury Cation Exchange. *J. Am. Chem. Soc.* **2011**, *133*, 24-26.

8.   Mirkovic, T.; Rossouw, D.; Botton, G. A.; Scholes, G. D. Broken Band Alignment in EuS-CdS Nanoheterostructures. *Chem. Mater.* **2011**, *23*, 181-187.

9.   Rivest, J. B.; Swisher, S. L.; Fong, L.-K.; Zheng, H.; Alivisatos, A. P. Assembled Monolayer Nanorod Heterojunctions. *ACS Nano* **2011**, *5*, 3811-3816.

10.   Luther, J. M.; Jain, P. K.; Ewers, T.; Alivisatos, A. P. Localized Surface Plasmon Resonances Arising from Free Carriers in Doped Quantum Dots. *Nat. Mater.* **2011**, *10*, 361-366.

11.   Zhao, Y.; Pan, H.; Lou, Y.; Qiu, X.; Zhu, J.; Burda, C. Plasmonic $Cu_{2-x}S$ Nanocrystals: Optical and Structural Properties of Copper-Deficient Copper(I) Sulfides. *J. Am. Chem. Soc.* **2009**, *131*, 4253-4261.

12.   Lotfipour, M.; Machani, T.; Rossi, D. P.; Plass, K. E. α-Chalcocite Nanoparticle Synthesis and Stability. *Chem. Mater.* **2011**, *23*, 3032-3038.

13.   Sitt, A.; Sala, F. D.; Menagen, G.; Banin, U. Multiexciton Engineering in Seeded Core/Shell Nanorods: Transfer from Type-I to Quasi Type-II Regimes. *Nano Lett.* **2009**, *9*, 3470-3476.

14.   Rainò, G.; Stöferle, T.; Moreels, I.; Gomes, R.; Kamal, J. S.; Hens, Z.; Mahrt, R. F. Probing the Wave Function Delocalization in CdSe/CdS Dot-in-Rod Nanocrystals by Time- and Temperature-Resolved Spectroscopy. *ACS Nano* **2011**, *5*, 4031-4036.

15.   Talapin, D. V.; Nelson, J. H.; Shevchenko, E. V.; Aloni, S.; Sadtler, B.; Alivisatos, A. P. Seeded Growth of Highly Luminescent CdSe/CdS Nanoheterostructures with Rod and Tetrapod Morphologies. *Nano Lett.* **2007**, *7*, 2951–2959.

16.   Carbone, L.; Nobile, C.; De Giorgi, M.; Sala, F. D.; Morello, G.; Pompa, P.; Hytch, M.; Snoeck, E.; Fiore, A.; Franchini, I. R.; Nadasan, M.; Silvestre, A. F.; Chiodo, L.; Kudera, S.; Cingolani, R.; Krahne, R.; Manna, L. Synthesis and Micrometer-Scale Assembly of Colloidal CdSe/CdS Nanorods Prepared by a Seeded Growth Approach. *Nano Lett.* **2007**, *7*, 2942–2950.

17.   Amirav, L.; Alivisatos, A. P. Photocatalytic Hydrogen Production with Tunable Nanorod Heterostructures. *J. Phys. Chem. Lett.* **2010**, *1*, 1051-1054.

18.   Pacifici, D.; Moreira, E. C.; Franzò, G.; Martorino, V.; Priolo, F.; Iacona, F. Defect Production and Annealing in Ion-Irradiated Si Nanocrystals. *Phys. Rev. B* **2002**, *65*, 144109.

19.   Patil, S. G. Optoelectronic Properties of Copper-Doped Cadmium Sulphide. *J. Phys. D: Appl. Phys.* **1972**, *5*, 1692-1699.

20.   Petre, D.; Pintilie, I.; Pentia, E.; Pintilie, I.; Botila, T. The Influence of Cu Doping on Opto-Electronic Properties of Chemically Deposited CdS. *Mat. Sci. Eng. B* **1999**, *58*, 238-243.

21.   Michenaud, J.-P.; Streydio, J.-M.; Luyckx, A. Kinetics of Optical Charge Excahnge in Copper-Doped Cadmium Sulphide Single Crystals. *J. Phys. Chem. Solids* **1967**, *28*, 1607-1616.

22.   Liang, G.-X.; Liu, H.-Y.; Zhang, J.-R.; Zhu, J.-J. Ultrasensitive Cu^{2+} Sensing by Near-Infrared-Emitting CdSeTe Alloyed Quantum Dots. *Talanta* **2010**, *80*, 2172-2176.

23. Norris, D. J.; Yao, N.; Charnock, F. T.; Kennedy, T. A. High-Quality Manganese-Doped ZnSe Nanocrystals. *Nano Lett.* **2001**, *1*, 3-7.

24. Erwin, S. C.; Zu, L.; Haftel, M. I.; Efros, A. L.; Kennedy, T. A.; Norris, D. J. Doping Semiconductor Nanocrystals. *Nature* **2005**, *436*, 91-94.

25. Turnbull, D. Formation of Crystal Nuclei in Liquid Metals. *J. Appl. Phys.* **1950**, *21*, 1022-1028.

26. Chan, E. M.; Marcus, M. A.; Fakra, S.; ElNaggar, M.; Mathies, R. A.; Alivisatos, A. P. Millisecond Kinetics of Nanocrystal Cation Exchange Using Microfluidic X-ray Absorption Spectroscopy. *J. Phys. Chem. A* **2007**, *111*, 12210–12215.

27. Wark, S.; Hsia, C.-H.; Son, D. H. Effects of Ion Solvation and Volume Change of the Reaction on the Equilibrium and Morphology in Cation-Exchange Reaction of Nanocrystals. *J. Am. Chem. Soc.* **2008**, *130*, 9550–9555.

28. Lippard, S. J.; Mayerle, J. J. Behavior of Tertiary Phosphine and Arsine Complexes of Copper(I) in Chloroform Solution. *Inorg. Chem.* **1972**, *11*, 753-756.

29. Sullivan, G. A. Diffusion and Solubility of Cu in CdS Single Crystals. *Phys. Rev.* **1969**, *184*, 796-805.

30. Page, D. J; Kayali, A. A.; Wright, G. T. Some Observations of Space Charge Limited Current in Cadmium Sulphide Crystals. *Proc. Phys. Soc.* **1962**, *80*, 1133-1142.

31. Meulenberg, R. W.; van Buuren, T.; Hanif, K. M.; Willey, T. M.; Strouse, G. F.; Terminello, L. J. Structure and Composition of Cu-Doped CdSe Nanocrystals Using Soft X-ray Absorption Spectroscopy. *Nano Lett.* **2004**, *4*, 2277-2285.

32. Fife, D. J.; Moore, W. M.; Morse, K. W. Solution Equilibria of Tertiary Phosphine Complexes of Copper(I) Halides. *Inorg. Chem.* **1984**, *23*, 1684-1691.

33. Pearson, R. G. Hard and Soft Acids and Bases. *J. Am. Chem. Soc.* **1963**, *85*, 3533-3543.

34. Acharya, S.; Pradhan, N. Insertion/Ejection of Dopant Ions in Composition Tunable Semiconductor Nanocrystals. *J. Phys. Chem. C* **2011**, *115*, 19513–19519

35. Steiner, D.; Dorfs, D.; Banin, U.; Della Sala, F.; Manna, L.; Millo, O. Determination of Band Offsets in Heterostructured Colloidal Nanorods Using Scanning Tunneling Spectroscopy. *Nano Lett.* **2008**, *8*, 2954-2958.

36. Yoskovitz, E.; Menagen, G.; Sitt, A.; Lachman, E.; Banin, U. Nanoscale Near-Field Imaging of Excitons in Single Heterostructured Nanorods. *Nano Lett.* **2010**, *10*, 3068-3072.

Chapter 3.

Ion Exchange Synthesis of III-V Nanocrystals

III-V nanocrystals displaying high crystallinity and low size dispersity are difficult to access by direct synthesis from molecular precursors. Here, we demonstrate that cation exchange of cadmium pnictide nanocrystals with group 13 ions yields monodisperse, crystalline III-V nanocrystals, including GaAs, InAs, GaP, and InP. This report highlights the versatility of cation exchange for accessing nanocrystals with covalent lattices.

3.1 Synthetic Challenge of III-V Nanocrystals

Colloidal synthesis of semiconductor nanocrystals has rapidly developed in the past several decades, expanding beyond the prototypical spherical CdSe[1] to encompass an expanding library of binary and ternary compound semiconductors of various morphologies and complex heterostructures[2-5] for use in biolabeling[6] and electronic devices.[7] However, III-V semiconductors, common materials for epitaxially grown quantum dots, have lagged behind in colloidal synthetic development as the covalency of these materials requires high temperatures for both nucleation and growth, making it difficult to discriminate the two, yielding polydisperse samples.[8,9]

The synthesis of III-V nanocrystals has largely relied upon the dehalosylation reaction of $P(SiMe_3)_3$[10-12] or $As(SiMe_3)_3$[13-15] with group 13 halides in coordinating solvents, though single source precursors[16] and transmetalation reactions[17] have been demonstrated as alternative methods. In these cases, high temperatures (typically at reflux of the solvent) or long annealing times (on the order of days) are needed to achieve crystalline products. More recently, studies have demonstrated that fatty acids in non-coordinating solvents can be used to lower reaction temperatures and significantly reduce growth and annealing times to achieve InP and InAs nanocrystals with dispersities comparable to their II-VI analogs.[18-21] To date, no equivalent synthesis has been developed for the gallium pnictides; thus, state-of-the-art syntheses produce polydisperse samples, many of which are contaminated with molecular impurities.[15,22,23]

3.2 Ion Exchange Synthesis of III-V Nanocrystals

Ion exchange has emerged as an alternative to conventional "hot-injection" synthesis for ionic nanocrystals, allowing rapid replacement of the cation between various II-VI, I-VI, and IV-VI semiconductors while preserving particle size and morphology.[24-30] The use of an existing crystal lattice as a template enables the development of syntheses of crystal phases[27] and novel heterostructures[28,31-34] not accessible by conventional synthesis. Though ion exchange has been demonstrated using higher valent ions,[35] these reports have been limited to ionic systems. Here we demonstrate the extension of ion exchange to synthesize monodisperse, highly crystalline III-V nanocrystals, including GaAs, InAs, GaP, and InP.

Recent synthetic developments in II-V, Cd_3P_2 and Cd_3As_2, semiconductor nanocrystals[36,37] have provided high quality template materials for the ion exchange synthesis of III-V nanocrystals. The thermodynamic driving force for this ion exchange is a balance between the solvation energy of the ions and the lattice binding energy before and after exchange.[24,30,31,35] For the II-V to III-V exchanges of interest, bulk lattice energies favor exchange. Thus, the solvation energies of the ions must be similar to permit facile exchange. Therefore, we selected tri-n-octylphosphine (TOP), a soft base, to minimize the binding preference for hard group 13 ions, Ga^{3+} or In^{3+}, relative to Cd^{2+}.

3.2.1 Formation of Group 13 Arsenides from Cd_3As_2

Our approach for the ion exchange synthesis of GaAs from Cd_3As_2 is the exposure Cd_3As_2 nanocrystal to $GaCl_3$ at elevated temperature in a bath of phosphines. Monodisperse Cd_3As_2 nanocrystals (Figure 3.1A), synthesized according to prior literature,[37] are dissolved in TOP and injected into a $GaCl_3$:TOP complex (Ga:Cd 100:1) at 300 °C for 15 minutes. The stronger energy of formation of GaAs compared to Cd_3As_2 (ΔG = -25 kcal/mol, bulk)[38,39] favors the 3:2 replacement of Cd^{2+} with Ga^{3+}. Transmission electron microscopy (TEM) of the GaAs nanocrystals after the ion exchange reaction (Figure 3.1B) displays a quasi-spherical morphology similar to the initial Cd_3As_2. High-resolution TEM confirm the crystallinity of the GaAs nanocrystals (Figure 3.1B inset) and x-ray diffraction (XRD) shows the conversion from the lower symmetry tetragonal phase of Cd_3As_2 ($P4_2/nmc$ space group) to the higher symmetry zinc blende phase of GaAs ($F\bar{4}3m$ space group). Likewise, similar reaction conditions can be used to produce InAs nanocrystals from the ion exchange reaction of Cd_3As_2 nanocrystals with an $InCl_3$:TOP complex (Figure 3.1C, D).
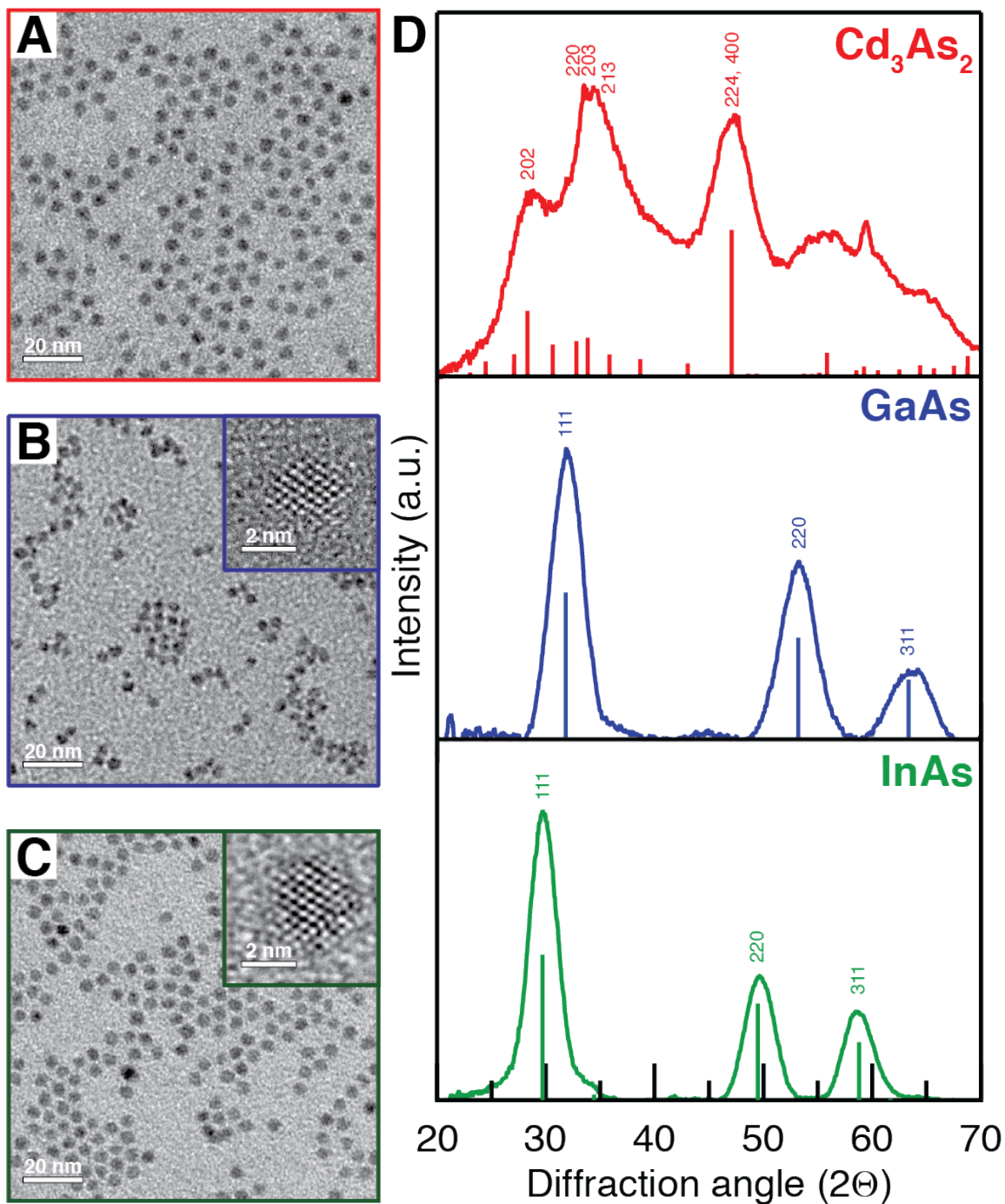
Figure 3.1. Group 13 cation exchange of Cd_3As_2 nanocrystals. (A) TEM images of the initial Cd_3As_2 nanocrystals and (B) GaAs and (C) InAs nanocrystals obtained from ion exchange. (B, C) Insets show HRTEM images. (D) XRD of the initial Cd_3As_2 nanocrystals (top) and GaAs (middle) and InAs (bottom) nanocrystals after ion exchange. Patterns from the Inorganic Crystal Structure Database (ICSD) for Cd_3As_2 (ICSD no. 23245), GaAs (ICSD no. 107946), and InAs (ICSD no. 24518) are provided for reference.

As no additional source of arsenic was present in the reaction, the formation of GaAs and InAs require either dissolution of the initial Cd_3As_2 nanocrystals and subsequent nucleation and growth of GaAs and InAs or a cation exchange reaction in which the Cd^{2+} ions are replaced by group 13 ions. Given the precedence for difficulty in synthesizing crystalline GaAs nanocrystals,[15] the 15-minute reaction time and monodispersity of the resulting particles argue against a new nucleation process. Furthermore, detailed sizing analysis shown in Figure 3.2A confirms conservation of the size dispersity during the ion exchange reaction, and that mean diameters are consistent with the predicted trend in volume change associated with the transformation to a denser unit cell.   The transformation from the tetragonal unit cell of Cd_3As_2 to the cubic GaAs and InAs should yield a volume contraction of 30% and 15%, respectively.   The observed 19% volume decrease for InAs is in line with expectation. For GaAs, an appreciably larger volume decrease of 55% is observed which we attribute to surface etching from phosphines and chlorides.[40] Notwithstanding, the monodispersity of each sample is maintained, as expected for an ion exchange reaction. The initial Cd_3As_2 nanocrystals have a well-controlled, narrow size dispersion of 9%. By using this as a template, we achieve GaAs and InAs particles with dispersities of 12% and 11%, respectively, the lowest dispersity reported for GaAs nanocrystals. Together, we can conclude that the GaAs and InAs nanocrystals were formed from the 3:2 replacement of Cd^{2+} with Ga^{3+} and In^{3+}.

Absorption spectroscopy shows the expected blue shift of the optical gap from the near infrared bandgap of Cd_3As_2 to InAs and GaAs (Figure 3.2B); however, in line with literature precedent for III-V nanoparticles with no shell, negligible photoluminescence was observed.[9] The expected quantum confinement blue shift of the bandgap when the exchange reaction is performed on smaller Cd_3As_2 nanocrystals is added substantiation of a cation exchange reaction as opposed to a dissolution and subsequent nucleation process (Figure 3.2C). The monodispersity of the nanocrystals synthesized by ion exchange is evident by the excitonic absorption in the InAs nanocrystals. However, the GaAs nanocrystals show a featureless absorption spectrum although the size dispersity is similar to the InAs. This may be due to Cd atoms residual from the ion exchange (see below) potentially broadening the spectrum; however, the same is true of the InAs nanocrystals. The lack of excitonic absorption is also in line with theoretical predictions of an indirect bandgap for strongly confined spherical GaAs quantum dots.[41] The ability to synthesize monodisperse GaAs nanocrystals through ion exchange provides a method for future work to more systematically investigate the evolution of the electronic structure and optical properties of GaAs as a function of size.
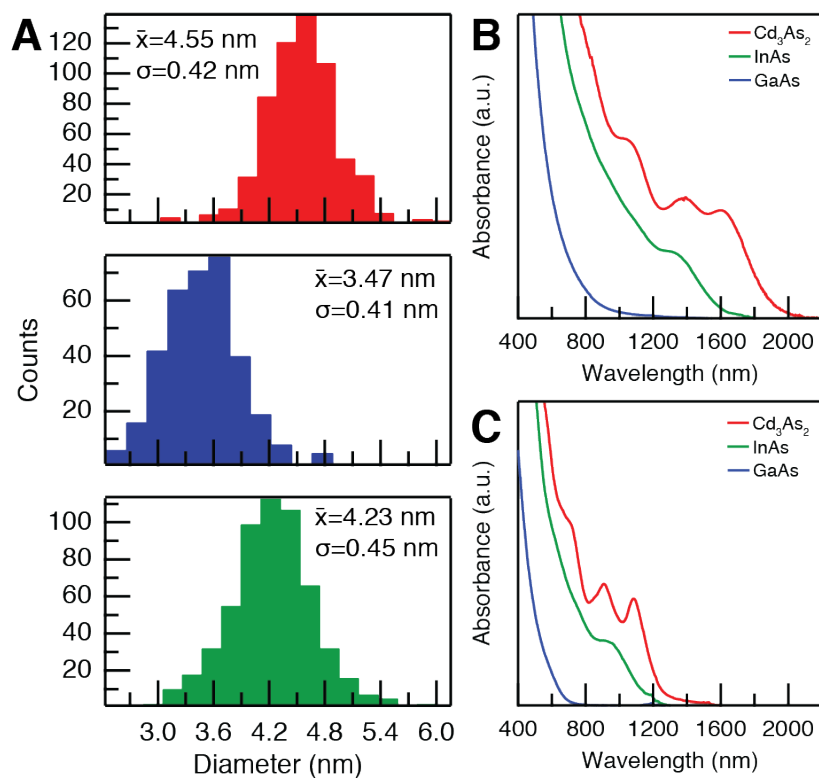
Figure 3.2. Evidence of cation exchange mechanism. (A) Particle size histograms of the initial Cd_3As_2 nanocrystals (top) and GaAs (middle) and InAs (bottom) nanocrystals after ion exchange showing preservation of size dispersity. (B) Absorption spectra of initial 4.5 nm Cd_3As_2 nanocrystals and those that have been exchanged to InAs and GaAs. (C) Absorption spectra of initial 3 nm Cd_3As_2 nanocrystals and those that have been exchanged to InAs and GaAs.

3.2.2 Formation of Group 13 Phosphides from Cd_3P_2

Further highlighting the versatility of ion exchange for the synthesis of III-V semiconductors, GaP and InP can also be synthesized by ion exchange of Cd_3P_2 nanocrystals (Figure 3.3). In each instance, similar size dispersities and morphologies are obtained after the cation exchange process and the absorption spectra blue shift from Cd_3P_2 to InP to GaP as expected from their bulk bandgaps (Figure A.2.1). XRD, shown in Figure 3.3D, confirms the conversion from the tetragonal Cd_3P_2 to the cubic crystal phase of GaP and InP, consistent with the results achieved for the arsenide materials.
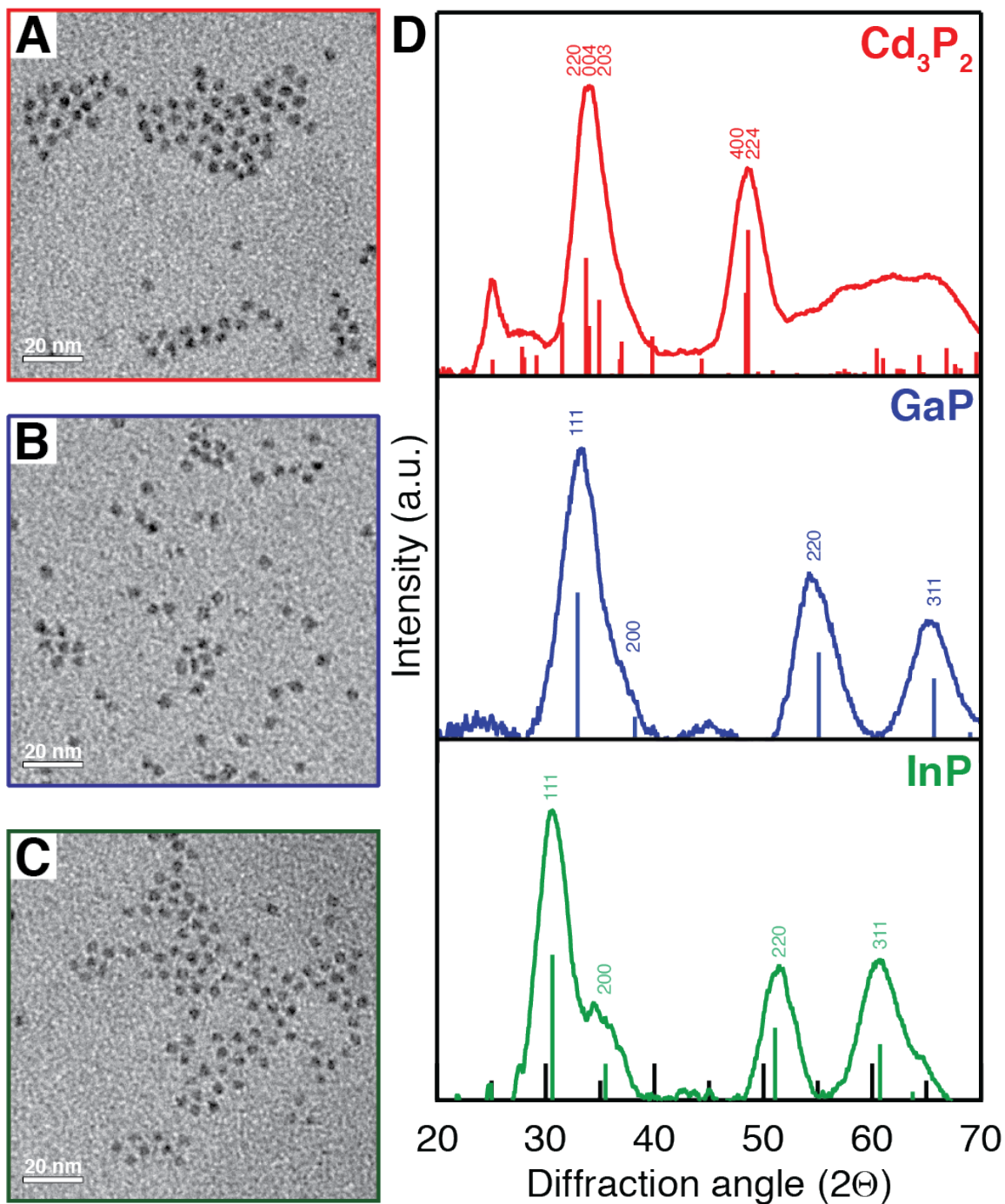
Figure 3.3. Group 13 cation exchange of Cd_3P_2 nanocrystals. (A) TEM images of the initial Cd_3P_2 nanocrystals and (B) GaP and (C) InP nanocrystals obtained from ion exchange. (D) XRD of the initial Cd_3P_2 (top) and GaP (middle) and InP (bottom) nanocrystals after ion exchange. Patterns from the ICSD for Cd_3P_2 (ICSD no. 158864), GaP (ICSD no. 77088), and InP (ICSD no. 24517) are provided for reference.

3.3 Ionic Versus Covalent Products by Cation Exchange Reactions

The diffusivity of ions can be orders of magnitude lower in covalent semiconductors compared to ionic systems.[42] Prior work has demonstrated that residual amounts of impurity ions may remain after cation exchange reactions in ionic nanocrystals;[43] thus, it might be expected that residual Cd may be present in the ion exchanged III-V nanocrystals given the increased activation energy for diffusion. Indeed, inductively coupled plasma atomic emission spectroscopy (ICP-AES) confirms residual Cd concentration of a few atomic percent remain in all samples post-exchange (Table A.2.1). While the Ga^{3+} ion exchange of Cd_3As_2 successfully yielded crystalline zinc blende GaAs in only 5 minutes at 200 °C, the amount of residual Cd is dependent on the reaction temperature, time, and particle size as expected for a thermally activated, diffusion limited process (Figure A.2.2, Table A.2.2), warranting the ion exchange to be performed at higher temperatures for longer times. For initial exchanges, the residual Cd concentration reaches a steady state at longer times; however, the residual Cd content can be further reduced by sequential exchanges (Table A.2.1). XRD and optical spectroscopy show no signs of the cadmium pnictide phases or signs of alloying, analogous to InAs nanocrystals intentionally doped with high Cd concentrations (2:1 In:Cd).[44] Preliminary etching experiments[45] imply the cadmium is distributed throughout the nanocrystals as opposed to being localized to the surface (Table A.2.1). This high solubility of Cd within a III-V is in stark contrast with bulk equilibrium phase diagrams which predict less than one atomic percent at 850 °C,[46] warranting further investigation; however, similar to a prior study,[44] the remnant Cd may be useful as a means to control the carrier concentration in nanocrystal solids, in line with previous examples of using cation exchange as a means of controlled doping.[47,48]

Ion exchange reactions for III-V nanocrystals differ from those in ionic II-VI nanocrystals in several key aspects. The majority of the II-VI ion exchange reactions can be performed reversibly at room temperature due to the high lability of metal M^{1+} and M^{2+} ions and by modulating the ion energy in solution to drive species in and out.[24-26,30,32,33] In contrast, the III-V ion exchange reactions demonstrated here are highly irreversible, largely driven by the difference in lattice energies of the reactant and product phases, and require higher temperatures to enhance diffusion of the exchanging ions, a process which is inhibited at room temperature in these materials.

In summary, we have demonstrated the extension of cation exchange to form nanocrystals with covalent lattices, enabling the synthesis of highly crystalline, monodisperse III-V nanocrystals. In particular, the availability of monodisperse semiconductor nanocrystals such as GaAs presents new opportunities for comparison studies of epitaxially grown and colloidally synthesized quantum dots.

3.4 Chapter 3 References

1. Murray, C. B.; Norris, D. J.; Bawendi, M. G. Synthesis and Characterization of Nearly Monodisperse CdE (E = Sulfur, Selenium, Tellurium) Semiconductor Nanocrystallites. *J. Am. Chem. Soc.* **1993**, *115*, 8706–8715.

2. Murray, C. B.; Kagan, C. R.; Bawendi, M. G. Synthesis and Characterization of Monodisperse Nanocrystals and Close-Packed Nanocrystal Assemblies. *Annu. Rev. Mater. Sci.* **2000**, *30*, 545–610.

3. Yin, Y.; Alivisatos, A. P. Colloidal Nanocrystal Synthesis and the Organic–Inorganic Interface. *Nature* **2005**, *437*, 664–670.

4. *Nanocrystal Quantum Dots,* 2nd ed.; Klimov, V. I., Ed.; CRC Press: Boca Raton, FL, 2010.

5. Park, J.; Joo, J.; Kwon, S. G.; Jang, Y.; Hyeon, T. Synthesis of Monodisperse Spherical Nanocrystals. *Angew. Chem. Int. Ed.* **2007**, *46*, 4630–4660.

6. Michalet, X.; Pinaud, F. F.; Bentolila, L. A.; Tsay, J. M.; Doose, S.; Li, J. J.; Sundaresan, G.; Wu, A. M.; Gambhir, S. S.; Weiss, S. Quantum Dots for Live Cells, in Vivo Imaging, and Diagnostics. *Science* **2005**, *307*, 538–544.

7. Talapin, D. V.; Lee, J.-S.; Kovalenko, M. V.; Shevchenko, E. V. Prospects of Colloidal Nanocrystals for Electronic and Optoelectronic Applications. *Chem. Rev.* **2010**, *110*, 389–458.

8. Nozik, A. J.; Mićić, O. I. Colloidal Quantum Dots of III-V Semiconductors. *MRS Bull.* **1998**, *23*, 24–30.

9. Heath, J. R.; Shiang, J. J. Covalency in Semiconductor Quantum Dots. *Chem. Soc. Rev.* **1998**, *27*, 65–71.

10. Wells, R. L.; Aubuchon, S. R.; Kher, S. S.; Lube, M. S.; White, P. S. Synthesis od Nanocrystalline Indium Arsenide and Indium Phosphide from Indium(III) Halids and Tris(trimethylsilyl)pnicogens. Synthesis, Characterization, and Decomposition Behavior of $I_3In•P(SiMe_3)_3$.*Chem. Mater.* **1995**, *7*, 793–800.

11. Guzelian, A. A.; Katari, J. E. B.; Kadavanich, A. V.; Banin, U.; Hamad, K.; Juban, E.; Alivisatos, A. P.; Wolters, R. H; Arnold, C. C.; Heath, J. R. Synthesis of Size-Selected, Surface-Passivated InP Nanocrystals. *J. Phys. Chem.* **1996**, *100*, 7212–7219.

12. Mićić, O. I.; Sprague, J. R.; Curtis, C. J.; Jones, K. M.; Machol, J. L.; Nozik, A. J.; Giessen, H.; Fluegel, B.; Mohs, G.; Peyghambarian, N. Synthesis and Characterization of InP, GaP, and $GaInP_2$ Quantum Dots. *J. Phys. Chem.* **1995**, *99*, 7754–7759.

13. Wells, R. L.; Pitt, C. G.; McPhail, A. T.; Purdy, A. P.; Shafieezad, S.; Hallock, R. B. The Use of Tris(trimethylsilyl)arsine to Prepare Gallium Arsenide and Indium Arsenide. *Chem. Mater.* **1989**, *1*, 4–6.

14. Guzelian, A. A.; Banin, U.; Kadavanich, A. V.; Peng, X.; Alivisatos, A. P. Colloidal Chemical Synthesis and Characterization of InAs Nanocrystal Quantum Dots. *Appl. Phys. Lett.* **1996**, *69*, 1432–1434.

15. Olshavsky, M. A.; Goldstein, A. N.; Alivisatos, A. P. Organometallic Synthesis of Gallum-Arsenide Crystallites, Exhibiting Quantum Confinement. *J. Am. Chem. Soc.* **1990**, *112*, 9438–9439.

16. Kim, Y.-H.; Jun, Y.-W.; Jun, B.-H.; Lee, S.-M.; Cheon, J. Sterically Induced Shape and Crystalline Phase Control of GaP Nanocrystals. *J. Am. Chem. Soc.* **2002**, *124*, 13656–13657.

17. Lauth, J.; Strupeit, T.; Kornowski, A.; Weller, H. A Transmetalation Route for Colloidal GaAs Nanocrystals and Additional III-V Semiconductor Materials. *Chem. Mater.* **2012**, *25*, 1377–1383.

18. Battaglia, D.; Peng, X. Formation of High Quality InP and InAs Nanocrystals in a Noncoordinating Solvent. *Nano Lett.* **2002**, *2*, 1027–1030.

19. Xie, R.; Battaglia, D.; Peng, X. Colloidal InP Nanocrystals as Efficient Emitters Covering Blue to Near-Infrared. *J. Am. Chem. Soc.* **2007**, *129*, 15432–15433.

20. Lucey, D. W.; MacRae, D. J.; Furis, M.; Sahoo, Y.; Cartwright, A. N.; Prasad, P. N. Monodispersed InP Quantum Dots Prepared by Colloidal Chemistry in a Noncoordinating Solvent. *Chem. Mater.* **2005,** *17*, 3754–3762.

21. Xu, S.; Kumar, S.; Naan, T. Rapid Synthesis of High-Quality InP Nanocrystals. *J. Am. Chem. Soc.* **2006**, *128*, 1054–1055.

22. Uchida, H.; Curtis, C. J.; Nozik, A. J. Gallium Arsenide Nanocrystals Prepared in Quinoline. *J. Phys. Chem.* **1991**, *95*, 5382–5384.

23. Uchida, H.; Curtis, C. J.; Kamat, P. V.; Jones, K. M.; Nozik, A. J. Optical Properties of Gallium Arsenide Nanocrystals. *J. Phys. Chem.* **1992**, *96*, 1156–1160.

24. Son, D. H.; Hughes, S. M.; Yin, Y.; Alivisatos, A. P. Cation Exchange Reactions in Ionic Nanocrystals. *Science* **2004**, *306*, 1009–1012.

25. Sadtler, B.; Demchenko, D. O.; Zheng, H.; Hughes, S. M.; Merkle, M. G.; Dahmen, U.; Wang, L.-W.; Alivisatos, A. P. Selective Facet Reactivity During Cation Exchange in Cadmium Sulfide Nanorods. *J. Am. Chem. Soc.* **2009**, *131*, 5285–5293.

26. Luther, J. M.; Zheng, H.; Sadtler, B.; Alivisatos, A. P. Synthesis of PbS Nanorods and Other Ionic Nanocrystals of Complex Morphology by Sequential Cation Exchange Reactions. *J. Am. Chem. Soc.* **2009**, *131*, 16851–16857.

27. Li, H.; Zanella, M.; Genovese, A.; Povia, M.; Falqui, A.; Giannini, C.; Manna, L. Sequential Cation Exchange in Nanocrystals: Preservation of Crystal Phase and Formation of Metastable Phases. *Nano Lett.* **2011**, *11*, 4964–4970.

28. Mews, A.; Eychmüller, A.; Giersig, M.; Schooss, D.; Weller, H. Preparation, Characterization, and Photophysics of the Quantum Dot Quantum Well System CdS/HgS/CdS. *J. Phys. Chem.* **1994**, *98*, 934–941.

29. Camargo, P. H. C.; Lee, Y. H.; Jeong, U.; Zou, Z.; Xia, Y. Cation Exchange: A Simple and Versatile Route to Inorganic Colloidal Spheres with the Same Size but Different Compositions and Properties. *Langmuir* **2007**, *23*, 2985–2992.

30. Wark, S.; Hsia, C.-H.; Son, D. H. Effects of Ion Solvation and Volume Change of the Reaction on the Equilibrium and Morphology in Cation-Exchange Reaction of Nanocrystals. *J. Am. Chem. Soc.* **2008**, *130*, 9550–9555.

31. Pietryga, J. M.; Werder, D. J.; Williams, D. J.; Casson, J. L.; Schaller, R. D.; Klimov, V. I.; Hollingsworth, J. A. Utilizing the Lability of Lead Selenide to Produce Heterostructured Nanocrystals with Bright, Stable Infrared Emission. *J. Am. Chem. Soc.* **2008**, *130*, 4879–4885.

32. Robinson, R. D.; Sadtler, B.; Demchenko, D. O.; Erdonmez, C. K.; Wang, L.-W.; Alivisatos, A. P. Spontaneous Superlattice Formation in Nanorods Through Partial Caiton Exchange. *Science* **2007**, *317*, 355–358.

33. Jain, P. K.; Amirav, L.; Aloni, S.; Alivisatos, A. P. Nanoheterostructure Cation Exchange: Anionic Framework Conservation. *J. Am. Chem. Soc.* **2010**, *132*, 9997–9999.

34. Li, H.; Brescia, R.; Krahne, R.; Bertoni, G.; Alcocer, M. J. P.; D'Andrea, C.; Scotognella, F.; Tassone, F.; Zanella, M.; De Giorgi, M.; Manna, L. Blue-UV-Emitting ZnSe(Dot)/ZnS(Rod) Core/Shell Nanocrystals Prepared from CdSe/CdS Nanocrystals by Sequential Cation Exchange. *ACS Nano* **2012**, *6*, 1637–1647.

35. Dong, C.; van Veggel, F. C. J. M. Cation Exchange in Lanthanide Fluoride Nanoparticles. *ACS Nano* **2008**, *3*, 123–130.

36. Xie, R.; Zhang, J.; Zhao, F.; Yang, W.; Peng, X. Synthesis of Monodisperse, Highly Emissive, and Size-Tunable Cd_3P_2 Nanocrystals. *Chem. Mater.* **2010**, *22*, 3820–3822.

37. Harris, D. K.; Allen, P. M.; Han, H.-S.; Walker, B. J.; Lee, J.; Bawendi, M. G. Synthesis of Cadmium Arsenide Quantum Dots Luminescent in the Infrared. *J. Am. Chem. Soc.* **2011**, *133*, 4676–4679.

38. Collaboration: Scientific Group Thermodata Europe (SGTE): Thermodynamic Properties of Compounds, Al2O3-SrO to GeAs. (ed.). SpringerMaterials - The Landolt-Börnstein Database (http://www.springermaterials.com). DOI: 10.1007/10652891_13

39. Collaboration: Authors and editors of the volumes III/17E-17F-41C: Cadmium arsenide (Cd3As2) entropies, enthalpies, free energy. Madelung, O., Rössler, U., Schulz, M. (ed.). SpringerMaterials - The Landolt-Börnstein Database (http://www.springermaterials.com). DOI: 10.1007/10681727_249

40. Traub, M. C.; Biteen, J. S.; Michalak, D. J.; Webb, L. J.; Brunschwig, B. S.; Lewis, N. S. Phosphine Functionalization of GaAs(111)A Surfaces. *J. Phys. Chem. C* **2008**, *112*, 18467–18473.

41. Luo, J.-W.; Franceschetti, A.; Zunger, A. Quantum-Size-Induced Electronic Transitions in Quantum Dots: Indirect Band-Gap GaAs. *Phys. Rev. B* **2008**, *78*, 035306.

42. Dutt, M. B., Sharma, B. L.: 3 Diffusion in compound semiconductors. Beke, D. L. (ed.). SpringerMaterials - The Landolt-Börnstein Database (http://www.springermaterials.com). DOI: 10.1007/10426818_10

43. Jain, P. K.; Beberwyck, B. J.; Fong, L.-K.; Polking, M. J.; Alivisatos, A. P. Highly Luminescent Nanocrystals From Removal of Impurity Atoms Residual From Ion-Exchange Synthesis. *Angew. Chem. Int. Ed.* **2012**, *51*, 2387–2390.

44. Geyer, S. M.; Allen, P. M.; Chang, L.-Y.; Wong, C. R.; Osedach, T. P.; Zhao, N.; Bulovic, V.; Bawendi, M. G. Control of the Carrier Type in InAs Nanocrystal Films Prepared by Predeposition Incorporation of Cd. *ACS Nano* **2010**, *4*, 7373–7378.

45. Battaglia, D.; Blackman, B.; Peng, X. Coupled and Decoupled Dual Quantum Systems in One Semiconductor Nanocrystal. *J. Am. Chem. Soc.* **2005**, *127*, 10889–10897.

46. Petzow, G.; Effenberg, G.; Aldinger, F., Eds. *Ternary Alloys: A Comprehensive Compendium of Evaluated Constitutional Data and Phase Diagrams*; VCH: New York, 1994; Vol 9.

47. Mocatta, D.; Cohen, G.; Schattner, J.; Millo, O.; Rabani, E.; Banin, U. Heavily Doped Semiconductor Nanocrystal Quantum Dots. *Science* **2011**, *332*, 77–81.

48. Sahu, A.; Kang, M. S.; Kompch, A.; Notthoff, C.; Wills, A. W.; Deng, D.; Winterer, M.; Frisbie, C. D.; Norris, D. J. Electronic Impurity Doping in CdSe Nanocrystals. *Nano Lett.* **2012**, *12*, 2587–2594.

Chapter 4.

Prospectus

Chemical transformations such as cation exchanges serve as unique synthetic tools available for the development of colloidal semiconductor nanocrystals, both as a complement to and a replacement for traditional hot-injection methods. The prior chapters of this dissertation have demonstrated several of these instances, including achieving comparable optical quality to conventionally synthesized materials (Chapter 3) and synthesizing previously inaccessible materials (Chapter 4). Here we describe select techniques and experiments that can further probe cation exchange reactions in colloidal semiconductor nanocrystals and lead to its increased adoption as a synthetic approach. It is important to note that while many of these techniques are often used in synthetic chemistry, they have been under-utilized in the nanocrystal field and can be broadly applicable to various nanocrystal reactions, in particular ligand studies.

4.1 Thermodynamics of Nanocrystal Cation Exchange Reactions

Cation exchange reactions continue to increase in prevalence as means to synthesize novel nanostructures, expanding beyond complete compositional transformation to include partial conversions such as heterostructure formation and doping.[1] However, a firm understanding of the thermodynamics of cation exchange and thus the ability to rationally design reactions is lacking. To date, a simplistic thermodynamic model has been invoked based on the difference in the bulk formation energies of the reactants and product phases and the solvation energy of the exchanging ions, with the latter portion usually relying upon qualitative intuition such as Pearson's hard-soft acid-base theory.[1,2] Strategies to quantitatively assess the thermodynamics of cation exchange reactions in colloidal nanocrystals, including nanostructuring and ligation effects, are needed to provide fundamental insight and inform new methods for ion exchange synthesis.

4.1.1 Quantitative Ligand Binding

The thermodynamics of cation exchange reactions in colloidal nanocrystals can be investigated in a similar fashion to the quantitative characterization of the binding of a small solute (ligand) to a biological macromolecule (acceptor). By determining the relative distribution of the ligand and acceptor in their free and complexed states, the equilibrium constant and other thermodynamic properties can be calculated.[3] We can treat the prototypical Ag exchange of CdSe as the binding of a ligand, Ag, to the nanocrystal, a multivalent acceptor in which the cation lattice sites of the crystal represent the binding sites. For displacement reactions like cation exchange, a secondary ligand, Cd, is released when a new ligand binds such that the relevant characterization is of differential binding. A binding saturation curve can then be constructed by determining the concentration of

free or bound ligand over the course of an equilibrium titration and interpreted with a binding function accounting for an appropriate model of acceptor-ligand interactions.[3,4] While numerous techniques are used in practice to determine the extent of binding, we will focus on those we deem suitable for the solution phase cation exchange of nanocrystals.

Isothermal titration calorimetry is one such technique that provides a direct measurement of the heat evolution of solution-phase reactions.[5] The ligand is titrated into a solution containing the acceptor and the heat released or absorbed in the sample cell is measured as the power necessary to maintain the sample in an isothermal condition relative to a reference. The amount of power expended is proportional to the amount of ligand bound. Beyond the directly measured heat, applying an appropriate binding function to ITC data enables the determination of the equilibrium constant, number of binding sites, and the standard enthalpy, entropy, and free energy change.

Figure 4.1A shows an isothermal titration calorimetry thermogram of the titration of silver hexafluorophosphate ($AgPF_6$) into CdSe nanocrystals in tetrahydrofuran (THF). $AgPF_6$ is used in place of the conventional $AgNO_3$ to enable solubility of both the Ag salt and nanocrystals in a single solvent. Upon addition of the Ag solution, power is applied to the reference cell to maintain the isothermal condition, indicating the exothermic nature of the Ag exchange of CdSe. By integrating the power versus time as a function of Ag addition, the differential heat per mol of Ag can be determined (Figure 4.1B). At low Ag/Cd ratios, essentially all the free Ag is incorporated into the particle leading to similar peak areas. However, as the binding sites of the nanocrystals are saturated the amount of heat evolved decreases and, at high Ag/Cd ratios, plateaus at the heat of dilution. This binding curve can be fit to the Wiseman isotherm,[6] a Langmuir-like model of n-independent sites, to extract a reaction enthalpy (ΔH) of -93 kJ/mol Ag, a stoichiometry (n) of 1.42 Ag/Cd, and an equilibrium constant (K) of 1.26×10^7 M^{-1}. The stoichiometry of less than 2, as expected by charge neutrality, may be related to a recent study in which the desorption of the surface ligand involves the removal of a surfactant bound Cd,[7] implying loss of the surface ligand during the cation exchange reaction (see below).

The relatively good agreement between the data and this simple binding function is interesting given the complexity of the inherent underlying solid-state transformation. In a bulk phase diagram of Ag_2Se and CdSe, at least three separate regions, and hence disparate equilibrium constants, would be expected corresponding to a solid solution of Ag_2Se within the CdSe phase, the coexistence of the Ag_2Se and CdSe phases, and a solid solution of CdSe within the Ag_2Se phase.[8] This simplistic binding curve may be indicative of the dominant role played by the solvation energies of the exchanging cations, overwhelming any contribution from the interconversion of the inorganic core. This observation highlights one of the limitations of the ITC technique: the calorimeter measures the heat evolved from all aspects of the reaction, preventing the isolation of the solid-state contribution. Nevertheless, ITC provides a means to directly measure the enthalpy of cation exchange reactions and may serve as an ideal method for measuring the solvation energies of common nanocrystal ligands/solvents and metal ions. Such results can inform strategies to drive new cation exchange reactions through preferential

solvation of ions or better understand the synthetic mechanism of nanocrystals via the conventional "hot injection" technique.
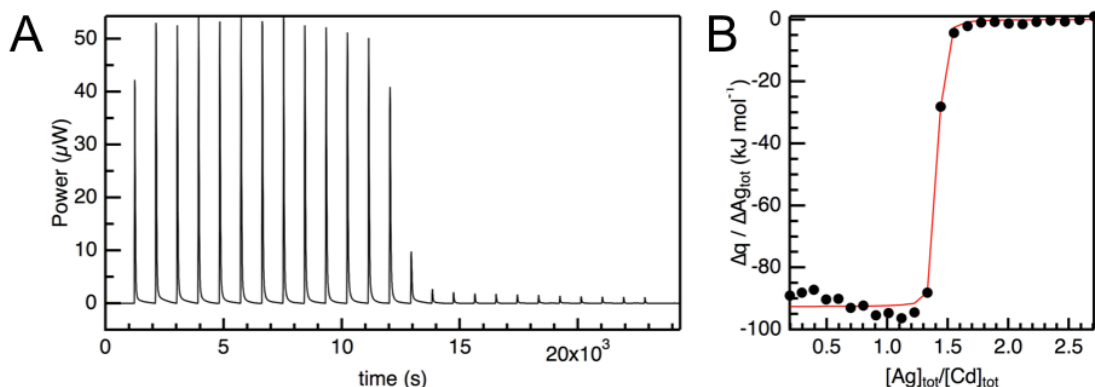

Figure 4.1. Isothermal titration calorimetry of Ag exchange of CdSe nanocrystals in THF. (A) Baseline-corrected thermogram and (B) differential heat per mol of Ag fit to the Wiseman isotherm.

Spectroscopic binding titrations serve as another method to investigate the equilibrium of cation exchange reactions. Nanocrystals have excellent optical properties including high quantum yields, narrow line-widths of fluorescence, and structured absorbance spectra that are sensitive to slight perturbations in the nanocrystal's core and surface structure.[7,9] Therefore, optical spectroscopy, in particular, can measure the changes concomitant with the formation of the ligand-acceptor (Ag-nanocrystal) complex to correlate with the extent of ligand binding. For instance, the absorbance and photoluminescence (PL) spectra of CdSe are significantly altered upon the addition of Ag (Figure 4.2A, B). The absorbance displays a pronounced red shift and broadening of the CdSe exciton, likely due to the solid solution of CdSe with Ag_2Se, with increased near infrared absorption due to the formation of the Ag_2Se phase with increasing Ag concentration. Likewise, the band edge emission of CdSe is dramatically reduced with increasing silver concentration as, on the order of, one or two Ag binding events per particle is expected to quench the CdSe emission.[10] If we assume each lattice site of the nanocrystal occupied by Ag leads to an equivalent change in absorbance, a fraction of sites bound can be determined to construct the binding curve and the relative intensity of the PL can be used as a measure of the unligated CdSe population (Figure 4.2C).

The sigmoidal shape of the integrated binding curve in Figure 4.2C is far more complex than the ITC binding curve, which would appear as a rectangular hyperbolic response when converted from a differential to integrated curve. This sigmoidal shape is indicative of a cooperative process in which the sites are no longer independent, as assumed in the Wiseman isotherm, but instead indicates that the binding of each site influences the
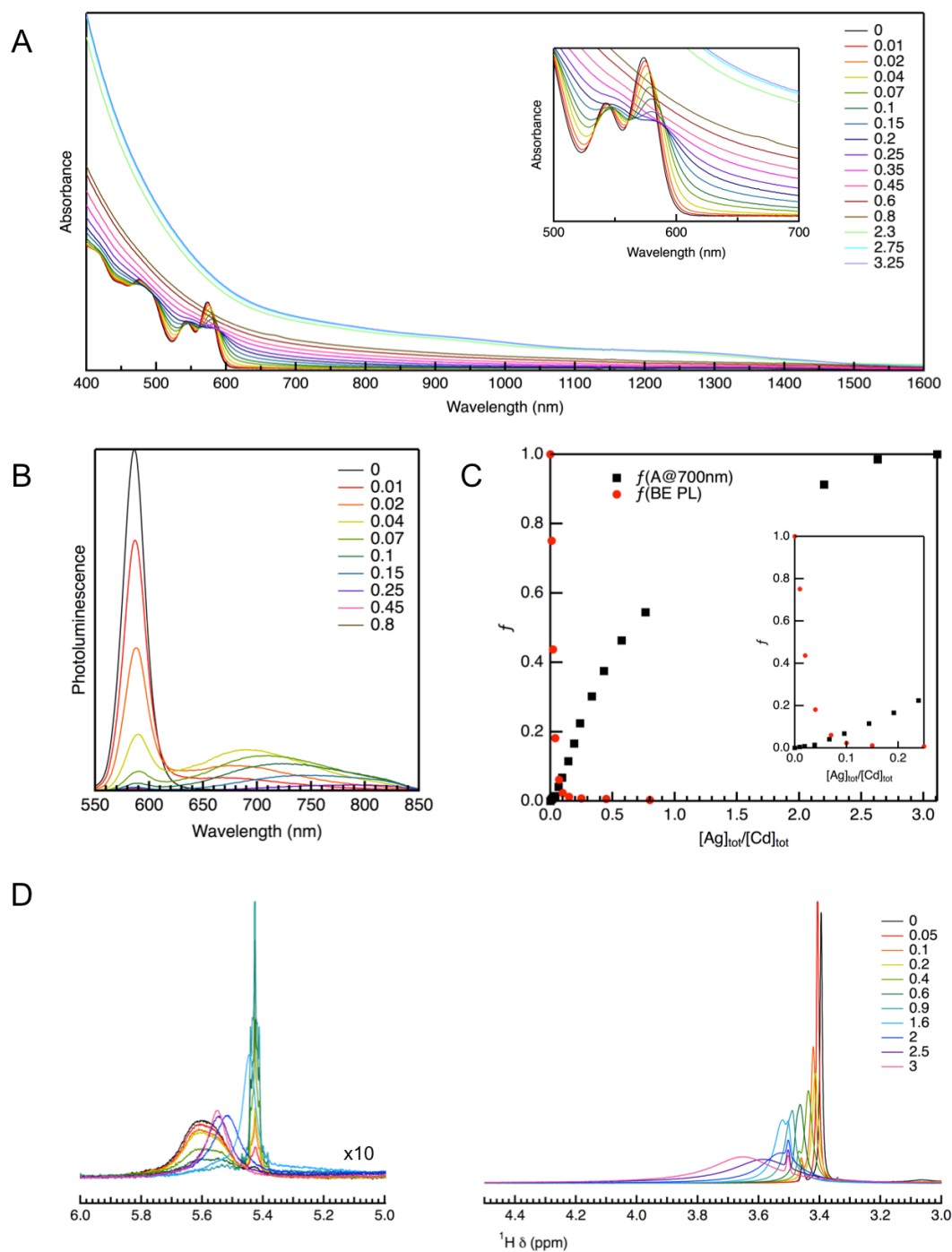
Figure 4.2. Spectroscopic titration experiments of Ag exchange of CdSe nanocrystals. Each legend denotes the ratio of the total [Ag] added relative to the total [Cd]. (A) Absorbance and (B) photoluminescence spectra as a function of Ag added. (C) Fraction of pure CdSe nanocrystals (red) based upon relative intensity of CdSe band edge (BE) emission and extent of Ag binding (black) from relative absorbance changes at 700 nm. Inset is fractional plot expanded at low ratios. (D) ^{1}H NMR spectra of CdSe nanocrystals as a function of Ag concentration showing the vinyl region of the oleate ligand (5.3-5.8 ppm) and the α-methylene region of 1-butanol (3.3-4 ppm).

binding of the next.[3,4] In fact, a recent study attempted to model a spectral binding titration of the Cu exchange of CdSe with the Hill equation, a well known binding model that provides a means to quantify the degree of cooperativity ;[11] however, the theoretical binding model used was far simpler than the current qualitative understanding of the solid-state transformations within nanocrystals and neglects the ongoing equilibrium between the nanocrystal's inorganic core and its surface ligand during the exchange reaction. For instance, a nuclear magnetic resonance (NMR) spectroscopic titration over the course of the Ag exchange of CdSe nanocrystals (Figure 4.2D) shows the vinyl region of the native oleate ligand sharpen and shift upfield while the α-methylene region of 1-butanol present in the reaction solution (see Appendix for methods) shifts downfield and broadens with increasing Ag concentration. These changes in line width and chemical shift[12] are indicative of desorption of the native Cd-oleate ligand from and the binding of 1-butanol to the nanocrystal surface during the cation exchange reaction.

From the above discussions, it is apparent that the key to deducing the thermodynamics of the cation exchange reaction relies on constructing an appropriate binding function that encapsulates the key ligand-acceptor interactions. While ITC or optical spectroscopy may be sufficient on their own to construct the binding curve, a myriad of techniques will be necessary to form a sufficiently complete picture of the exchange reaction to enable this endeavor.

4.1.2 Advanced Ligand Architectures

Beyond directly quantitating the role of ion solvation in the thermodynamics of cation exchange reactions in colloidal nanocrystals, the known approach to utilize preferential ion solvation to drive exchange reactions remains underutilized and implemented only in a simplistic manner. These methods rely on monodentate ligands to drive exchanges through ligand-ion-solvent miscibility limitations[13] or, most often, through qualitative hard-soft acid-base interactions to exchange from a soft Ag- or Cu-based material to a harder ion, such as Cd with the use of a soft phosphine. We propose the use of more advanced ligand architectures for stronger and more selective ion solvation as a strategy for achieving new materials through the cation exchange reaction.

A tangible approach for increasing the driving force of the exchange reaction is to increase the denticity of the ligands selected for preferential ion solvation. Provided steric hindrances allow for the increased number of binding sites to coordinate the metal ion without interference, the stability constant of the metal complex, and thus the overall driving force of the exchange reaction, would increase as the denticity of the ligand increases owing to the chelate effect. For example, the stability constant of a Cd^{2+} complex increases from log β = 6.52 with four monodentate methylamine ligands to log β = 10.6 with two bidentate ethylenediamine ligands, amounting to a decrease in free energy of 23.5 kJ/mol.[14] While selecting polydentate chelating ligands for the ion to be extracted from the lattice will increase the thermodynamic driving force of the exchange reaction, it is important that the ion being inserted into the lattice is available at a

sufficiently free concentration in solution such that the exchange reaction occurs. Therefore, properly selected chelators will have large differences in the stability constants of the ion to be extracted relative to the one to be inserted and will also have a low stability constant for the ion to be inserted. As a proof-of-principle, the exchange of Cu_2S to CdS was performed using both the canonical tertiary phosphine, a soft base that strongly binds to the soft Cu^+, and a well known Cu^+ chelator, neocuproine (2,9-dimethyl-1,10-pehananthroline) (Figure 4.3). Both ligands have high affinities for Cu^+ and are able to drive the exchange as evident by the similar featured optical spectra of CdS following the exchange reaction, demonstrating the successful use of a chelator to drive a cation exchange through preferential solvation. Extension of this concept may provide sufficient driving force to make new material systems thermodynamically accessible by these post synthetic chemical transformations.
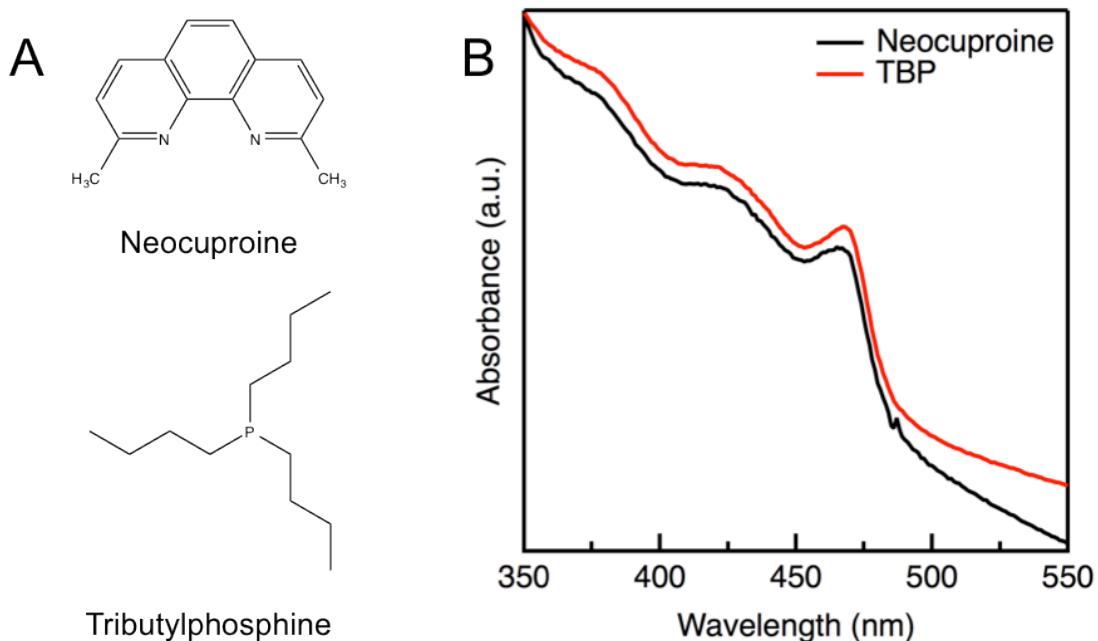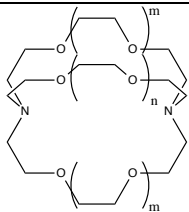
Figure 4.3. Chelation mediated cation exchange. (A) Ligands for selective solvation of Cu ions. (B) Absorbance spectra of CdS nanocrystals recovered after exchange from Cu_2S using tributylphosphine and neocuproine. The red absorbance tail is from scattering due to decreased solubility of the nanocrystals following forward and reverse exchange.

Beyond denticity, geometric constraints can be employed to enhance the selectivity of a ligand used to drive the exchange reaction. The three dimensional structure of macropolycyclic compounds such as cryptands creates a strong correlation between the

thermodynamic stability of the complex and the similarity in size of the cation with the cryptand cavity.[15] This geometric selectivity of cryptands is most noteworthy for their ability to discriminate between alkali metal cations such as Na^+ and K^+; however, it also translates to transition metal ions (Table 4.1).[16] While the nature of the binding sites remains constant (ether oxygen atoms and amine nitrogen at the end of the cage, see inset of Table 4.1 for structure and naming convention), the size of the pocket increases from cryptand [2.1.1] to cryptand [2.2.2], creating nonmonotonic variations in the stability constants. For example, the thermodynamic stability of the cryptand-ion complex transitions from favoring Ni^{2+} over Co^{2+} at large cavity size to favoring Co^{2+} over Ni^{2+} at small cavity size.

Table 4.1. Stability constants (Log β) of various cryptands and transition metal ions.[16] Values in parentheses denote ionic radii of ion or cryptand cavity.

Cryptand [(m+1).(m+1).(n+1)]	[2.1.1] (0.8)	[2.2.1] (1.10)	[2.2.2] (1.40)
Cu^{2+} (0.72)	7.78	7.56	6.81
Ni^{2+} (0.78)	4.5	4.28	3.5
Zn^{2+} (0.83)	5.3	4.28	3.5
Co^{2+} (0.82)	4.7	5.40	2.5
Cd^{2+} (0.95)	5.5	10.04	7.10
Pb^{2+} (1.18)	7.93	13.12	12.72
Ag^+ (1.15)	8.52	10.60	9.85

The selectivity of cryptands for the size, instead of solely the electronic nature, of the ion may enable exchanges that are routinely performed as a sequential exchange through a Cu- or Ag-based intermediate material to be done directly. The ability to perform direct exchanges can be advantageous in instances where the potential deleterious optical effects of residual Cu or Ag ions is of concern.[10,17,18]

4.2 Kinetics for Mechanistic Investigations

Replacement reactions are highly complex, involving numerous atomic motions, mass transport phenomena, and elementary reactions. For instance, a typical ion exchange can

be divided into a series of many steps: transport of reactants by diffusion to the particle-solution boundary, adsorption to the surface, decomposition/dissociation of the reactant, transport across the boundary into the crystal, solid state diffusion in the particle away from the interface, etc. Mechanistic pictures of ion replacement reactions in minerals[19] and thin films[20] have been constructed; however, the intermediate size scale of nanocrystals between that of molecules and bulk solids makes it unwise to simply extrapolate these findings. In fact, preliminary mechanistic studies of replacement reactions in nanocrystals imply the rate-limiting step is a surface mediated process as opposed to a solid-state diffusional process that is found in thin film studies.[21] Clearly, a detailed description of the mechanism and rate-determining step in cation exchange at the nanoscale is key for our understanding of the cation exchange reaction across various size scales and would provide insight into developing future reactions.

To postulate a mechanism, an empirical rate law is constructed in which the influence of reaction conditions on the rate are investigated. The rate law can then be subdivided into a series of elementary steps consistent with experimental observations to construct a reaction mechanism.[22] While the reaction rates can be measured by a number of techniques in which the observable can be correlated with the extent of reaction, stopped flow absorption spectroscopy is ideally suited for kinetic studies of ion exchange reactions in colloidal nanocrystals. As discussed above, the changes in the optical properties of nanocrystals, such as fluorescence intensity or extinction, can be correlated with the extent of reaction. For instance, the prototypical Ag exchange of CdSe involves the transformation of the visible band gap CdSe to the NIR absorbing Ag_2Se, enabling the extinction at a wavelength below the band gap of the CdSe to be used to construct a rate law. While the determination of a rate law and consistent mechanism requires methodical collection of a wealth of kinetic data including reactant order dependencies and rate constants at various temperatures to determine an activation energy, we will limit this discussion to a select few stopped flow absorption experiments of reaction rates that highlight the unique insights available by this technique.

The pathway for ligand interchange of coordination complexes is typically classified as an associative or dissociative substitution.[23] If we consider the nanocrystal as a Se sublattice (metal center) with interchanging cations (ligands), we can analogously treat the cation exchange reaction of a nanocrystal as either an associative or dissociative substitution of a coordination complex (Figure 4.4). For associative substitutions, the rate of interchange is influenced strongly by the nature of the entering ligand (Ag); however, the rate is invariant with the nature of the entering group for dissociative substitutions and it instead shows a strong dependence on the nature of the departing group (Cd).[23] A simple investigation of the rate law's dependence on the initial [Ag] and [Cd] in solution should enable cation exchange reactions to be classified in a similar manner to coordination complexes.

Morphology effects on the reaction rate should also provide insight into the mechanism. As discussed in Chapter 1, the examples in literature imply a surface reaction (molecular-like) being rate limiting for the Ag exchange of 3.5 nm CdSe dots[21] while solid-state diffusion (bulk-like) is rate limiting for CdSe nanowires.[24] Investigating the reaction rate

with various sizes of CdSe nanocrystals may enable this size dependent transition to be mapped out. Furthermore, the scaling of the rate with particle size should be indicative of the mechanism, as the rate should scale as surface area/volume for a rate limiting surface event. While many stopped flow absorption experiments benefit from the simplicity of using spherical nanocrystals, the litany of other nanocrystal shapes that are synthetically accessible provides additional mechanistic aspects to be investigated. How does the reaction rate change with shape? A facet selective exchange would be strongly dependent on the shape of the nanocrystal; for example, the rate of a facet selective exchange of a nanorod should scale as the inverse of the length as the diffusion front propagates.
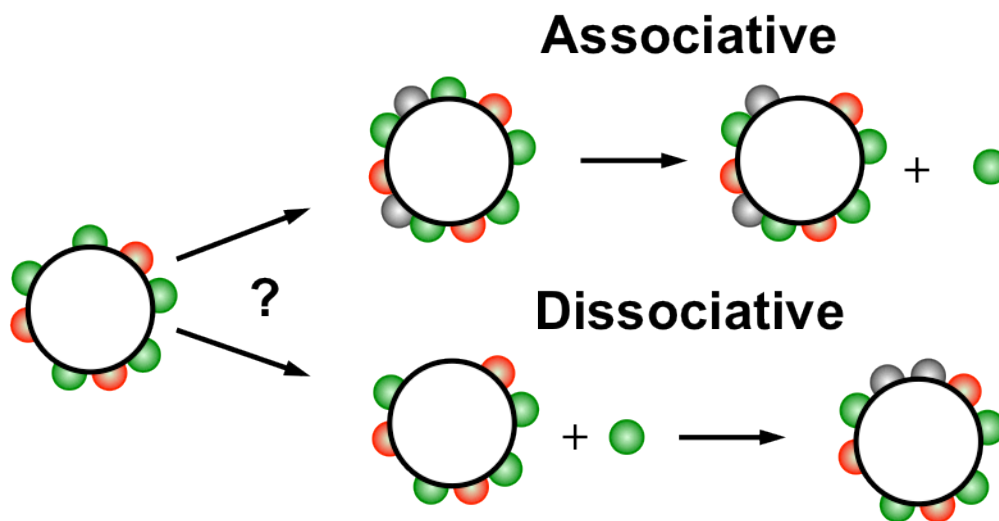
Figure 4.4. Classification of ion interchange. The green spheres represent Cd, red Se, and gray Ag. Only the surface layer of the nanocrystal is shown for simplicity.

In addition to the inorganic core, the organic surfactant that provides colloidal stability may play a key role in the mechanism of the ion exchange reaction of nanocrystals. Chapter 1 and the prior section highlight the dramatic role the ligand plays in the thermodynamics of these reactions but its role in the kinetics of the experiment is often neglected. A prior study claims a simple bimolecular rate law for the Ag exchange of CdSe yet showed a strong rate dependence on the concentration of ligand in solution, though the ligand was not included in the rate law.[21] Experiments investigating the order dependence on free ligand concentration and the type of ligand (binding group, chain length, cone angle) can elucidate if the role of the ligand is to decrease collision frequency between free ions and bare sites on the nanocrystal surface, to simply ligate free metal ions in solution effectively reducing their concentration, or if the ligand serves a more complex role in the mechanism.

As can be seen from these select examples, kinetic studies using stopped flow absorption spectroscopy can form a picture of the mechanism of cation exchange reactions in colloidal nanocrystals and identify the rate-limiting step. With knowledge of the rate limiting step, methods can be devised that may be able to accelerate or change which step is rate limiting, effectively providing a means to catalyze cation exchange reactions. This would provide a route to new materials that are thermodynamically favorable but whose formation is kinetically sluggish.

4.3 Isotopic Labeling

In conjunction with kinetic data, mechanistic information can be inferred through comparison of physical properties before and after the exchange reaction, though often relying on indirect evidence. For example, the size and shape preservation of cation exchange reactions in nanocrystals is commonly attributed to the anion framework of the particle remaining relatively static over the course of the reaction.[25] This proposal is based upon TEM images of samples before and after exchange showing negligible morphology changes[25] as well as minimal changes in optical data of CdSe/CdS dot-in-rod nanocrystal heterostructures before and after ion exchange, implying negligible intermixing of the anion sublattices.[26] These techniques provide only indirect evidence that the anion sublattice remains relatively static, an interesting hypothesis considering the complete replacement of cations within the lattice must involve a large-scale breakage and formation of bonds with the anion sublattice. Often during mechanistic investigations, it is desirable to isolate the role of a specific component of a complex participating in the reaction; in these cases the suspected participant (atom or molecule) may be replaced with its compositionally equivalent but isotopically unique counterpart.[22,23] Here we propose the extension of this technique to isotopically label nanocrystals to serve as an additional, and at times, more direct probe for characterization before, during, and after cation exchange.

Nanocrystal synthesis has developed methods to construct sharp, compositionally disparate interfaces within particles for the creation of heterostructures with high quantum yields or charge separation capabilities.[27] One of the more generalized techniques that has played a prominent role in this development is successive ion layer adsorption and reaction (SILAR).[28] Through this technique, approximately monolayer coverage of a material can be added to a seed nanocrystal, allowing precise radial engineering of the composition of nanocrystals including graded compositions.[29] This SILAR approach can be extended to our proposed purpose of isotopic engineering of nanocrystals (see Appendix for methods). A typical cadmium sulfide nanocrystal synthesis is followed using enriched sulfur-34 to yield $Cd(^{34}S)$ nanocrystals (Figure 4.5A). These seed nanocrystals are then overcoated with cadmium sulfide (natural sulfur abundance is 95% sulfur-32) approximately one monolayer at a time (Figure 4.5B) to yield a compositionally homogeneous but isotopically heterostructured core/shell $Cd(^{34}S)/Cd(^{32}S)$ nanocrystal (Figure 4.5C).

The isotopic SILAR technique allows the creation of nanocrystals well-suited to probe various nanocrystal reactions and many tenets of the ion exchange reaction. For instance, the core/shell $Cd(^{34}S)/Cd(^{32}S)$ nanocrystals can serve as an indicator of the rigidness of the anion framework. Controlled etching[30] (Figure 4.5D) coupled with mass spectroscopy would enable the radial isotopic profile of a nanocrystal before and after sequential cation exchanges to be compared, thus testing the hypothesis of a static anion sublattice. A truly static framework would demonstrate a discrete, step-like change in the $[^{34}S]$ as the nanocrystal is etched (Figure 4.5E); however, if the framework is more mobile, the discrete isotopic profile will be blurred following exchange (Figure 4.5F). A similar sample and technique can be used to probe another proposed mechanism of the cation exchange reaction: the reaction zone (see Chapter 1 for discussion). If the particle size is less than the reaction zone, the anion framework should be highly fluid yet as the particle grows larger, the framework should become more rigid.[25,31] A similar map of the isotopic profile and measure of the degree of anion mobility would provide a method to investigate this proposal.
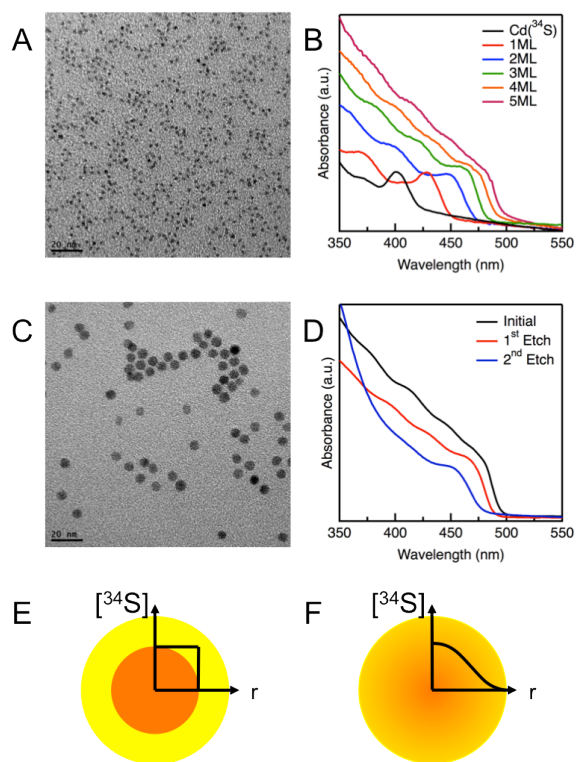
Figure 4.5. Isotopically labeled nanocrystals. (A) TEM image of $Cd(^{34}S)$ nanocrystals. (B) Absorbance spectra evolution during the overcoating process of $Cd(^{34}S)$ core nanocrystals with $Cd(^{32}S)$ monolayers (ML) to produce a compositionally homogeneous but isotopically heterogeneous nanocrystal. (C) TEM image of final $Cd(^{34}S)/Cd(^{32}S)$ core/shell nanocrystal. (D) Characteristic blue shift of CdS absorbance demonstrating controllable etching of isotopically labeled core/shell nanocrystal. (E, F) Proposed isotopic profile from radial etching coupled with mass spectroscopy for static and mobile anion sublattice models, respectively.

In addition to mass spectroscopy, the ability to controllably create isotopic interfaces within a nanocrystal can integrate with other isotope sensitive techniques, perhaps most noteworthy NMR given its the sensitivity to chemical environments, to provide a powerful probe of nanocrystal reactions. NMR has only recently become a standard technique in nanocrystal characterization, with the majority of studies probing ^{1}H, ^{31}P, and ^{13}C to investigate the organic ligand of the particle.[12] Due to the lower sensitivity factors and natural abundances of unpaired spin isotopes of the metals that are prototypical core materials (Cd, S, Se), only a limited number of reports exist probing the inorganic component of nanocrystals, relying on advanced solid-state NMR techniques to enhance signals,[32,33,34] preventing the study of solution phase reactions ubiquitous with colloidal nanocrystals. Isotopic enrichment of nanocrystal samples can yield sufficient concentrations of NMR active ^{113}Cd, ^{77}Se, or other relevant nuclei to enable solution phase monitoring of the inorganic component of the nanocrystal (Figure 4.6). Following a similar isotopic SILAR method, the core or surface of the nanocrystal can be selectively enriched with the NMR active metals to probe their role in solution phase nanocrystal reactions.
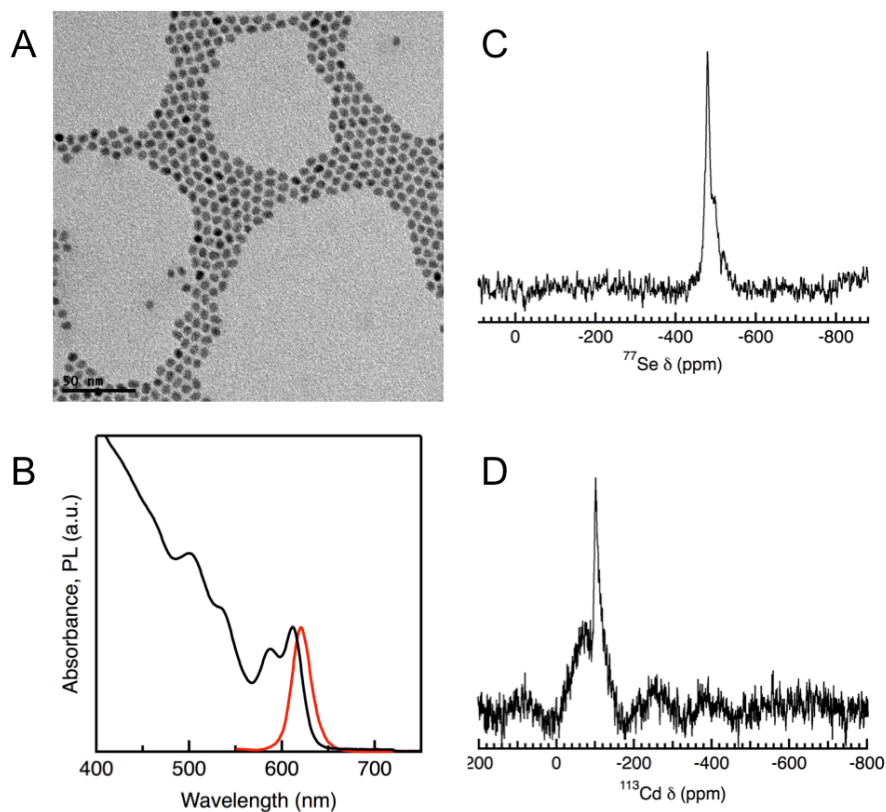

Figure 4.6. ^{113}Cd(^{77}Se) enriched NMR active nanocrystals. (A) TEM image and (B) absorbance and photoluminescence of ^{113}Cd(^{77}Se) nanocrystals. (C, D) ^{77}Se and ^{113}Cd NMR of enriched nanocrystals, respectively.

4.4 Concluding Thoughts

Cation exchange reactions in colloidal nanocrystals have continually developed as a synthetic method; yet, as this chapter has demonstrated, there is still a great deal to investigate. The overarching challenge remains for cation exchange to produce a technologically relevant, high quality material that is infeasible to produce by other means, vaulting the exchange reaction to prominence. Transition metal chalcogenides may be this target material class, given their promise as low cost catalysts for the oxygen reduction reaction[35] and the promising thin film literature demonstrating the use of ion exchange for their synthesis.[36] The morphology preservation accompanying cation exchange reactions on the nanoscale opens up the possibility of catalytic studies of quantum size and shape effects of transition metal chalcogenides that may yield even more exciting results.

4.5 Chapter 4 References

1.   Beberwyck, B. J.; Surendranath, Y.; Alivisatos, A. P. Cation Exchange: A Versatile Tool for Nanomaterials Synthesis. *J. Phys. Chem. C* **2013**, *117*, 19759-19770.

2.   Dong, C.; van Veggel, F. C. J. M. Cation Exchange in Lanthanide Fluoride Nanoparticles. *ACS Nano* **2008**, *3*, 123–130.

3.   Winzor, D. J.; Sawyer, W. H. *Quantitative Characterization of Ligand Binding*; Wiley-Liss: New York, 1995.

4.   Wyman, J.; Gill, S. J. *Binding and Linkage*; University Science Books: Mill Valley, 1990.

5.   Jelesarov, I.; Bosshard, H. R. Isothermal Titration Calorimetry and Differential Scanning Calorimetry as Complementary Tools to Investigate the Energetics of Biomolecular Recognition. *J. Mol. Recognit.* **2012**, *12*, 3-18.

6.   Herrera, I.; Winnik, M. A. Differential Binding Models for Isothermal Titration Calorimetry: Moving beyond the Wiseman Isotherm. *J. Phys. Chem. B* **2013**, *117*, 8659-8672.

7.   Anderson, N. C.; Hendricks, M. P.; Choi, J. J.; Owen, J. S. Ligand Exchange and the Stoichiometry of Metal Chalcogenide Nanocrystals: Spectroscopic Observation of Facile Metal-Carboxylate Displacement and Binding. *J. Am. Chem. Soc.* **2013**, *135*, 18536-18548.

8.   Tomashyk, V; Feychuk, P.; Shcherbak, L. *Ternary Alloys Based on II-VI Semiconductor Compounds*; CRC Press: Boca Raton, 2014.

9.   Smith, A. M.; Nie, S. Semiconductor Nanocrystals: Structure, Properties, and Band Gap Engineering. *Acc. Chem. Res.* **2010**, *43*, 190-200.

10.   Ingole, P. P.; Abhyankar, R. M.; Prasad, B. L. V.; Haram, S. K. Citrate-Capped Quantum Dots of CdSe for the Selective Photometric Detection of Silver Ions in Aqueous Solutions. *Mat. Sci. Eng. B* **2010**, *168*, 60-65.

11. White, S. L.; Smith, J. G.; Behl, M.; Jain, P. K. Co-operativity in a Nanocrystalline Solid-State Transition. *Nat. Commun.* **2013**, *4*, 2933.

12. Hens, Z.; Martins, J. C. A Solution NMR Toolbox for Characterizing the Surface Chemistry of Colloidal Nanocrystals. *Chem. Mater.* **2013**, *25*, 1211-1221.

13. Wark, S.; Hsia, C.-H.; Son, D. H. Effects of Ion Solvation and Volume Change of the Reaction on the Equilibrium and Morphology in Cation-Exchange Reaction of Nanocrystals. *J. Am. Chem. Soc.* **2008**, *130*, 9550–9555.

14. Cotton, F. A.; Wilkinson, G.; Murillo, C. A.; Bochmann, M. *Advanced Inorganic Chemistry*, 6th ed; Wiley-Interscience: New York, 1999.

15. Lehn, J. M. Cryptates: Inclusion Complexes of Macropolycyclic Receptor Molecules. *Pure & Appl. Chem.* **1978**, *50*, 871-892.

16. Arnaud-Neu, F.; Spiess, B.; Schwing-Weill, M.-J. Stability in Aqueous Solution of Some Complexes of Heavy Metals with Diaza-Polyoxamacrocyclic Ligands. *Helvetica Chimica Acta* **1977**, *60*, 2633-2643.

17. Sahu, A.; Kang, M. S.; Kompch, A.; Notthoff, C.; Wills, A. W.; Deng, D.; Winterer, M.; Frisbie, C. D.; Norris, D. J. Electronic Impurity Doping in CdSe Nanocrystals. *Nano Lett.* **2012**, *12*, 2587–2594.

18. Jain, P. K.; Beberwyck, B. J.; Fong, L.-K.; Polking, M. J.; Alivisatos, A. P. Highly Luminescent Nanocrystals From Removal of Impurity Atoms Residual From Ion-Exchange Synthesis. *Angew. Chem. Int. Ed.* **2012**, *51*, 2387–2390.

19. Putnis, A. Mineral Replacement Reactions: From Macroscopic Observations to Microscopic Mechanisms. *Mineral. Mag.* **2002**, *66*, 689–708.

20. Fedorov, V. A.; Ganshin, V. A.; Korkishko, Y. N. Ion Exchange in II-VI Crystals: Thermodynamics, Kinetics, and Technology. *Phys. Status Solidi A* **1993**, *139*, 9–65.

21. Chan, E. M.; Marcus, M. A.; Fakra, S.; ElNaggar, M.; Mathies, R. A.; Alivisatos, A. P. Millisecond Kinetics of Nanocrystal Cation Exchange Using Microfluidic X-ray Absorption Spectroscopy. *J. Phys. Chem. A* **2007**, *111*, 12210–12215.

22. Espensen, J. H. *Chemical Kinetics and Reaction Mechanisms*, 2nd ed.; McGraw-Hill: New York, 1995.

23. Shriver, D. F.; Atkins, P. W.; Overton, T. L.; Rourke, J. P.; Weller, M. T.; Armstrong, F. A. *Inorganic Chemistry*, 4th ed.; W. H. Freemand and Company: New York, 2006.

24. Dorn, A.; Allen, P. M.; Harris, D. K.; Bawendi, M. G. In Situ Electrical Monitoring of Cation Exchange in Nanowires. *Nano Lett.* **2010**, *10*, 3948–3951.

25. Son, D. H.; Hughes, S. M.; Yin, Y.; Alivisatos, A. P. Cation Exchange Reactions in Ionic Nanocrystals. *Science* **2004**, *306*, 1009-1012.

26. Jain, P. K.; Amirav, L.; Aloni, S.; Alivisatos, A. P. Nanoheterostructure Cation Exchange: Anionic Framework Conservation. *J. Am. Chem. Soc.* **2010**, *132*, 9997-9999.

27. Carbone, L., Cozzoli, P.D. Colloidal Heterostructured Nanocrystals: Synthesis and Growth Mechanisms. *Nanotoday* **2010**, *5*, 449-493.

28. Li, J. J.; Wang, Y. A.; Guo, W.; Keay, J. C.; Mishima, T. D.; Johnson, M. B.; Peng, X. Large-Scale Synthesis of Nearly Monodisperse CdSe/CdS Core/Chell

Nanocrystals Using Air-Stable Reagents via Successive Ion Layer Adsoprtion and Reaction. *J. Am. Chem. Soc.* **2003**, *125*, 12567-12575.

29. Xie, R.; Kolb, U.; Basché, T.; Mews, A. Synthesis and Characterization of Highly Luminescent CdSe-Core CdS/Zn$_{0.5}$Cd$_{0.5}$S/ZnS Multishell Nanocrystals. *J. Am. Chem. Soc.* **2005**, *127*, 7480-7488.

30. Ivanov, S. A.; Piryantinski, A.; Nanda, J.; Tretiak, S.; Zavadil, K. R.; Wallace, W. O.; Werder, D.; Klimov, V. I. Type-II Core/Shell CdS/ZnSe Nanocrystals: Synthesis, Electronic Structures, and Spectroscopic Properties. *J. Am. Chem. Soc.* **2007**, *129*, 11708-11719.

31. Backhaus-Ricoult, M. Solid-State Reactivity at Heterophase Interfaces. *Annu. Rev. Mater. Res.* **2003**, *33*, 55–90.

32. Berrettini, M. G.; Braun, G.; Hu, J. G.; Strouse, G. F. NMR Analysis of Surfaces and Interfaces in 2-nm CdSe. *J. Am. Chem. Soc.* **2004**, *126*, 7063-7070.

33. Lovingood, D. D.; Achey, R.; Paravastu, A. K.; Strouse, G. F. Size- and Site-Dependent Reconstruction in CdSe QDs Evidenced by ^{77}Se{^{1}H} CP-MAS NMR Spectroscopy. *J. Am. Chem. Soc.* **2010**, *132*, 3344-3354.

34. Ratcliffe, C. I.; Yu, K.; Ripmeester, J. A.; Zaman, M. B.; Badarau, C.; Singh, S. Solid State NMR Studies of Photoluminescent Cadmium Chalcogenide Nanoparticles. *Phys. Chem. Chem. Phys.* **2006**, *8*, 3510-3519.

35. Zhu, L.; Susac, D.; Teo, M.; Wong, K. C.; Wong, P. C.; Parsons, R. R.; Bizzotto, D.; Mitchell, K. A. R. Investigation of CoS2-Based Thin Films as Model Catalysts for the Oxygen Reduction Reaction. *J. Catal.* **2008**, *258*, 235-242.

36. Engelken, R. D.; Ali, S.; Chang, L. N.; Brinkley, C.; Turner, K.; Hester, C. Study and Development of a Generic Electrochemical Ion-Exchange Process to Form M$_x$S Optoelectronic Materials from ZnS Precursor Films Formed by Chemical-Precipitation Solution Deposition. *Mater. Lett.* **1990**, *10*, 264–274.

Appendix.

A.1. Supporting Information for Highly Luminescent Nanocrystals from Removal of Impurity Atoms from Ion Exchange Synthesis

Unless otherwise noted, all manipulations were performed using standard air-free techniques on a Schlenk line (Ar, vacuum P<100 mTorr) or in a glovebox (Ar, O_2<2 ppm).

Synthesis

Hot Injection Synthesis

CdSe nanocrystals, CdSe/CdS dot/rods, and CdS rods were synthesized and purified following Carbone et al.,[1] Talapin et al.,[2] and Sadtler et al.,[3] respectively.

Cation Exchange Synthesis

Cu(I) and Cd(II) cation exchange reactions were carried out in a similar manner to Jain et al.[4] Additional precipitation and re-dissolution steps were performed on several samples to ensure removal of excess free cations from solution. We ascertained that the cleaning steps did not lead to any significant effect on the PL yield.

Defect Purification

CdSe/CdS dot/rods obtained from the Cu(I) exchange and subsequent back-exchange to Cd(II) were purified by heating on a temperature controlled hot plate at 60-100 °C (depending on the solvent) for a period of several hours to a few days. Absorbance and PL were acquired periodically throughout this time to observe the progress of the defect purification. Prior to PL and absorption measurements, samples were allowed to cool to room temperature and sit for a couple hours to minimize temperature effects on PL intensity and allow surface ligand population to equilibrate.

Characterization Methods

Optical Spectra

Spectra were acquired in sealed cuvettes to prevent oxygen exposure to limit photobleaching effects on the samples. UV-visible absorbance spectra of the CdSe/CdS dot/rods and CdS nanorods were measured in toluene or hexane on a Shimadzu UV-3600 scanning spectrophotometer (full range: 185–3300 nm) with 1-nm step size and the appropriate solvent as background. Visible region photoluminescence (PL) spectra of

CdSe/CdS dot/rods and CdS nanorods were measured in toluene or hexane on a Horiba Jvon Yobin Fluoromax system equipped with a Triax 320 spectrometer and a photomultiplier tube (PMT), using a step size of 1 nm and an excitation wavelength of 400 (CdS nanorods) or 450 nm (CdSe/CdS dot/rods). Slit sizes and integration times were kept consistent between all samples being compared.

X-ray-Diffraction

X-ray diffraction patterns were collected on a GADDS Hi-Star D8 diffractometer (Bruker) using Co Kα radiation (1.790 Å) and a general area detector. The scan resolution was 0.02° in 2θ. Samples were prepared by deposition of a concentrated solution of nanocrystals on a glass plate followed by drying in air. The patterns were background-subtracted by the Bézier method and compared with those published in the Joint Committee of Powder Diffraction Standards (JCPDS) database for bulk materials (Hexagonal CdS #01-070-2553; Cubic CdS #03-065-2887).

Electron Microscopy

Low-resolution electron microscopy images were acquired on a FEI Tecnai G2 20 200kV LaB$_6$ transmission electron microscope. High-resolution transmission electron microscopy (HRTEM) images were acquired on a modified Philips CM300FEG/UT 300kV field-emission transmission electron microscope. The CdSe/CdS dot/rods with a 3.9-nm dot were selected for HRTEM characterization. Samples were prepared by drop-casting a few drops of the nanorod solution in toluene on either standard amorphous carbon on Cu grids (low resolution) or ultrathin carbon (< 3 nm) over holey carbon film, followed by rinsing with methanol and drying in air.

Characterization Results

Structural Defects

Formation and removal of structural defects were investigated as a possible source for the poor optoelectronic properties as a result of cation exchange and subsequent recovery of PL following defect purification. Low-resolution TEM (Figure A.1.1) and sizing distributions (Figure A.1.2) of the diameter and length of the nanorods from cation exchange and those from post-exchange purification confirm no substantial morphology changes (within standard deviation) as is the case for nanorods before and after cation exchange.[4] It is worth noting that at high excess Cu exchange concentrations, the nanorods will begin to form chains, likely through oriented attachment that persist after back-exchange with Cd. Simple sonication allows the chains to be broken down into individual nanorods. The lengths of these individual nanorods were used for the sizing comparison.

XRD and HRTEM indicate the presence of crystallographic defects in the CdSe/CdS dot/rods synthesized from cation exchange. The XRD pattern (Figure 3.2A) shows a strong suppression of the 002 peak for the sample from cation exchange compared to that synthesized from hot-injection. This implies the presence of crystallographic defects (grain boundaries) disrupting the single crystal domain along the long axis of the wurtzite CdSe/CdS dot/rods. Additionally, the nanorods synthesized from cation exchange have an increase in reflections attributable to zinc blende, implying the formation of zinc blende and associated stacking faults and/or grain boundaries upon exchange. Additionally, HRTEM confirms the presence of these defects (Figure 3.2B). However, no noticeable change in the density of these defects in the XRD pattern (Figure 3.2A) or HRTEM (Figure 3.2C) occurs upon purification, implying that these structural crystallographic defects are not the dominant source of the PL suppression and recovery upon annealing.

Determination of PL Yield and Enhancement and Comparison to Control Experiments

To compare the relative PL of samples synthesized from hot-injection, cation exchange, and post-exchange purification, band-gap PL intensities were integrated using IGOR Pro. PL spectra were corrected for absorbed intensity using the optical density (OD) at the excitation wavelength and for self-absorption using OD at the emission wavelength, as per the formula:

$$Multiplier_{PLCorrection} = \frac{1}{(1-10^{-(OD_{excitation}-OD_{baseline})})(10^{-OD_{emission}})}$$

No corrections for refractive index changes were accounted for between nanocrystal samples as the PL intensity appeared relatively independent of the solvent, likely because the dielectric environment of the nanocrystal is dominated by the ligands.

Quantum yields of the various samples were obtained by comparing the corrected integrated PL intensity of the nanocrystals to that of a standard (Coumarin 540 in methanol with QY = 91%) with similar PL spectra settings, as per the formula:

$$QY_{NC} = \frac{PLInt_{NC}}{PLInt_{C450}} * \left(\frac{n_{NC}}{n_{C540}}\right)^2 * QY_{C540}$$

The times and temperatures for the defect purification process of different samples and corrected PL intensities and quantum yields are reported for the CdSe/CdS dot/rods with 3.9 nm dot, 2.5 nm dot, and CdS nanorods in Tables A.1.1, A.1.2, and A.1.3, respectively. As mentioned in the text, several controls were performed to investigate the source of the increase in the PL yield following purification. Insignificant increase in the PL yield of samples treated with oleic acid compared to those kept at room temperature or those that were heated imply that the lack of surface passivation does not seem to be the dominant mechanism for PL deterioration. Hot-injection controls heated under the same temperature/time conditions as the impurity purification process showed no PL

enhancement, rather a marginal decrease in the PL yield possibly due to some loss of ligand passivation (see Tables A.1.1-A.1.3). In order to ensure that washing steps performed on cation-exchanged samples are not responsible for their drastically low PL yield, we performed the same washing steps on a hot-injection synthesized nanorod control. There was a marginal decrease in PL probably due to ligand loss but no drastic PL deterioration as seen in cation-exchanged samples.

Intentional Cu Doping and Subsequent Purification

To confirm the role of Cu impurities, we doped CdSe/CdS dot/rods from hot-injection with small concentrations of Cu impurities. A solution of 2 mg tetrakis(acetonitrile)copper(I) hexafluorophosphate in 10 mL methanol was added drop-wise in small increments (amounting cumulatively to 1.5, 3, 4.5, 6, 11, 19.5, and 27 nmol) to a vigorously stirred solution of the seeded rods (0.648 μmol Cd) in 3 mL toluene. Assuming 100% of the added Cu is incorporated into then nanorod, this amounts to 0.02 up to 0.4% Cu doping. PL and absorption spectra were taken immediately following the addition of the Cu solution. No change in absorption was seen from doping even at the highest 0.4% Cu doping, implying no formation of Cu_2S domains or morphological changes.

The intentionally added Cu impurities were removed by the addition of 10 μL of TBP, a known Cu(I) binding agent, to hot-injection-synthesized CdSe/CdS dot/rods doped with 0.4% Cu. The Cu impurity removal was probed by following the PL yield. Likewise, a control of sample of CdSe/CdS dot/rods from hot-injection without Cu impurities was exposed to TBP, to ensure that any PL change is not due to surface passivation effects. The PL yield of the Cu-doped sample increased 38-fold upon exposure to TBP for 24 hours, while the control sample decreased in PL yield over the same time under similar conditions (Figure A.1.3).
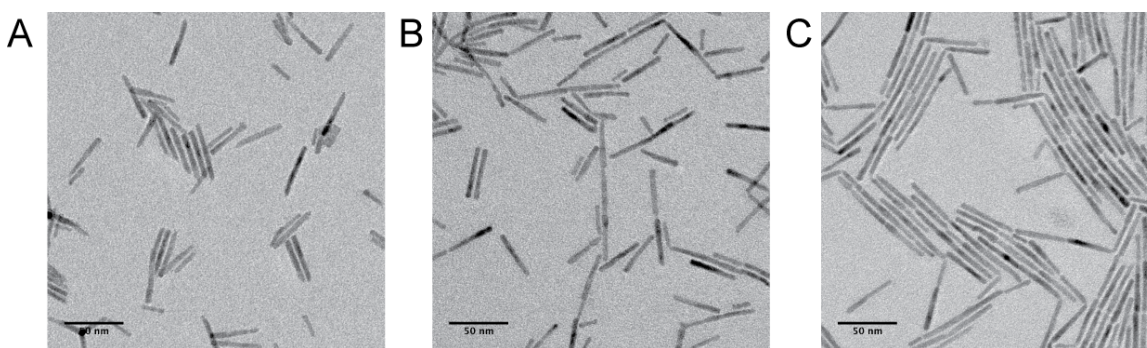

Figure A.1.1. Morphology effect of ion exchange and defect purification. Low res-TEM of CdSe/CdS dot/rods with 3.9 nm dot obtained from (A) hot-injection, (B) cation exchange, (C) and post-exchange purification.

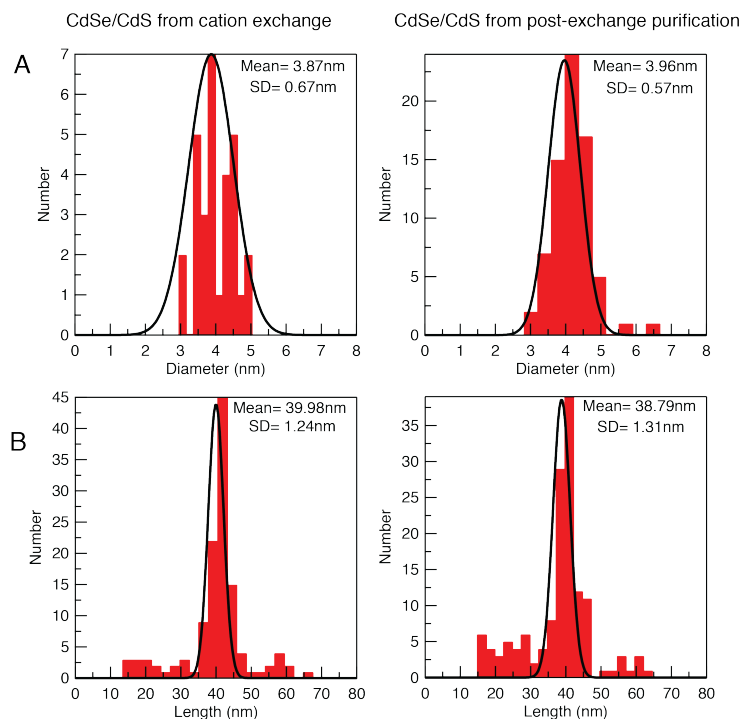CdSe/CdS from cation exchange   CdSe/CdS from post-exchange purification

Figure A.1.2. Size histograms of nanoheterostructures from cation exchange and post-exchange purification. (A) Diameters and (B) length distributions for CdSe/CdS dot/rods with 3.9 nm dot obtained from cation exchange (left) and post-exchange purification (right). Size distributions confirm negligible change (within standard deviation) of the length or diameter of the CdSe/CdS dot/rods as a result of the defect purification process.

Table A.1.1. Photoluminescence properties of CdSe/CdS dot/rods with 3.9 nm dot.

Sample	Corrected Integrated PL	Quantum Yield
Coumarin 540 in methanol	5.41×10^7	0.91
CdSe/CdS from hot-injection	2.72×10^7	0.5559
CdSe/CdS from exchange	3.51×10^4	0.0007
CdSe/CdS post-exchange purified at 100 °C for 30 hr	1.45×10^7	0.2959
CdSe/CdS post-exchange purified at 25 °C for 30 hr	3.54×10^6	0.0723
Hot-injection sample heated at 100 °C for 30 hr	1.67×10^7	0.3419

Table A.1.2. Photoluminescence properties of CdSe/CdS dot/rods with 2.5 nm dot.

Sample	Corrected Integrated PL	Quantum Yield
Coumarin 540 in Methanol	1.49×10^8	0.91
CdSe/CdS from hot-injection	3.40×10^7	0.2521
CdSe/CdS from exchange	2.29×10^5	0.0017
CdSe/CdS post-exchange purified at 60 °C for 21 hr and 100 °C for 43 hr	7.99×10^6	0.0592
CdSe/CdS post-exchange purified at 25 °C for 64 hr	1.00×10^6	0.0074
CdSe/CdS from hot-injection heated at 60 °C for 21 hr and 100 °C for 43 hr	1.94×10^7	0.1442
CdSe/CdS post-exchange oleic acid treatment at 25 °C for 21 hr	1.35×10^6	0.0100
CdSe/CdS post-exchange purified at 25 °C for 21 hr	5.56×10^5	0.0041
CdSe/CdS from hot-injection heated at 60 °C for 21 hr	5.77×10^6	0.0428

Table A.1.3. Photoluminescence properties of CdS nanorods.

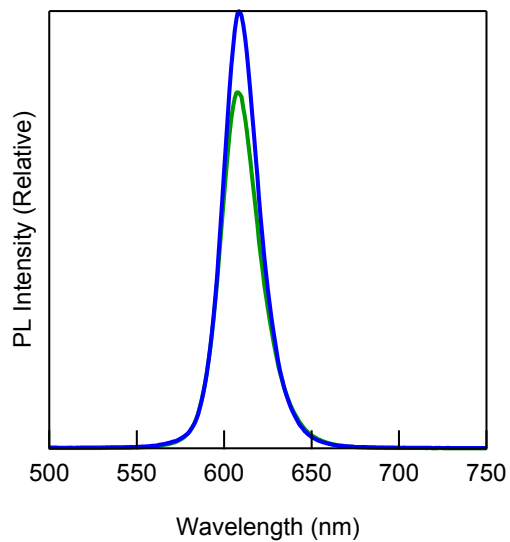| Sample	Corrected Integrated PL
Hot-injection synthesized CdS	5.23×10^7
CdS from exchange	8.34×10^4
CdS post-exchange purified at 65 °C for 61 hr	3.03×10^7
Hot-injection synthesized CdS heated at 65 °C for 61 hr	1.77×10^7

Figure A.1.3. Effect of tri-n-butylphosphine on nanoheterostructures PL. Corrected PL intensity of CdSe/CdS dot/rods from hot-injection control (blue) and after exposure to TBP for 24 hours (green). Unlike the case where CdSe/CdS dot/rods doped intentionally with Cu impurities increased in PL yield after exposure to TBP, the control showed a decrease in PL yield.

A.2. Supporting Information for Ion Exchange Synthesis of III-V Nanocrystals

All manipulations were performed using standard air-free techniques on a Schlenk line (Ar, vacuum P<100 mTorr) or in a glovebox (Ar, O_2<2 ppm).

Synthesis

Synthesis of Template Nanocrystals

Cd_3As_2 and Cd_3P_2 nanocrystals were synthesized according to literature protocols.[5,6]

Ion Exchange Synthesis

The procedure for the In^{3+} ion exchange of Cd_3As_2 and Cd_3P_2 is similar. A 1 M $InCl_3$:TOP stock solution was prepared by combining 10 mmol $InCl_3$ and 10 mL TOP in a flame dried 25 mL flask and heated to 270 °C under Ar for 1 hour, cooled, and transferred into the glovebox. In a typical In^{3+} ion exchange reaction, 1 mL of the 1 M $InCl_3$:TOP stock solution and an additional 1 g TOP were loaded into a flame dried 25 mL flask under Ar atmosphere. The solution was heated to 270 °C under Ar and either Cd_3P_2 or Cd_3As_2 nanocrystals (7.5 μmol Cd^{2+} (100x excess In:Cd) as determine by ICP-AES) dissolved in 0.83 g TOP were rapidly injected into the ion exchange solution. The reaction was kept at 270 °C for 15 minutes before the heating mantle was removed and the reaction cooled to room temperature. The raw solution was transferred into a glovebox and 2 mL chloroform and 10 mL 1:1 EtOH:MeOH solution was added to induce flocculation. The solution was centrifuged and the supernatant discarded. The precipitate was redispersed in chloroform and the cleaning procedure repeated an additional 2-3x. The final precipitate was dispersed in chloroform and passed through a 0.2 μm PTFE syringe filter.

The procedure for the Ga^{3+} ion exchange of Cd_3As_2 and Cd_3P_2 is similar. A 1 M $GaCl_3$:TOP stock solution was prepared in a glovebox by combining 10 mmol $GaCl_3$ with 10 mL TOP and stirred overnight at room temperature. In a typical Ga^{3+} ion exchange reaction, 1 mL of the 1 M $GaCl_3$:TOP stock solution and an additional 1 g TOP were loaded into a flame dried 25 mL flask under Ar atmosphere. The solution was heated to 300 °C under Ar and either Cd_3P_2 or Cd_3As_2 nanocrystals (7.5 μmol Cd^{2+} (100x excess Ga:Cd) as determine by ICP-AES) dissolved in 0.83 g TOP were rapidly injected into the ion exchange solution. The reaction was kept at 300 °C for 15 minutes before the heating mantle was removed and the reaction cooled to room temperature. The raw solution was transferred into a glovebox and 2 mL chloroform and 10 mL 1:1 EtOH:MeOH solution was added to induce flocculation. The solution was centrifuged and the supernatant discarded. The precipitate was redispersed in chloroform and the cleaning procedure repeated an additional 2-3x. In many situations, alcohols caused the flocculation of the nanocrystals as well as precipitated large amounts of white, residual

Ga-complex. When this occurred, a few drops of octylamine were added to the solution to redissolve the Ga-complex and the cleaning procedure continued. The final precipitate was dispersed in chloroform and passed through a 0.2 μm PTFE syringe filter.

Characterization Methods

Absorption Spectroscopy

Absorbance spectra were acquired using a Shimadzu 3600 spectrophotometer with 1 nm increments with solvent background subtraction. For absorbance measurements, the 4.5 nm Cd_3As_2 nanocrystals were dispersed in carbon tetrachloride and the remaining samples were dispersed in chloroform.

Electron Microscopy

TEM grids were prepared by drop-casting dilute solutions of nanocrystals onto amorphous carbon on 400 mesh Cu grids (Electron Microscopy Sciences) for low-resolution or ultrathin carbon on holey carbon film on 400 mesh Au grids (Ted Pella) for high resolution. Low resolution images were acquired using a 200 kV LaB_6 FEI G20 20 Tecnai and high-resolution images were acquired on a 200 kV FEG FEI monochromated F20 UT Tecnai. Particle sizes were measured using ImageJ (http://rsbweb.nih.gov/ij/).

X-ray Diffraction

XRD scans was collected on a Bruker GADDS Hi-Star D8 diffractometer with Co K_α (λ=1.790 Å) operating at 45 kV/35 mA. Samples were prepared in a glovebox by drop casting concentrated nanocrystal solutions onto a silicon crystal plate. Air sensitive samples were measured using an airtight silicon crystal specimen holder (Bruker) to minimize air exposure. Patterns were background subtracted by the Bézeir method and compared to reference patterns from the Inorganic Crystal Structure Database (ICSD).

Inductively Coupled Plasma Atomic Emission Spectroscopy (ICP-AES)

Cd^{2+} concentrations of the Cd_3P_2 and Cd_3As_2 nanocrystal solutions and residual Cd^{2+} concentrations in the ion exchanged nanocrystals were determined using an Optima 7000 DV ICP-AES (Perkins Elmer). Cd, Ga, In, and As ICP/DCP standard solutions (Fluka) were serially diluted to prepare a linear calibration curve spanning several orders of magnitude, ensuring sample concentrations fell within this linear range. Samples were prepared by drying nanocrystals solution under Ar and the solids digested using concentrated nitric acid (65%, TraceSELECT® Ultra, Fluka). These solutions were subsequently diluted to 10 mL total volume with Milli-Q™ (Millipore) water and passed through a 0.2 μm nylon syringe filter. Nitric acid concentrations were 2% wt/wt in all samples and standard solutions.
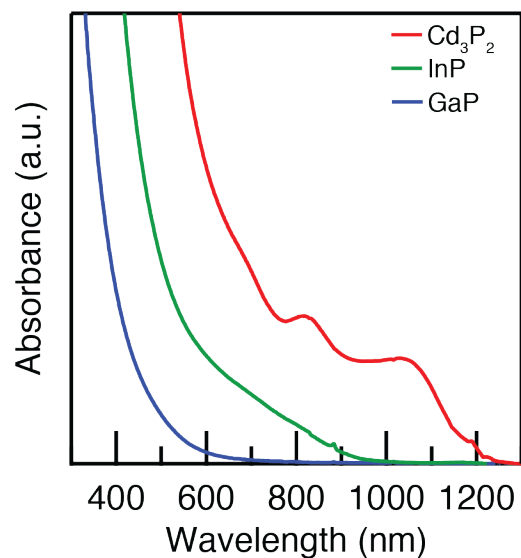
Figure A.2.1. Absorption spectra of the cation exchange of initial Cd_3P_2 nanocrystals to InP and GaP. The initial Cd_3P_2 shows a bimodal size distribution leading to a broad absorption feature for the InP.

Table A.2.1. ICP-AES results of III-V ion exchange synthesis. Ga^{3+} ion exchanges were performed at 300 °C for 15 min and In^{3+} ion exchanges at 270 °C for 15 min. Results are normalized to Cd concentration. *Note for the sequential exchanged InAs, the higher In concentration is due to residual In from the exchange procedure.

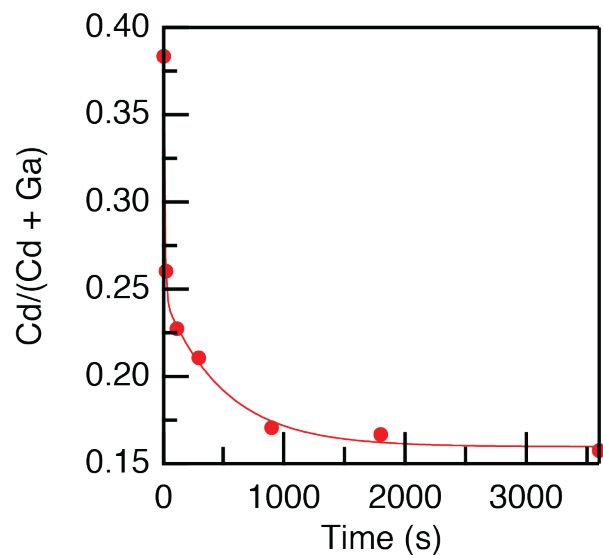| Sample	Ga	In	As	Cd
In^{3+} exchange of 3 nm Cd_3As_2	-	13.4	8	1
In^{3+} exchange of 4.5 nm Cd_3As_2	-	15.8	11.4	1
Sequential In^{3+} exchange of previously In^{3+} exchanged 4.5 nm Cd_3As_2	-	70*	19.5	1
In^{3+} exchange of 4.5 nm Cd_3As_2 followed by surface etch[7]	-	15.8	10.6	1
In^{3+} exchange of 3.5 nm Cd_3P_2	-	22.3	-	1
Ga^{3+} exchange of 3 nm Cd_3As_2	4.7	-	4.8	1
Ga^{3+} exchange of 4.5 nm Cd_3As_2	4.3	-	5.7	1
Ga^{3+} exchange of 3.5 nm Cd_3P_2	8.8	-	-	1

Figure A.2.2. Ratio of residual Cd as a function of time for Ga^{3+} ion exchange of 4.5 nm Cd_3As_2 at 300 °C.

Table A.2.2. ICP-AES results of residual Cd after Ga^{3+} ion exchange of Cd_3As_2 as a function of temperature, time, and size.

T (°C)	t (min)	d (nm)	Cd/(Cd+Ga)
200	5	2.2	0.10
		3	0.17
		4.5	0.26
300	5	4.5	0.21
	60		0.16
350	5	4.5	0.17
	60		0.13

A.3 Supporting Information for Prospectus

Isothermal Titration Calorimetry

ITC data was collected on a TA Instruments Nano ITC Standard Volume System with 24-carat gold cylindrical cells. The titration cell was filled with 1.2 mL of a 2 nm phosphonate-passived CdSe[1] nanocrystal-tetrahydrofuran (THF) solution (0.261 mM Cd measured by ICP-AES) and the reference cell was filled with 1 mL THF. The syringe (250 µL) was filled with a 2.775 mM $AgPF_6$-THF solution. The titration was performed by injecting 10 µL of titrant 25 times, waiting 900 s between injections to allow the instrument to return to baseline, while stirring at 300 rpm. The titration was performed at 25 °C and began only after the instrument achieved a stability of 0.2 ± 0.02 µW/hr.

Ag exchange of CdSe titration experiments

Ag(I) exchanges are modified from the report of Son et al.[8] $AgPF_6$ is used in place of $AgNO_3$ for enhanced salt solubility in nonpolar solvents and exchanges are performed in a mixed solvent system of 10% v/v 1-butanol/toluene to ensure particle solubility at low and high Ag/Cd ratios. Ag additions to solutions of CdSe nanocrystals are performed under vigorous stirring in an isopropanol dry ice bath (-77 °C) to ensure a homogeneous concentration of Ag within the nanocrystal solution is reached before the reaction proceeds.

Optical Titrations

3.7 nm phosphonate-passivated CdSe nanocrystals[1] were dispersed in the mixed solvent to yield a concentration of 0.5 mM Cd as determine by ICP-AES. For each titration point, 3 mL of the CdSe nanocrystal solution was cooled in the dry ice bath. Under vigorous stirring, the appropriate volume (as determined by the desired Ag/Cd ratio) of a 15 mM $AgPF_6$ mixed solvent solution, held in the dry ice bath, was added by microsyringe under Ar. After several seconds of vigorous stirring, the Ag-CdSe solution was removed from the dry ice bath to a stir plate at room temperature and allowed to equilibrate for > 24 hours prior to optical characterization. Absorbance spectra were collected on a Shimadzu 3600 spectrophotometer with 1 nm increments with solvent background subtraction from 1600-400 nm and corrected for volumetric dilution. Photoluminescence spectra were measured on a Horiba Jvon Yobin Fluoromax system equipped with a Triax 320 spectrometer and a photomultiplier tube (PMT) using a step size of 1nm. The excitation wavelength (500 nm), slit widths (2 nm), and integration time (0.5 s/nm) were held constant for all samples. Titration points were subsequently characterized by TEM to confirm particle aggregation and ripening did not contribute to changes in the absorbance. As seen in Figure A.3.1, an intermediate concentration range exists in which the particles ripen and aggregate. These concentrations were excluded from the analysis in Chapter 4 and warrant further study.

NMR titrations

Ag(I) exchanges were performed similar to above but with deuterated solvents (1-butanol-d$_{10}$, toluene-d$_8$). A 100 μM solution of 3.4 nm oleate-passivated CdSe nanocrystals[9] (~38mM Cd) in the mixed solvent was created as determined by absorbance.[10] For each titration point, 400 μL of the CdSe solution was loaded into a NMR tube and cooled in the dry ice bath. An appropriate amount (as determined by the desired Ag/Cd ratio) of a 225 mM AgPF$_6$ mixed solvent solution was added via micropipette. The NMR sample was shaken several times and removed to room temperature for > 24 hours prior to NMR analysis. ^{1}H NMR spectra were acquired on a Bruker AVB-400 400 MHz spectrometer.

Chelation Mediated Cation Exchange

Cd(II) exchange of Cu$_2$S nanocrystals were performed in a similar manner to Jain et al.[4] with the substitution of 2,9-dimethyl-1,10-pehananthroline (neocuproine) for tri-n-butylphosphine.

Isotopically Labeled Nanocrystals and Controlled Etching

Cd(^{34}S) cores were synthesized and purified according to Yang et al.[11] using enriched sulfur-34. Overcoating of Cd(^{34}S) was performed through modification of a published protocol.[12] Briefly, a 0.1 M cadmium oleate in octadecene (Cd:ODE) solution is prepared by heating CdO with 2.1 equivalents of oleic acid in ODE at 300 °C under Ar until clear and subsequently placing under vacuum at 100 °C for 1 hour before storing under Ar at room temperature. A 0.1 M sulfur:ODE (S:ODE) solution is prepared by heating elemental sulfur in ODE under vacuum at 120 °C for 1 hour and further heating at 200°C under Ar until clear before storing under Ar at room temperature. In a separate 25 mL 3-neck round bottom flask, 6 mL ODE and 1.5 g ocatdecylamine are degassed at room temperature for 15 minutes. Under Ar, a hexane solution of Cd(^{34}S) cores corresponding to 100 nmol of nanocrystals based on absorbance[10] is added. The solution is placed under vacuum for 1 hour at room temperature and then 20 minutes at 120 °C. Next, the flask is heated to 240 °C under Ar and a syringe pump is used to controllably added alternating amounts of the 0.1 M Cd:ODE and S:ODE solution at a rate of 0.1 mL/min, waiting 15 minutes in between each addition. The amount of Cd:ODE and S:ODE to be added is calculated according to Xie et al[12] to grow approximately 1 monolayer at a time. Samples are purified as previously reported.

Cd(^{34}S)/Cd(^{32}S) core/shell nanocrystals were controllably etched following Ivanov et al.[13]

^{113}Cd(^{77}Se) Enriched NMR Active Nanocrystals

^{113}Cd(^{77}Se) nanocrystals were synthesized and purified following Carbone et al.[1] with isotopically enriched ^{113}CdO and ^{77}Se powders. Purified ^{113}Cd(^{77}Se) nanocrystals were dispersed in CDCl$_3$. ^{113}Cd NMR spectra were collected on a Bruker AV-600 600 MHz

spectrometer and ^{77}Se spectra were collected on AVB-400 400 MHz spectrometer, each with a relaxation delay of 200 s.
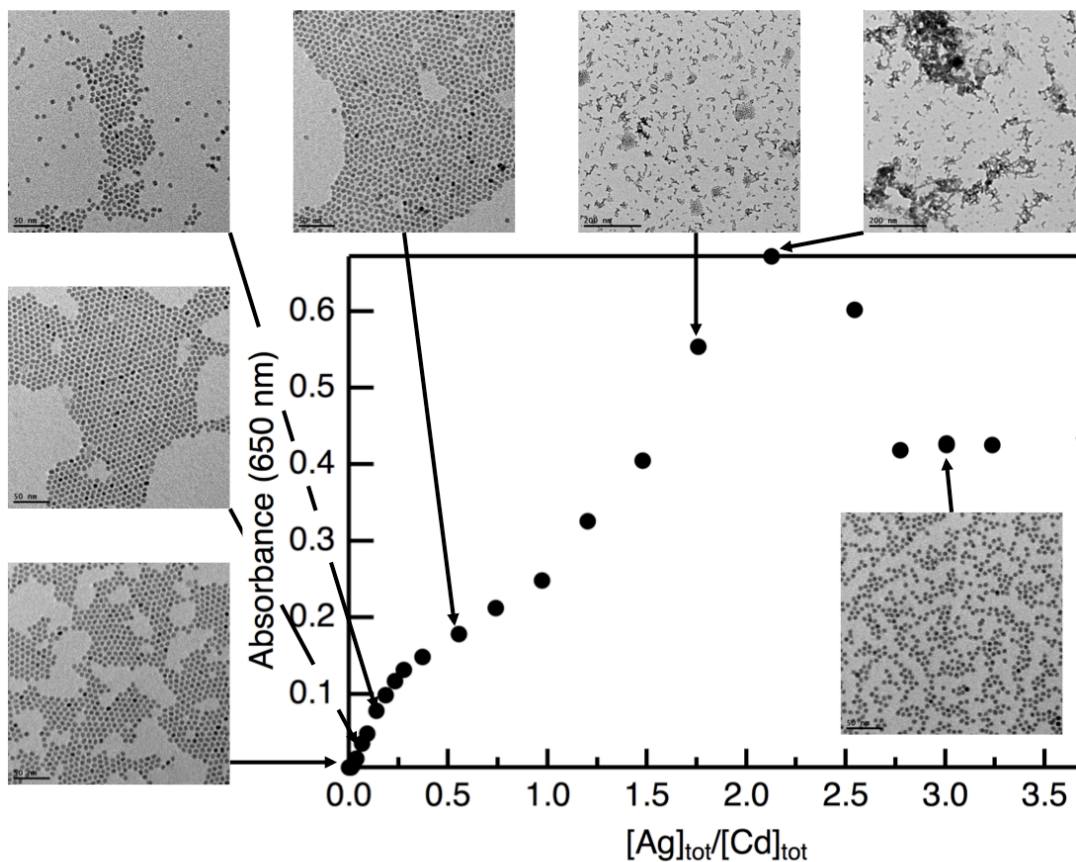

Figure A.3.1. Correlated TEM images to absorption titration of Ag exchange of CdSe nanocrystals. There is an intermediate Ag/Cd range (~1-2.5) that leads to ripening and aggregation.

A.4 Appendix References

1. Carbone, L.; Nobile, C.; De Giorgi, M.; Sala, F. D.; Morello, G.; Pompa, P.; Hytch, M.; Snoeck, E.; Fiore, A.; Franchini, I. R.; Nadasan, M.; Silvestre, A. F.; Chiodo, L.; Kudera, S.; Cingolani, R.; Krahne, R.; Manna, L. Synthesis and Microrrmeter-Scale Assembly of Colloidal CdSe/CdS Nanorods Prepared by a Seeded Growth Approach. *Nano Lett*. **2007**, 7, 2942–2950.
2. Talapin, D. V.; Nelson, J. H.; Shevchenko, E. V.; Aloni, S.; Sadtler, B.; Alivisatos, A. P. Seeded Growth of Highly Luminescent CdSe/CdS

Nanoheterostructures with Rod and Tetrapod Morphologies. *Nano Lett.* **2007**, *7*, 2951–2959.

3. Sadtler, B.; Demchenko, D. O.; Zheng, H.; Hughes, S. M.; Merkle, M. G.; Dahmen, U.; Wang, L.-W.; Alivisatos, A. P. Selective Facet Reactivity During Cation Exchange in Cadmium Sulfide Nanorods. *J. Am. Chem. Soc.* **2009**, *131*, 5285–5293.

4. Jain, P. K.; Amirav, L.; Aloni, S.; Alivisatos, A. P. Nanoheterostructure Cation Exchange: Anionic Framework Conservation. *J. Am. Chem. Soc.* **2010**, *132*, 9997-9999..

5. Harris, D. K.; Allen, P. M.; Han, H.-S.; Walker, B. J.; Lee, J.; Bawendi, M. G. Synthesis of Cadmium Arsenide Quantum Dots Luminescent in the Infrared. *J. Am. Chem. Soc.* **2011**, *133*, 4676–4679.

6. Xie, R.; Zhang, J.; Zhao, F.; Yang, W.; Peng, X. Synthesis of Monodisperse, Highly Emissive, and Size-Tunable Cd_3P_2 Nanocrystals. *Chem. Mater.* **2010**, *22*, 3820–3822.

7. Battaglia, D.; Blackman, B.; Peng, X. Coupled and Decoupled Dual Quantum Systems in One Semiconductor Nanocrystal. *J. Am. Chem. Soc.* **2005**, *127*, 10889–10897.

8. Son, D. H.; Hughes, S. M.; Yin, Y.; Alivisatos, A. P. Cation Exchange Reactions in Ionic Nanocrystals. *Science* **2004**, *306*, 1009-1012.

9. Flamee, S.; Cirillo, M.; Abe, S.; De Nolf, K.; Gomes, R.; Aubert, T.; Hens, Z. Fast, High Yield, and High Solid Loading Synthesis of Metal Selenide Nanocrystals. *Chem. Mater.* **2013**, *25*, 2476-2483.

10. Yu, W. W.; Qu, L.; Guo, W.; Peng, X. Experimental Determination of the Extinction Coefficient of CdTe, CdSe, and CdS Nanocrystals. *Chem. Mater.* **2003**, *15*, 2854-2860.

11. Yang, Y.; Chen, O.; Angerhofer, A. Cao, Y. C. Radial-Position-Controlled Doping in CdS/ZnS Core/Shell Nanocrystals. *J. Am. Chem. Soc.* **2006**, *128*, 12428-12429.

12. Xie, R.; Kolb, U.; Basché, T.; Mews, A. Synthesis and Characterization of Highly Luminescent CdSe-Core $CdS/Zn_{0.5}Cd_{0.5}S/ZnS$ Multishell Nanocrystals. *J. Am. Chem. Soc.* **2005**, *127*, 7480-7488.

13. Ivanov, S. A.; Piryantinski, A.; Nanda, J.; Tretiak, S.; Zavadil, K. R.; Wallace, W. O.; Werder, D.; Klimov, V. I. Type-II Core/Shell CdS/ZnSe Nanocrystals: Synthesis, Electronic Structures, and Spectroscopic Properties. *J. Am. Chem. Soc.* **2007**, *129*, 11708-11719.